INFORMATION TO USERS

This manuscript has been reproduced from the microfilm master. UMI films the text directly from the original or copy submitted. Thus, some thesis and dissertation copies are in typewriter face, while others may be from any type of computer printer.

The quality of this reproduction is dependent upon the quality of the copy submitted. Broken or indistinct print, colored or poor quality illustrations and photographs, print bleedthrough, substandard margins, and improper alignment can adversely affect reproduction.

In the unlikely event that the author did not send UMI a complete manuscript and there are missing pages, these will be noted. Also, if unauthorized copyright material had to be removed, a note will indicate the deletion.

Oversize materials (e.g., maps, drawings, charts) are reproduced by sectioning the original, beginning at the upper left-hand corner and continuing from left to right in equal sections with small overlaps. Each original is also photographed in one exposure and is included in reduced form at the back of the book.

Photographs included in the original manuscript have been reproduced xerographically in this copy. Higher quality 6" x 9" black and white photographic prints are available for any photographs or illustrations appearing in this copy for an additional charge. Contact UMI directly to order.

UMI®

Bell & Howell Information and Learning
300 North Zeeb Road, Ann Arbor, MI 48106-1346 USA
800-521-0600

A COMPARATIVE STUDY OF MODIFIED PASSENGER RAILWAY VEHICLE TRUCKS

Srinivasan Narayanaswamy

A thesis in

The Department

of

Mechanical Engineering

Submitted in Partial Fulfillment of the Requirements
for the Degree of Doctor of Philosophy at
Concordia University
Montreal, Quebec, Canada

December, 1998

Abstract

A Comparative Study of Modified Passenger Railway Vehicle Trucks

Srinivasan Narayanaswamy, Ph.D.
Concordia University, 1998

There has been renewed interest in rail transportation driven by the need for alternatives to congested highways and environmental concerns. The conventional railway truck designed for operation at high speed of approximately 200 km/hr makes use of stiff primary suspension elements to provide good dynamic stability. The curving performance of such a vehicle is poor because of wheelset misalignment in curves resulting in increased wheel and rail wear. This increases the maintenance cost. The wheelset misalignment also leads to increased lateral forces which raises the potential for derailment due to wheel climb. One of the aspects of the railway truck design that needs improvement is better compatibility between dynamic stability at high speeds and the ability of the vehicle to steer around curves.

In this thesis, modified truck designs are considered with an objective to improve both the high speed stability and curving behaviour. The performance of the following designs are compared: (i) Conventional truck (*C truck*) (ii) Radial truck (*R Truck*) (iii) Conventional truck with yaw damper (*CD truck*) and (iv) Unsymmetric Suspension truck with yaw damper (*USD truck*). The *USD truck* has longitudinal asymmetry in the suspension according to direction of motion i.e. the primary stiffness in the leading axle is

different from the trailing axle. Another truck considered for evaluation is the Unsymmetric Wheelset truck (*UW truck*) in which the trailing axle is an Independently Rotating Wheelset (IRW).

By choosing suitable values of primary yaw dampers, it is possible for *CD truck* and *USD truck* to achieve higher critical speed in comparison to *C truck* and *US truck* for a given bending stiffness. The non-linear curving analysis has shown that *USD truck* achieves better curving performance in comparison to other truck designs on curvatures up to 12 degrees. Thus it is possible for a properly designed *USD truck* to achieve near perfect steering *as well as* maintain good dynamic stability.

Validation of the results from this study has been carried out using the software New and Untried Car Analytic Regime Simulation (NUCARS). NUCARS is a multi-body dynamic program for railway vehicle design and performance evaluation and is an industry-wide standard in North America. The analysis of performance using NUCARS also shows that USD truck has better curving behaviour compared to other truck designs for curvatures up to 12 degrees.

ACKNOWLEDGMENTS

The author wishes to acknowledge the support and guidance given by his supervisors Prof. M.O.M. Osman, Department of Mechanical Engineering and Dr. R.V. Dukkipati, Adjunct Professor, Department of Mechanical Engineering. The author also thanks the management of the Canadian Pacific Railway for permission to use the software NUCARS for validation purposes. It is also appropriate to mention with gratitude the cooperation extended by the author's family during the course of this thesis work.

TABLE OF CONTENTS

List of Figures x

List of Tables xvi

Nomenclature xvii

1.0 Introduction and Literature Review 1

1.1 Background 1

1.2 Literature Review 4

1.2.1 Conventional Rail Vehicles 5
1.2.2 Steering Trucks 7
1.2.3 Railway Vehicle Trucks with Independently Rotating Wheelsets 11
1.2.4 High Speed Ground Transportation 20

1.3 Research Outline 21

1.3 Summary 23

2.0 Modelling Considerations and Simulation Environment 26

2.1 Introduction 26

2.2 Wheel/Rail Geometry 26
2.2.1 Linear Model of Wheel/Rail Geometry 26
2.2.2 Non-Linear Model for Wheel-Rail Geometry 29

2.3 Wheel/Rail Contact Forces 33
2.3.1 Creep Forces for Linear Stability Model 36
2.3.2 Creep Forces for Linear Curving Model 38
2.3.3 Creep Forces for Steady State Non-Linear Curving Model 40

2.4 Gravitational Stiffness Forces 42
2.4.1 Gravitational Stiffness for Linear Stability Model 44
2.4.2 Gravitational Stiffness for Linear Curving Model 44

2.5 Conventional Rail Vehicle Model 45
2.5.1 Wheelset Force Balance 45
2.5.2 Linear Stability Model 46
2.5.3 Linear Curving Model 47

2.6 Summary 47

3.0 Lateral Stability Models for Modified Truck Designs 51

3.1 Introduction 51

3.2 Radial Trucks 51

3.3 Unsymmetric Suspension Truck 57

3.4 Unsymmetric Wheelset Truck 65

3.5 Conventional Truck with Yaw Damper 65

3.6 Unsymmetric Suspension Truck with Yaw Damper 66

3.7 Tangent Track Stability Analysis 70

3.8 Stability Properties 74

3.9 Summary 80

4.0 Linear Curving Models and Curving/Stability Trade-Off 83

4.1 Introduction 83

4.2 Linear Curving Model 83
4.2.1 *C Truck* and *R Truck* 84
4.2.2 *US Truck* 86
4.2.3 *UW Truck* 89

4.3 Off-flange curving/stability trade-off 91

4.4 On-flange curving 104

4.5 Summary 108

5.0 Lateral Stability Behaviour of Modified Truck Designs 110

5.1 Introduction 110

5.2 Conventional Truck 111

5.3 Conventional Truck with Primary Yaw Damper 114

5.4 Radial Truck 119

5.5 Unsymmetric Suspension Truck with Yaw Damper 119

5.6 Summary 123

6.0 Steady State, Non-Linear Curving Analysis and Comparison with NUCARS 126

6.1 Introduction 126

6.2 Analysis of Simulation Results 126

6.2.1 Angle of Attack of Leading Axle 131
6.2.2 Lateral Force on the Leading Axle 133
6.2.3 Truck Wear Index 136
6.2.4 Summary of Simulation Results 139

6.3 Curving Analysis using NUCARS 139

6.3.1 Angle of Attack 143
6.3.2 Lateral Force on the Leading Axle 143
6.3.3 Wheel/Rail Resistance 144
6.3.4 Comparison of NUCARS with SS curving model 153

6.4 Summary 160

7.0 Summary, Conclusions and Recommendations for Future Research 161

7.1 Summary 161

7.2 Conclusions 162

7.3 Recommendations for Future Research 164

References 166

Appendix A 174

Appendix B 180

Appendix C 191

Appendix D 206

Appendix E 208

LIST OF FIGURES

Number	*Title*	*Page*
1.1	H-Frame Truck	3
1.2	Cross Braced Truck	8
1.3	Radial Truck	9
1.4	Stub Axle Design of IRW	12
1.5	Single Axle Design of IRW	13
1.6	Creep Controlled Wheelset	17
1.7	Axle-less Truck Design	19
2.1	Wheel/Rail Geometric Parameters	27
2.2	Wheel and Rail Profiles	31
2.3	Geometric constraint functions generated from WHRAILA for AAR 1:20	32
2.4	Wheelset Axis System	34
2.5	Non-Linear Creep Force Law	37
2.6	Free body diagram of wheelset	37
2.7	Suspension Arrangement of a Conventional Truck	49
2.8	Carbody Suspension Model	50
3.1	Inter-Wheelset Stiffnesses	53
3.2	Schematic of a radial truck	55

Number	*Title*	*Page*
3.3	Stiffness values that characterize different truck designs	56
3.4	Definition of US Index and Generalized Coordinates for US Trucks	58
3.5	Schematic of Unsymmetric Suspension Truck	60
3.6	Equivalent Shear Stiffness for US Truck	61
3.7	CD Truck Model	67
3.8	USD Truck Model	68
3.9	USD Truck with Switched Damper	71
3.10	Stability Plot for C Truck	75
3.11	Stability Plot for R Truck	76
3.12	Stability Plot for US Truck	78
3.13	Comparison of Stability for Different Truck Designs	79
3.14	Stability Zone for UW Truck	81
3.15	Variation of Critical Speed for UW Truck	81
4.1	Definition of Degree Curve	85
4.2	Stiffness Relationships for US Truck	90
4.3	Stiffness Ratio and Unsymmetric Index for US Truck	90
4.4	Lateral Displacement of Lead Wheelset	93
4.5	Tread Wear Index on Lead Outer Wheel	93
4.6	Trade Off Plot for C Truck, $\lambda = 0.15$	95

Number	*Title*	*Page*
4.7	Trade Off Plot for C Truck, $\lambda = 0.25$	97
4.8	Trade Off Plot for R Truck, $\lambda = 0.15$	98
4.9	Trade Off Plot for US Truck, $\lambda = 0.15$	99
4.10	Trade Off Plot for US Truck, $\lambda = 0.25$	100
4.11	Trade Off Plot for UW Truck, $\lambda = 0.15$	101
4.12	Trade Off Plot for UW Truck, $\lambda = 0.25$	101
4.13	Trade Off Comparison for Different Truck Types, $\lambda = 0.15$	103
4.14	Trade Off Comparison for Different Truck Types, $\lambda = 0.25$	103
4.15	Variation of AOA for Different Truck Types, $\lambda = 0.15$	106
4.16	Variation of Flange Wear for Different Truck Types, $\lambda = 0.15$	106
4.17	Variation of AOA for Different Truck Types, $\lambda = 0.25$	107
4.18	Variation of Flange Wear for Different Truck Types, $\lambda = 0.25$	107
5.1	Critical Velocity for C Truck	112
5.2	10% Modal Velocity for C Truck	112
5.3	Effect of Creep Coefficient on C Truck Stability	113
5.4	Effect of Damper Parameters for CD Truck	116

Number	*Title*	*Page*
5.5	Critical Velocity for CD Truck	117
5.6	10% Modal Velocity for CD Truck	117
5.7	Effect of Creep Coefficient for CD Truck	118
5.8	Comparison of Critical Velocity for C and CD Trucks	118
5.9	Critical Velocity for R Truck	120
5.10	10% Modal Velocity for R Truck	120
5.11	Effect of Creep Coefficients in R Truck	121
5.12	Variation of Critical Velocity with Damper Coefficient	122
5.13	Critical Velocity for USD Truck – Half Creep	122
5.14	Critical Velocity for USD Truck - Full Creep	124
6.1	Steady State Curving Attitude for C Truck	129
6.2	Steady State Curving Attitude for USD Truck	130
6.3	Angle of Attack for Leading Axle (100% Kalker Creep Coefficient)	132
6.4	Angle of Attack for Leading Axle (50% Kalker Creep Coefficient)	134
6.5	Lateral Force on Lead High Rail Wheel (100% Kalker Creep Coefficient)	137
6.6	Lateral Force on Lead High Rail Wheel (50% Kalker Creep Coefficient)	138

Number	*Title*	*Page*
6.7	Wear Index per Truck (100% Kalker Creep Coefficient)	140
6.8	Wear Index per Truck (50% Kalker Creep Coefficient)	141
6.9	Angle of Attack from NUCARS, Critical Speed 60 m/s (K_b values correspond to 1/2 creep)	145
6.10	Angle of Attack from NUCARS, Critical Speed 60 m/s (K_b values correspond to full creep)	146
6.11	Angle of Attack from NUCARS, Critical Speed 80 m/s (K_b values correspond to half creep)	147
6.12	Angle of Attack from NUCARS, Critical Speed 80 m/s (K_b values correspond to full creep)	148
6.13	Lateral force on the high rail wheel, Critical Speed 80 m/s (K_b values correspond to half creep)	149
6.14	Lateral force on the high rail wheel, Critical Speed 80 m/s (K_b values correspond to full creep)	150
6.15	Total Wheel/Rail Resistance predicted by NUCARS Critical Speed 80 m/s (K_b values correspond to half creep)	151
6.16	Total Wheel/Rail Resistance predicted by NUCARS Critical Speed 80 m/s (K_b values correspond to full creep)	152
6.17	Steady State Curving Attitude of USD Truck predicted by NUCARS	157
6.18	Comparison of AOA from NUCARS with SS Curving for C Truck	158
6.19	Comparison of Lateral Force from NUCARS with SS Curving for C Truck	158

Number	*Title*	*Page*
6.20	Comparison of AOA from NUCARS with SS Curving for USD Truck	159
6.21	Comparison of Lateral Force from NUCARS with SS Curving for USD Truck	159
A-1	Axis System for Wheelset Model	175
A-2	Axis System at Wheel/Rail Contact Points	177
B-1	Wheelset Axes and Velocity Centre of Mass	181
B-2	Load Distribution during Curving	187
C-1	Free Body Diagram of a Wheelset	194
C-2	Free Body Diagram of Front Truck	197
C-3	Free Body Diagram of Car	199

LIST OF TABLES

Number	*Title*	*Page*
4.1	Optimized stiffness parameters for different truck configurations	105
5.1	Bending Stiffness for different truck configurations	124
6.1	Angle of Attack of front and rear wheelsets in mrad on a 12 degree curve	135
6.2	Lead wheelset lateral forces in Newtons on a 12 degree curve	135
6.3	Wear Index per Truck in Nm/m on a 12 degree curve	142
6.4	Comparison of Angle of Attack on a 12 degree curve, Critical Speed = 80 m/s	154
6.5	Comparison of Lateral Force on a 12 degree curve, Critical Speed = 80 m/s	154
6.6	Comparison of Wear Index on a 12 degree curve, Critical Speed = 80 m/s	155

NOMENCLATURE

a	half of track gauge
a_s	unsymmetric parameter
a_{ps}	unsymmetric index for perfect steering
b	half of wheelbase
C_{px}, C_{py} & C_{pz}	primary longitudinal, lateral and vertical damping coefficients
C_{sx}, C_{sy} & C_{sz}	secondary longitudinal, lateral and vertical damping coefficients
$C_{p\psi}$	damping coefficient for the primary yaw damper
D	curvature in degrees
d_p	half of lateral spacing between primary longitudinal springs
d_s	half of lateral spacing between secondary vertical springs
f_{11}	longitudinal creep coefficient
f_{22}	lateral creep coefficient
f_{23}	lateral/spin creep coefficient
f_{33}	spin creep coefficient
F_{xl}, F_{xr}	longitudinal creep force at the left & right wheels
F_{yl}, F_{yr}	lateral creep force at the left & right wheels
F_c	lateral force due to cant deficiency
F_f	flange force on the wheel
h_{tp}	vertical distance from primary suspension to truck cg
h_{ts}	vertical distance from truck cg to secondary suspension
h_{cs}	vertical distance from secondary suspension to carbody cg
h_{cg}	distance from rail top to vehicle cg
I_{wy}	moment of inertia of wheelset about the axle axis
I_{wz}	yaw moment of inertia of a wheelset
I_{tx}	roll moment of inertia of a truck frame
I_{tz}	yaw moment of inertia of the truck frame
I_{cx}	roll moment of inertia of a car body
I_{cz}	yaw moment of inertia of the car body
K_b	generalized bending stiffness

K_s generalized shear stiffness

k_b bending stiffness between wheelsets

k_s shear stiffness between wheelsets

K_{px}, K_{py} & K_{pz} primary longitudinal, lateral and vertical stiffness

K_{sx}, K_{sy} & K_{sz} secondary longitudinal, lateral and vertical stiffness

$K_{d\psi}$ series stiffness coefficient for the yaw damper

M_z spin creep moment

M_c mass of carbody

M_t mass of truck frame

M_w mass of wheelset

N_l normal load at the left wheel

N_r normal load at the right wheel

N_w nominal load per wheel

N_y Lateral gravitational stiffness force

N_ψ Yaw gravitational stiffness moment

r_o centered wheel radius

r_l, r_r radius at left and right wheels

R curve radius

R_{cl}, R_{cr} position vectors of left and right wheel contact points

V vehicle speed

W_A axle load

y_w wheelset lateral displacement

y_t truck lateral displacement

y_c car lateral displacement

Δy inter-wheelset lateral displacement

$\dot{y}_w$, $\dot{y}_t$, $\dot{y}_c$ lateral velocity for wheelset, truck & car respectively

$\ddot{y}_w$, $\ddot{y}_t$, $\ddot{y}_c$ lateral acceleration for wheelset, truck & car respectively

α_i real part of i^{th} eigen value

β_i imaginary part of i^{th} eigen value

ζ_i eigen value of the i^{th} mode

β wheel spin

Δ coefficient for wheelset contact angle difference

Γ wheelset roll coefficient

λ wheel conicity

ψ wheelset yaw rotation

ψ_t	truck yaw rotation
ψ_c	car yaw rotation
$\Delta\psi$	inter-wheelset yaw rotation
$\dot{\psi}_w$, $\dot{\psi}_t$, $\dot{\psi}_c$	yaw velocity for wheelset, truck and car respectively
$\ddot{\psi}_w$, $\ddot{\psi}_t$, $\ddot{\psi}_c$	yaw acceleration for wheelset, truck and car respectively
ϕ_w	wheelset roll angle
ϕ_t	truck roll angle
ϕ_c	car body roll angle
$\dot{\phi}_w$, $\dot{\phi}_t$, $\dot{\phi}_c$	roll velocity for wheelset, truck and car respectively
$\ddot{\phi}_w$, $\ddot{\phi}_t$, $\ddot{\phi}_c$	roll acceleration for wheelset, truck and car respectively
ϕ_d	cant deficiency
δ_l	left wheel contact angle
δ_r	right wheel contact angle
δ_o	contact angle for centered wheelset
ξ_x, ξ_y & ξ_s	creepages in longitudinal, lateral and normal directions
ξ_c	resultant creepage
ξ_d	damping ratio
μ	coefficient of friction between wheel and rail
Ω	angular velocity of wheelset axes (excl. wheelset rolling velocity)
ω	rigid body angular velocity (nominal wheel rolling velocity)
ω_{ni}	natural frequency of the i^{th} mode
i_b, j_b & k_b	body coordinate system
i_e, j_e & k_e	equilibrium coordinate system
i_l, j_l & k_l	left wheel contact plane axes
i_r, j_r & k_r	right wheel contact plane axes

Chapter 1

INTRODUCTION AND LITERATURE REVIEW

1.1 Background

There has been an increased effort devoted to railway vehicle research and development in recent years. The renewed interest in the rail transportation stems from a number of factors. As population and income growth spurs additional travel demand, inter city transportation by air and automobiles increasingly suffer from congestion and delay. High Speed Ground Transportation (HSGT) is a passenger transportation option that can best link metropolitan areas lying about 200 km to 1000 km apart to meet the pressing transportation needs. It is less polluting compared to other modes of transportation like automobiles and aircraft. The rail transportation system also requires significantly less space than highway systems. It is relatively safer and does not lead to the high social costs associated with road accidents. Hence rail transportation has the potential to become the most effective means of moving passengers and freight over intermediate distances. However, the railway industry faces more and more competition from the road and air transportation systems because of the speed of the air travel and amenities of a private car. To achieve improved operational efficiency, railroad industry continues to look for innovations that will help improve the performance. It is also a fact that the rail road industry, especially in North America, is essentially conservative. Only in recent years have modern scientific methods of computer simulation been applied to address the problems of rail vehicle dynamics.

The 'conventional' truck, shown in Figure 1.1, denotes the complete assembly of wheels, axles, truck frame and suspension elements. In a conventional wheel-axle set, commonly referred as wheelset, the wheels are rigidly mounted on the axle. The wheels are tapered to provide a self-centering action for the railway vehicle. If the wheelset is initially disturbed from the center of the track, it will pursue a sinusoidal path at low speeds, assuming no suspension restraint. The frequency of this motion for an unrestrained wheelset is given by $V\sqrt{\frac{\lambda}{ar}}$ in radians/second. This state of neutral stability at the low speed develops into divergent oscillations at higher speeds. Consequently, the wheelsets are restrained by means of suspension elements that provide dynamic stability to the truck. The suspension elements connecting the wheelset with the truck frame is referred to as primary suspension. The secondary suspension connects the truck frame with the car body.

The coupled oscillation of the restrained wheelset in yaw and lateral displacement -- known as hunting -- will be damped at low speeds. As speed increases, a critical speed is reached above which any disturbance of the wheelset or truck from equilibrium will increase with time. Wickens had indicated, for good guidance on straight track, the frequency of this hunting mode should be high to facilitate fast response of the self centering action for which λ should be high [1]. If λ is too large, critical speed will be less, thus creating a design conflict between the stability and tangent track guidance.

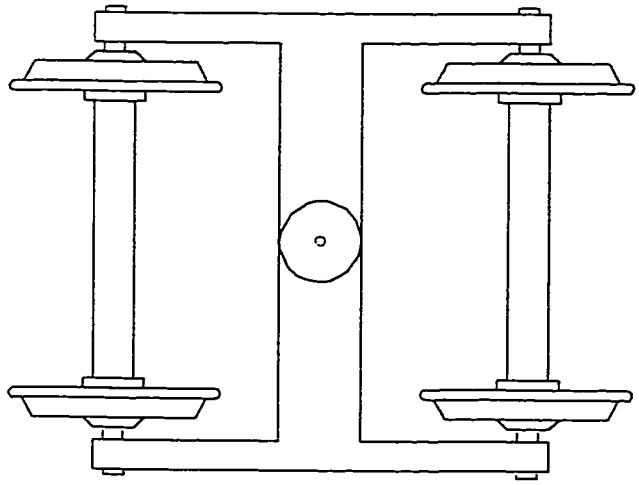

H-Frame Truck

Figure 1.1

The railway vehicle with flexible suspension and large conicity of the wheel profile achieves better steering ability without flange contact in curves as studies by Newland and Boocock have shown [2], [3]. But such a design leads to hunting phenomenon due to self induced oscillations of the rigid axle wheelsets. Vehicle hunting imposes operating speed limits and increases component wear.

A conventional rail vehicle suspension system is designed to provide high-speed dynamic stability on tangent track by using stiff primary suspension elements. The curving performance of such a vehicle is poor because of wheelset misalignment in curves resulting in increased wheel and rail wear. This increases the maintenance cost of track and wheels. The wheelset misalignment also leads to increased lateral forces which raises the potential for derailment due to wheel climb. One of the aspects of the railway truck design that needs improvement is better compatibility between dynamic stability at high speeds and the ability of the vehicle to steer around curves.

Thus requirements for good curving ability conflict with the requirements for dynamic stability.

1.2 Literature Review

In the following section review is done on the work carried out on rail vehicles to achieve compatibility between dynamic stability and curving behavior. Research carried

out in the development of rail vehicles with Independently Rotating Wheelset (IRW) are also discussed.

1.2.1 Conventional Trucks

The book on rail vehicle dynamics by Garg and Dukkipati is a comprehensive source for information on modeling and aspects of computer simulation of railway vehicles [4]. Law and Cooperider presented a survey of the research concerned with the dynamics of single, conventional rail vehicles and discussed the often conflicting objectives for railway vehicle suspension design and the research done to understand the design implications of these objectives [5]. Wickens presented the theory on steering and dynamic stability of railway vehicles in [6]. He showed that the stiffness and kinematic properties of all possible inter wheelset connections could be characterized by the generalized bending stiffness and the generalized shear stiffness.

A design methodology was proposed by Wormley et al for passenger railway trucks [7]. The procedure for the selection of truck design parameters to meet dynamic performance indices is based in partitioning the design task into three trade-off studies: (i) a vertical ride quality- secondary stroke trade-off (ii) a lateral ride quality-secondary stroke trade-off (iii) a stability-curving trade-off. The stability and forced vibrations of a railway vehicle to harmonic and stochastic track excitation were reported in reference [8] with the aid of a general multi-body program.

In these investigations, predominantly linear models of rail vehicles were considered. Because of the non-linearities inherent in the rail vehicle design and in the wheel/rail interaction, a linear analysis retains validity only for small amplitude motions. Linear models thus usually provide a qualitative, rather than a quantitative, measure of the system response. Hedrick and Arslan developed a model for studying the forced lateral response and stability considering important nonlinearities such as wheel profile and suspension effects [9]. They made use of the method of statistical linearization. The nonlinear curving theory for the railway vehicle was presented and validated with curving tests by Elkins and Gostling [10]. The improvements made to the nonlinear wheel/rail force prediction method of Elkins and Gostling was reported in reference [11]. The experimental equipment, that were developed over the years in British Rail Research and used to provide input data for the predictions, were described. Results of series of curving tests were compared with model predictions and were shown to give excellent agreement with the improved theory. Subsequently, Elkins and Allen used the validated computer model to evaluate the performance of a transit truck in terms of wheel/rail wear [12].

Analyses were conducted on the influence of axle load, track gauge, and wheel profile on the hunting behaviour of simplified models of wheelsets for typical freight and passenger car suspensions and reported in reference [13]. Hull and Cooperrider investigated influence of non-linear wheel/rail contact geometry on stability of railway freight cars with three-piece trucks using describing function techniques [14]. A non-

linear analysis for rail passenger truck stability and response to track alignment irregularities was developed by Horak and Wormley [15]. The analysis was used to illustrate the effect of track roughness, wheel profile parameters and creep on wheelset flanging and truck stability.

1.2.2 Steering Trucks

Development of two different types of steering trucks will be discussed in this section: (i) self-steering trucks in which wheelsets are interconnected through cross-braces or steering arms (ii) body-steered trucks in which wheelsets are steered by linkages connected to the car body.

The dynamics of a flexible truck are strongly affected by inter wheelset forces either through the truck frame as in the case of a conventional truck or through the interconnection elements as in the case of a self-steering truck. The impetus for the development of self-steering truck designs, like cross-braced trucks and radial trucks, has come from increasing demands of railways for higher operating speeds combined with good curving behaviour. The cross-anchor freight car bogies developed in South Africa and shown in Figure 1.2, use diagonal links pin-jointed to the journal boxes or side frames [16,17]. In USA and Canada, radial trucks for freight cars use steering arms mounted on the journal boxes and pin-jointed together as shown in Figure 1.3 [18].

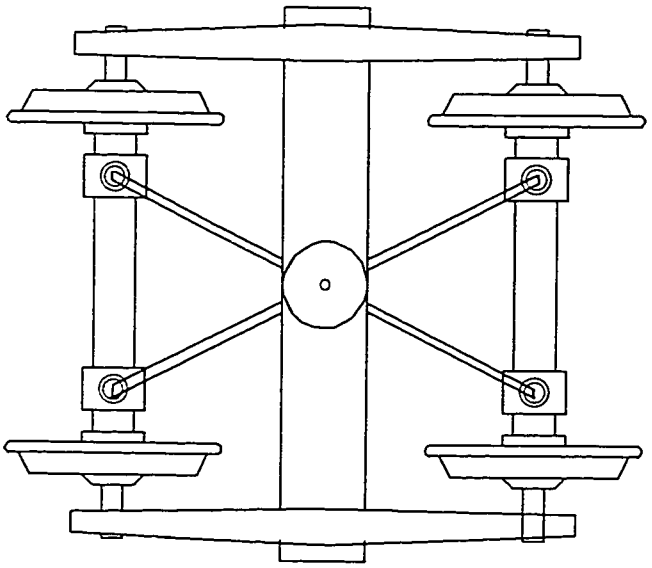

Cross Braced Truck

Figure 1.2

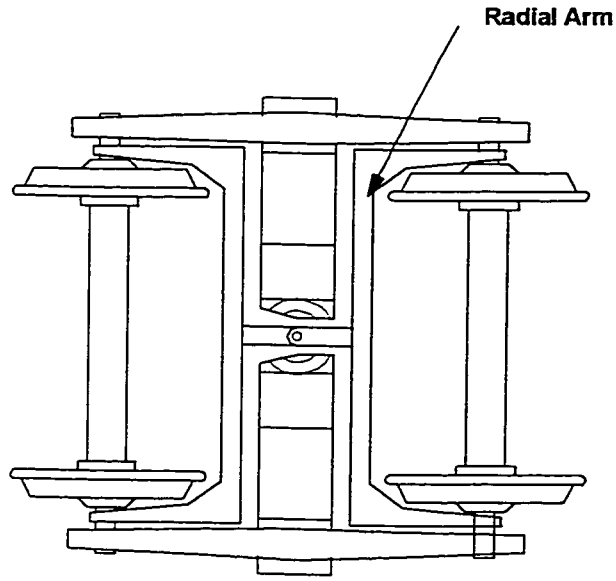

Radial Truck

Figure 1.3

References 19 to 21 presented the research efforts to quantify the benefits that can be obtained through cross bracing a three-piece truck for a freight car. The technique of cross-bracing did not eliminate the requirement for a non-zero bending stiffness between the wheelsets but it did provide greater stability for a given bending stiffness than was otherwise achievable. Using low order, predominantly linear models, Horak et al analyzed the stability andcurving mechanics of conventional and self-steering radial trucks for railway passenger cars [22]. It was shown that trucks with low value of bending stiffness had good curving behavior. However the choice of shear stiffness depended upon the severity of curves to be negotiated. A low value of shear stiffness improves the ability of the truck to stay off the flange for intermediate curves while a high value of shear stiffness results in lower flange forces once flange contact occurs. The effects of primary suspension and conicity were evaluated to find the trade-off between dynamic stability and curving performance for the case of conventional and radial truck designs.

In the body steered trucks, wheelsets are steered by means of linkages connected to the car body through the truck frame. In most designs, the linkages ensure that the yaw angle of the truck frame relative to the body is used to achieve the radial orientation of the wheelsets on curved track. Development of body steered trucks have been dealt with extensively in references [23] and [24] . In these trucks, an oscillatory instability can occur at low speeds due to kinematics of the linkage mechanism. These oscillations could be avoided by very careful selection of suspension parameters. However, these designs

have been found to be potentially sensitive to misalignments and manufacturing errors. Steering errors occur on curve entry and reverse curves.

One way of extending limits of performance obtainable with passive suspension is to use active suspension elements. Actively controlled suspensions have been the subject of research and development for a number of years and the main thrust has been towards the improvement of ride [25, 26]. Dynamics of actively guided vehicles in which steering is carried out in response to signals from a controller seeking to follow a given path or track has been reviewed by Wickens [27]. The performance of a rail car equipped with IRW having yaw control was discussed in [28]. However, for wider applications to railway environment, increased complexity of active systems may possibly outweigh the benefits.

1.2.3 Railway Vehicle Trucks with Independently Rotating Wheelsets

In a conventional rail vehicle, the hunting phenomenon imposes operational speed limits. Hunting is due to the coupling existing between the lateral and yaw motion of the rigid axle. In railway trucks provided with IRW, hunting is eliminated. In an IRW, wheels are decoupled and they can rotate independent of each other at different angular velocities. In all other ways, the IRW acts as a rigid wheelset thus avoiding problems at track features such as switch and crossing. The survey paper by Dukkipati et al provides an extensive review of rail vehicle systems with IRW [29]. Figure 1.4 shows the two-part

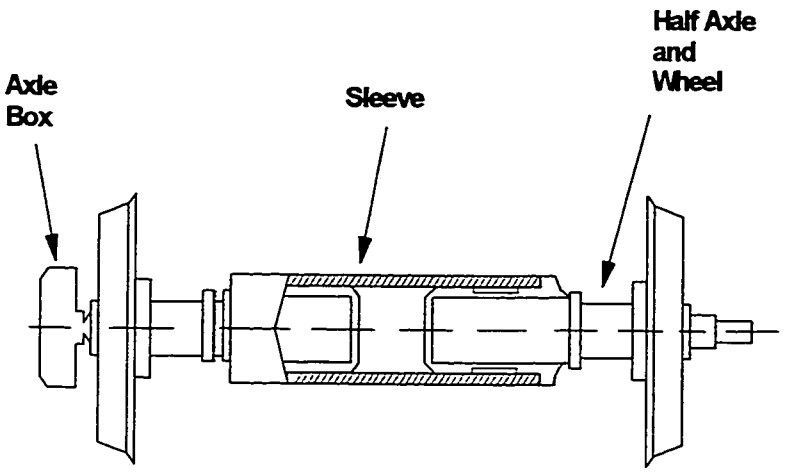

Stub Axle Design of IRW

Figure 1.4

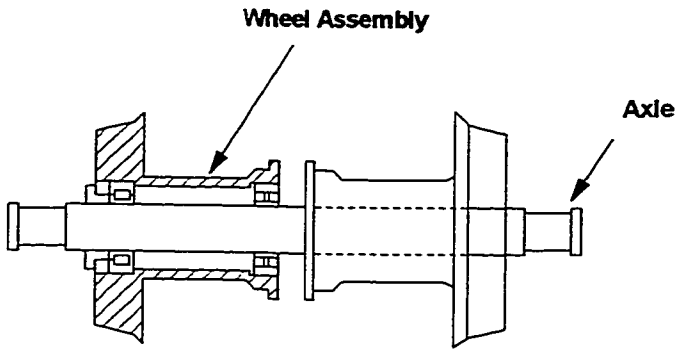

Single Axle Design of IRW

Figure 1.5

axle design of IRW in which two axle parts are joined by a common sleeve. The sleeve is fastened to the truck by tie rods and thus prevented from rotating. Each axle part is connected to the outer sleeve via two spherical roller bearings. Another design of IRW consists of two wheel assemblies mounted on a shaft through bearings as shown in Figure 1.5. Trucks with IRW do not have guidance capability, because independent wheels are unable to generate any steering torque due to rolling radius difference. This results incontinuous flange contact of one of the wheels.

Talgo train in Spain is a practical example of a railway system with IRW. The success of the Talgo train is due to its articulated construction whose trucks are coupled in the form of a draw bar chain, thus ensuring proper guidance for the vehicle. The ride quality of this high speed train is better compared to other conventional designs. But this train is not bi-directional.

An analytical investigation was initiated through a preliminary study of the application of IRW with a concave contour profile to the high speed Tube Vehicle System [30]. The response of the vehicle with IRW to lateral rail irregularities was compared to the performance of a conventional rail vehicle. It was found with respect to lateral ride qualities the modified vehicle appeared to be potentially superior to the conventional vehicle.

The dynamics of rail vehicles with IRW were analyzed theoretically by Eickhoff

and Harvey of British Rail Research and validated with experimental comparison [31, 32]. During testing it was observed that the truck fitted with IRW showed a definite tendency to run offset from the track center line, particularly with the softer suspension characteristics. One of the possible reasons for this behaviour is due to wheelset misalignment. In conventional trucks, wheelset misalignments of 0.1-0.5 milliradians are allowable. This is equivalent to making straight track look like a curve of several thousand metres radius. The conventional wheelset moves laterally and the small lateral offset produces a rolling radius difference. The resulting torque in the yaw direction compensates for the misalignment.

In the case of IRW, the wheelset has to move laterally until the contact angle difference produces sufficient force or rotates such that an angle of attack to the rail produces a lateral creep force. This is because, an IRW can not generate a yaw torque when it is laterally moved. It was found that a small misalignment of the order of 0.1 mrad would force an IRW into flange contact with one rail. However, the trucks with IRW were stable even at high speeds and for identical suspension parameters, the unweighted body lateral acceleration reduced by 50% in the case of the vehicle with IRW compared to the conventional one.

Elkins proposed a simple retrofit modification of the three piece freight car truck with IRW [33]. Various configurations of trucks with IRW were tested. It was observed that if hunting was the only consideration, then a truck with both axles with IRW would

be the best choice. However, the predicted curving performance of this configuration was worse than that of a conventional three piece truck. The configuration in which only the trailing axle was an IRW had substantially better predicted performance in both hunting and curving than a conventional truck. Such a design, however, is not bi-directional.

Another method of providing guidance to the IRW system is by a partial coupling of the axle. Benington showed that the dynamic behaviour of a single, conventional, elastically restrained wheelset could be improved by replacing the rigid torsional coupling between the wheels with a coupling having variable viscous characteristics [34]. In a detailed study, Ahmed investigated the performance of a freight car system with an Elasto-Damper Coupled Wheelset (EDCW). This concept is seen as a compromise between the excellent guiding characteristics of a conventional wheelset and improved hunting performance of an IRW [35]. An EDCW primarily consists of an axle with two independently rotating wheels coupled through an elasto-damper combination. The stability analysis revealed that by using a speed dependent damper in the coupler, the critical speed of a freight truck with EDCW is improved by over 100% in comparison to a conventional freight truck. However, analysis of the curving behaviour revealed that, due to torsional compliance of the EDCW, there is some loss of curving performance.

The partial coupling of the wheel-axle is provided by means of a magnetic coupling in a creep controlled wheelset developed in Germany . The wheels rotate independently on a fixed axle and are connected by means of a hollow shaft to a

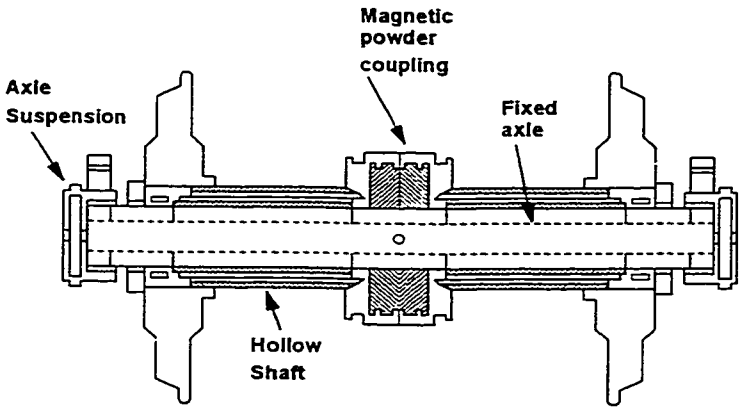

Creep Controlled Wheelset

Figure 1.6

magnetic powder coupling as shown in Figure 1.6. The frame and the primary suspension of the conventional truck are replaced by a fibre composite structure. Such a design was developed and tested by MBB GmbH and its excellent characteristics in terms of stability, guidance, force level and ride comfort are reported in reference [36].

In a creep controlled wheelset, the creep conditions at the two wheel/rail contact points are influenced directly by adjusting the torque transmission characteristics of the magnetic powder coupling, the main effort being directed at reducing the longitudinal component of the creep forces. The potential benefits of such a design are:

- Extension of the economically viable speed range upto 350 km/hr
- Reduction of lateral dynamic forces on tangent track and curves
- Decrease of wear on the tread profile
- Reduction of noise

The adverse effects of using a conventional rigid axle wheelset can be eliminated by completely de-coupling the wheels. Such a truck concept, in which forces necessary for guidance arise in the wheel-rail contact patch, has been advanced by Frederich [37]. The truck consists of individual wheels aligned one behind the other to form a so-called wheel block. Two such wheel blocks, with the wheels located in the fork shaped ends of the truck side frames, are linked to each other with a flexible joint as shown in Figure 1.7. The car body rests on two air springs mounted on the truck side frames. A lateral damper in the center of the truck and a vertical damper on each side of the air springs

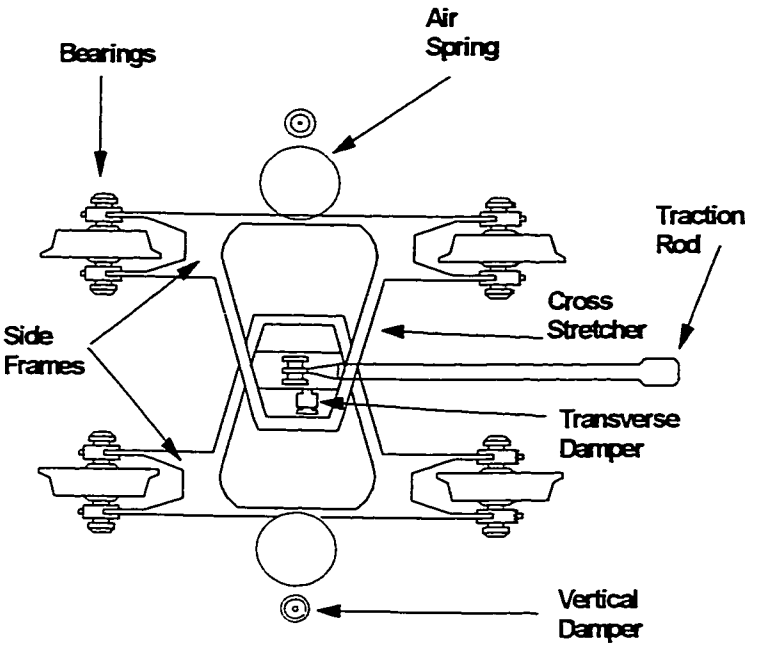

Axle-less truck design

Figure 1.7

together form the secondary suspension. A longitudinally aligned rod is provided to transmit traction and braking effort between the body and the truck. The analytical investigations and the subsequent experiments revealed the superior performance of the new truck design.

1.2.4 High Speed Ground Transportation

The progress made in the railway technology has found wide spread commercial applications in Railways in Europe and Japan. More recently in the United States,activities for the improvement, adaptation and integration of state-of-the-art technologies have been undertaken to promote high-speed passenger rail service [38,39,40,41]. To provide an objective basis for transport policy formulation and planning at the State and Federal levels, the report on ground transportation prepared by the Department of Transportation in the United States examined the economics of bringing HSGT to well-populated groups of cities [42]. The report classified HSGT options into three groups: accelerated rail service ("Accelerail"), new high-speed rail systems ("New HSR"), and magnetic levitation ("Maglev"), in order of increasing performance capabilities and initial cost Accelerail constitutes upgraded intercity rail passenger service on existing railroad rights-of-way, most of which belong to the freight railways. Examples of Accelerail-type systems include tilt trains such as the X-2000 in Sweden, Talgo in Spain, Pendolino in Italy and the InterCity 225 service in the United Kingdom. The top speeds attained in these systems are up to 240 km/h. New HSR

represents advanced steel-wheel-on-rail passenger systems on almost completely new rights-of-way with the maximum operating speed of approximately 300 km/h. Examples of New HSR include French TGV, the Japanese Shinkansen, and the German Intercity Express (ICE). Recently, the TGV technology developed in France has been chosen for the high speed train service in the North East Corridor of the United States [43].

Maglev is an advanced transport technology in which magnetic forces lift, propel and guide a vehicle over a specially designed guide way. There are no commercially operating Maglev systems currently. Germany and Japan have tested Maglev technology up to speeds of 450 km/h. These systems, if commercially made viable, have a potential to compete with air transportation over longer distances.

1.3 Research Outline

The challenge of railway vehicle suspension design has been to resolve the conflict between curving and dynamic stability. This conflict between curving and stability is quite fundamental and inherent in the railway vehicle design. As Wickens has shown, the conventional railway vehicle truck should have zero primary longitudinal stiffness for perfect steering on a curve [6]. However, such a vehicle with zero critical speed, will lack the dynamic stability. Thus, for the conventional truck, optimization involves a trade-off in the choice of suspension stiffnesses consistent with the required critical speed and curving performance. The radial truck design consists of minimizing

the longitudinal or yaw suspension stiffness that will help to align the wheelsets better on a curve and providing higher shear stiffness with wheelset interconnections to achieve a given critical speed. Studies in the past have shown that the self-steering radial truck allows an improved stability/curving trade-off, but it does not *eliminate* the trade-off [22].

In this thesis, potential for improving the performance envelops of existing designs is explored through investigation of modified truck designs. The modified truck design has an asymmetry in the plan view primary suspension. The asymmetry is introduced in two ways: in the unsymmetric suspension truck the primary suspension in the leading axle is different from the trailing axle; in the unsymmetric wheelset truck the trailing axle has independently rotating wheels. Appropriate linear models are developed for the study of dynamic stability and curving. It is shown that under certain conditions the unsymmetric suspension truck can achieve perfect steering *as well as* maintain dynamic stability. The models are evaluated to choose optimum suspension parameters to achieve the best trade-off between curving performance and tangent track stability.

Models of the conventional truck and unsymmetric truck are further modified by providing yaw dampers in the primary suspension to improve the dynamic stability. If the primary yaw dampers are used, the longitudinal restraint is removed for the low velocity steering motions; for higher frequency motions the damper resistance increases and the higher resistance helps to achieve desired critical speeds. The tangent track

stability of these advanced designs are then evaluated. Their curving performance is analyzed using a non-linear model that takes into account the non-linear wheel/rail profiles, non-linear creep forces and the yaw break away between truck and car body.

The technology that would hasten the deployment of a high-speed rail passenger service is that which can improve the safety, reliability, cost-effectiveness and revenue generating potential of such a service. It is shown that the unsymmetric suspension truck with primary yaw damper achieves better compatibility between the dynamic stability and curving behaviour than existing truck designs. Such a railway vehicle with the unsymmetric suspension trucks and primary yaw dampers can potentially be operated on existing rights-of-way without the need for massive investments for new track infrastructure.

1.4 Summary

In this chapter, a review is done on the research in railway vehicle suspension that has been carried out with an objective to achieve good curving performance and dynamic stability at high speeds. In Chapter 2, aspects of modelling a conventional railway vehicle will be discussed and equations of motion will be formulated for lateral stability analysis. Equations of equilibrium will also be derived for the study of curving behaviour.

In Chapter 3, concepts of modified truck designs will be introduced and equations of motion for a simple, two-axle truck model will be formulated to aid in understanding of

the stability characteristics. The following truck designs will be evaluated: a conventional truck that has symmetric plan view primary suspension, referred to as the *C truck*; a self-steering radial truck that has a steering arm interconnecting the wheelsets, referred to as the *R truck*; an unsymmetric suspension truck that has an unsymmetric plan view primary suspension, referred to as the *US truck*; and an unsymmetric wheelset truck that has an independently rotating wheelset in the trailing axle, referred to as the *UW truck*.

In chapter 4, linear curving models will be used to evaluate the off-flange and on-flange curving performance of the trucks mentioned above. A trade-off analysis is carried out to optimize suspension parameters for the different truck designs.

In Chapter 5, the *C truck* and the *US truck* will be modified with yaw dampers in the primary suspension in order to improve the dynamic stability at high speeds. These are referred to as *CD truck* and *USD truck* respectively. A sensitivity study will be done to evaluate the effects of varying bending stiffness, wheel conicity and creep coefficients for the *C truck*, *R truck*, *CD truck* and *USD truck* designs.

In Chapter 6, results of curving analysis using a non-linear, steady state curving program will be presented for the *C truck*, *R truck*, *CD truck* and *USD truck* designs. The program will be validated by comparing the results with those obtained from NUCARS simulation.

Chapter 7 will summarize main conclusions of research with recommendations for future work.

Chapter 2

MODELLING CONSIDERATIONS AND SIMULATION ENVIRONMENT

2.1 Introduction

The guidance of a railway vehicle is determined by interaction between wheelsets and rails. Thus the mechanics of wheel-rail interaction is fundamental to the dynamics of railway vehicles. The kinematics of guidance is based on the geometry of wheelsets and rails. On the other hand, the dynamics of guidance depend on the wheel-rail interaction forces and moments developed as a result of the vehicle's forward velocity.

Wickens developed realistic theory of dynamics of railway vehicles on straight track taking into account flexibility between the wheelsets and the frame in the longitudinal, lateral, and vertical directions, and the influence of wheel and rail profiles [44, 45]. In this chapter, aspects of modelling a conventional truck including wheel-rail geometry, wheel-rail contact forces and suspension forces will be discussed. The creepage expressions are derived in Appendix B. The suspension forces and the equations of motion are derived in Appendix C.

2.2 Wheel-Rail Geometry

2.2.1 Linear Model of Wheel-Rail Geometry

Rear View

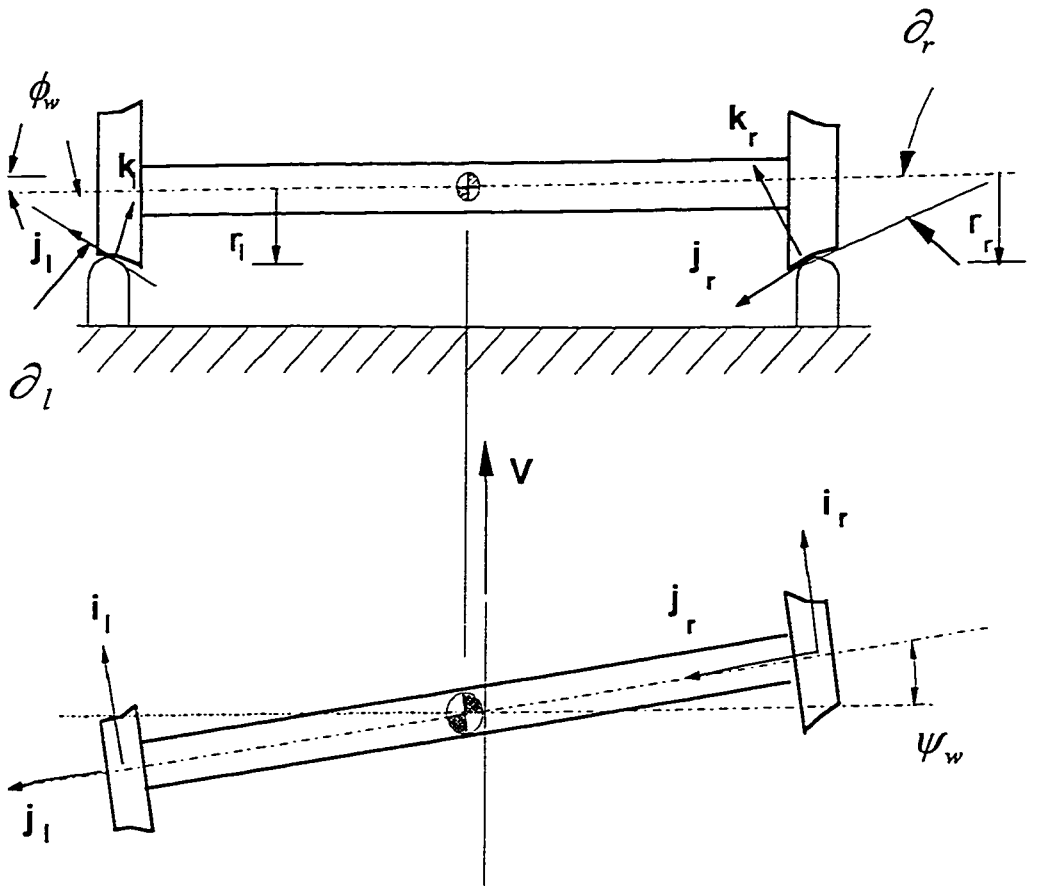

Top View

Wheel/Rail Geometric Parameters

Figure 2.1

A number of geometric parameters are required to adequately simulate the wheel/rail interface as shown in Figure 2.1. They are:

r_l, r_r = rolling radii of the left and right wheels
∂_l, ∂_r = contact angles for the left and right wheels
ϕ_w = wheelset roll angles

In the linear hunting model and linear curving model, these variables are approximated by linear functions of the lateral wheel set displacement as given below:

$$r_l, r_r = r_o \pm \lambda y_w \tag{2.1}$$

$$\partial_l, \partial_r = \partial_o \pm \frac{\Delta}{a} y_w \tag{2.2}$$

$$\phi_w = \frac{\Gamma}{a} y_w \tag{2.3}$$

In the above equations,

r_o = centered wheel radius
λ = wheel conicity
∂_o = centered contact angle
Δ = contact angle difference coefficient
Γ = wheelset roll coefficient

Referring to the equation (2.1), the rolling radii enter the wheelset equations of motion because there is a difference between the rolling radii of the wheelset as the whelset is laterally displaced. When the wheelset is displaced from a centered position between the rails, the difference between the rolling radii at the left and right wheels requires that the velocity of the wheel at the contact point on the wheel with a larger

rolling radius be greater than the velocity of the other wheel at the contact point. The resulting creepage at the wheel/rail interface gives rise to a moment which tends to steer the wheelset towards the centered position of the rails. This difference in rolling radii with lateral displacement has a dominant effect on the nature and stability of the rail vehicle motion. If the conicity is zero, like in a cylindrical tread profile, the vehicle will never experience hunting, but must rely on wheel flanges for guidance. Increasing the effective conicity has a destabilizing effect, since the critical speed for onset of hunting is lower for higher conicities.

2.2.2 Non-Linear Model for Wheel-Rail Geometry

The equations (2.1) to (2.3) are valid for the tread contact of wheels. For the linear hunting model, the above linearized wheel/rail geometry provide reasonably accurate results. During curving, wheels are guided by the flange and wheel/rail contact conditions depend on the wheelset lateral position.

The nature of the forces exerted between the wheel and rail, both in the plane of contact and normal to it, is determined by the geometry of the wheel and rail. The wheelset is constrained to move laterally and vertically in a prescribed space determined by the geometry of the wheels, rails and track structure. The wheelset position is described by its lateral position of its geometric center relative to the track center line and the yaw angle of the wheelset. The roll angle and vertical displacement of the wheelset are determined by the geometric constraints. To predict the wheel-rail geometric parameters

like contact angle, roll angle, rolling radius for any particular value of lateral displacement, Cooperrider and Heller developed a numerical technique [46].

A linear analysis that assumes conical wheel tread profile is a poor approximation for worn or intentionally profiled wheels. The new and worn profiles for the wheel and rail are shown in figures 2.2. The following steps are involved in using the program Asymmetric Wheel and Rail Characterization Program , WHRAILA, developed by Cooperrider and Heller:

1. Obtain digital wheel and rail profile data
2. Specify the wheel and rail gauge (lateral separation) and cant angles (relative orientations)
3. Solve numerically for wheel/rail contact positions over a range of wheelset lateral positions
4. Use the contact position results to compute desired wheel/rail geometric constraint functions.

Typical results from the wheel-rail geometry analysis for an AAR 1:20 profile is shown in figure 2.3. The normalized rolling radius difference, $\frac{r_l - r_r}{2a}$ and one half contact angle difference, $\frac{\delta_l - \delta_r}{2}$, are nearly linear before the flange contacts the rail, and jump abruptly at flange contact.

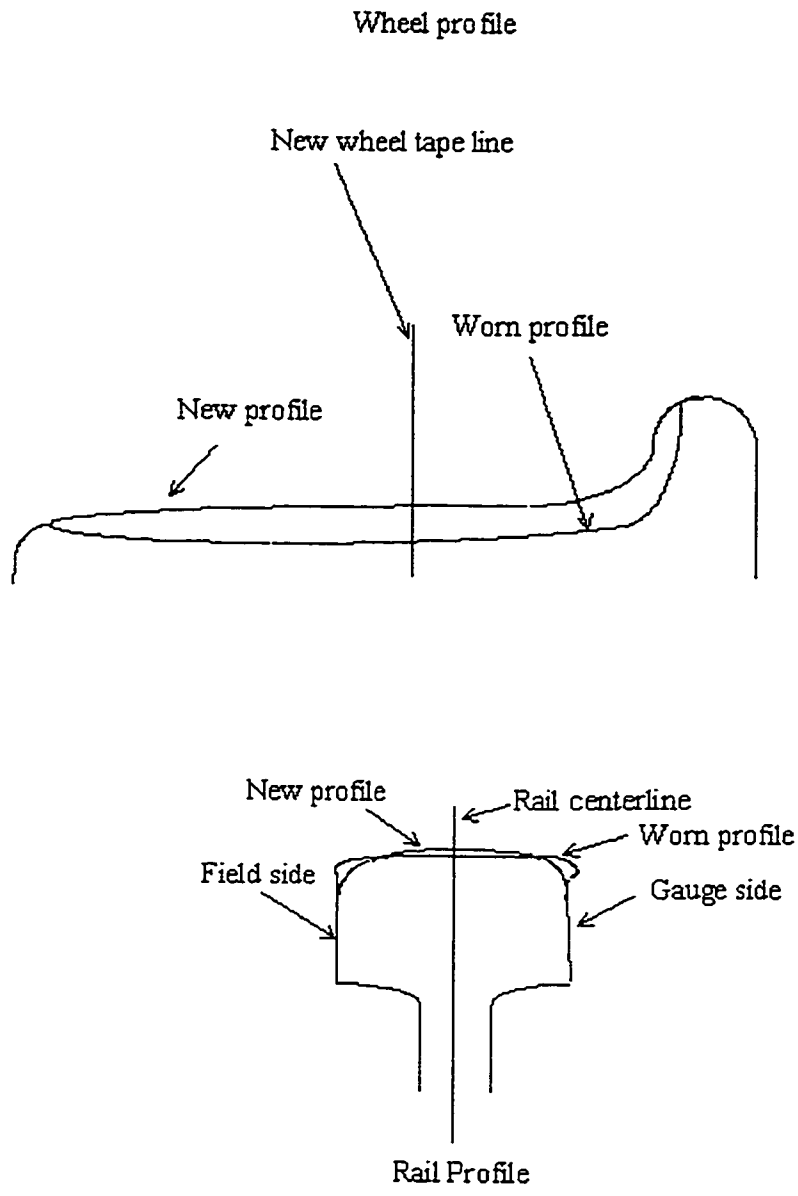

Wheel and Rail Profiles

Figure 2.2

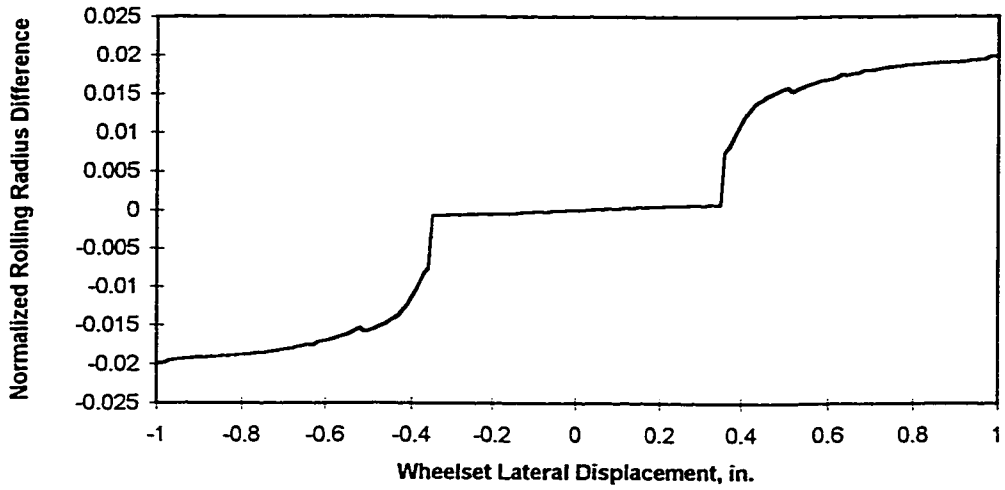

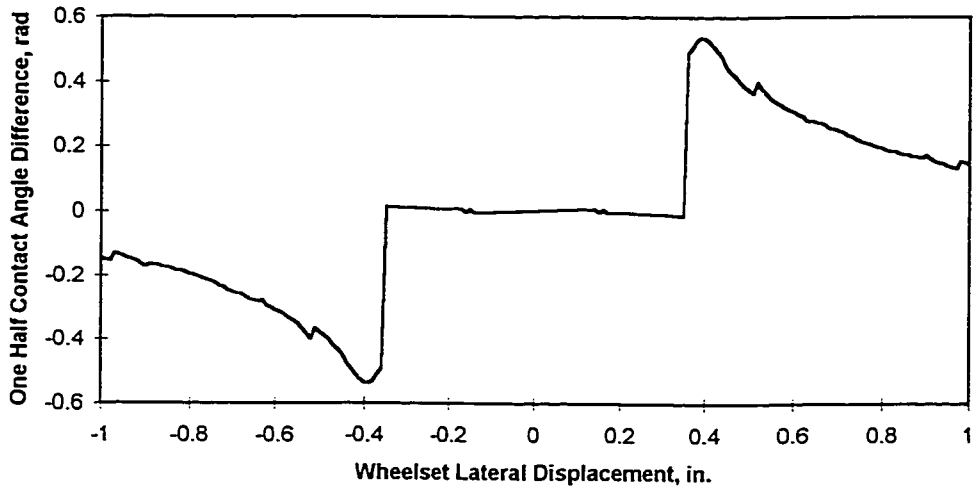

Geometric constraint functions generated from WHRAILA for AAR 1:20 wheel/rail profile

Figure 2.3

2.3 Wheel-rail Contact Forces

Wheel-rail forces are generated in the contact patches between the wheels and the rails. Each wheel and rail are pressed against each other by the normal loads and due to the material elasticity, deform to create a contact area. A contact plane is defined from the orientation of the track and the magnitude of the contact angle. Creep forces are tangential to the contact plane and normal forces are perpendicular to it. Creep forces are generated by the partial slip called creepage between the rolling wheel and the rail. The creepage can be defined as a state between pure rolling and overall sliding. Creep forces can be computed according to the linear theory of creep formulated by Kalker [47].

Forces and moments in the plane of the contact patch at each wheel are a function of the creepages ξ_i and creep coefficients f_{ij} as given by the following equation:

$$\begin{bmatrix} F_x \\ F_y \\ M_z \end{bmatrix} = \begin{bmatrix} -f_{11} & 0 & 0 \\ 0 & -f_{22} & -f_{23} \\ 0 & f_{23} & -f_{33} \end{bmatrix} \begin{bmatrix} \xi_x \\ \xi_y \\ \xi_s \end{bmatrix} \tag{2.4}$$

The creepages are calculated with respect to the contact plane axes shown in Figure 2.1. The relationship between the contact axes and the equilibrium axes are derived in Appendix A. The generalized expressions for creepages are derived in Appendix B based on the velocity of wheelset centre of mass as shown in Figure 2.4 . The longitudinal creepage for the left wheel is derived as

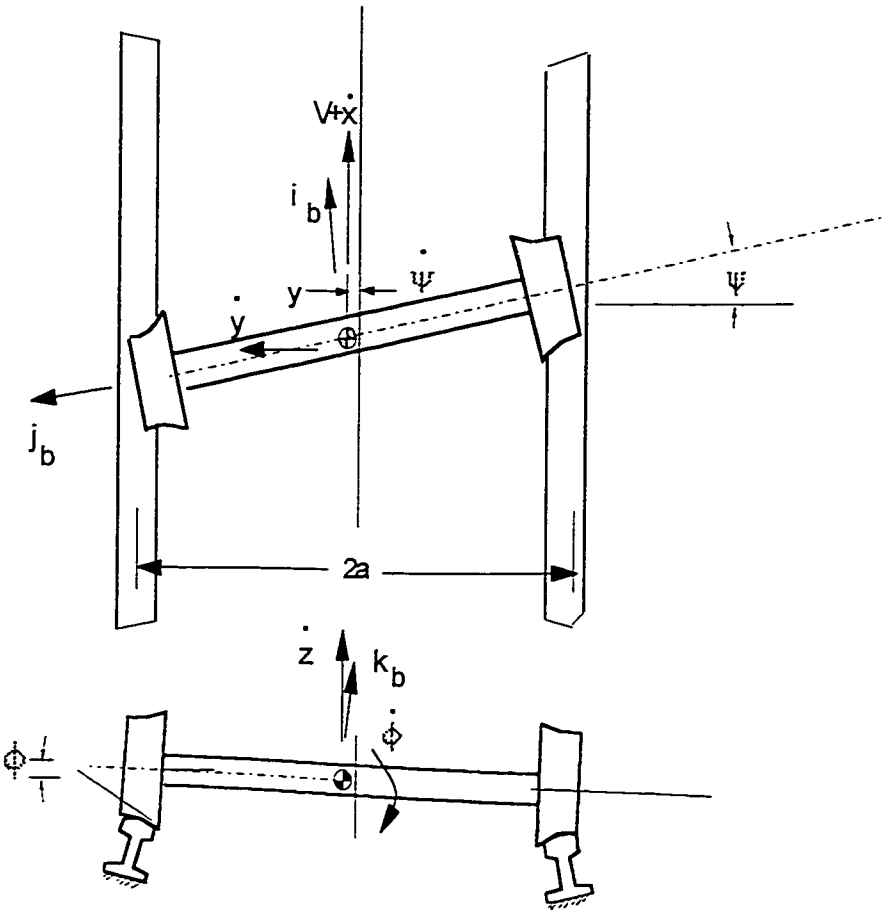

Wheelset Axis System

Figure 2.4

$$\xi_{xl} = \frac{V - a(\frac{V}{R} + \dot{\psi}_w) - (\omega + \dot{\beta})r_l}{V} \tag{2.5}$$

The lateral creepage is given by

$$\xi_{yl} = \frac{(\dot{y}_w - V\psi_w + r_l\dot{\phi})}{V\cos\partial_l} \tag{2.6}$$

and the spin creepage is

$$\xi_{sl} = \frac{(\frac{V}{R} + \dot{\psi}_w)\cos\partial_l - (\omega + \dot{\beta})\sin\partial_l}{V} \tag{2.7}$$

The corresponding creepage values for the right wheel are given by

$$\xi_{xr} = \frac{V + a(\frac{V}{R} + \dot{\psi}_w) - (\omega + \dot{\beta})r_r}{V} \tag{2.8}$$

$$\xi_{yr} = \frac{(\dot{y}_w - V\psi_w + r_r\dot{\phi})}{V\cos\partial_r} \tag{2.9}$$

$$\xi_{sr} = \frac{(\frac{V}{R} + \dot{\psi}_w)\cos\partial_r + (\omega + \dot{\beta})\sin\partial_r}{V} \tag{2.10}$$

Creep forces are non-linear functions of the creepages, normal wheel loads and wheel-rail geometry, mainly due to dry friction saturation limit equal to μN where μ is the coefficient of friction and N is the normal wheel load. The creep force variation as a function of creepage, for a given wheel load and contact geometry, is shown in Figure 2.5.

The slope at the origin is the creep coefficient.

2.3.1 Creep Forces for Linear Stability Model

For stability analysis, linearized creepage expressions are obtained by using equations (2.1), (2.2) and (2.3) in the generalized expressions above.

Left wheel:

$$\xi_{xl} = -\left(\frac{\lambda}{r_o} y_w + \frac{a\dot{\psi}_w}{V}\right) \tag{2.11}$$

$$\xi_{yl} = \frac{\dot{y}_w}{V} - \psi_w + \frac{\Gamma r_o \dot{y}_w}{Va} \tag{2.12}$$

$$\xi_{sl} = \frac{\dot{\psi}_w}{V} - \frac{\delta_l}{r_o} \tag{2.13}$$

Right wheel:

$$\xi_{xr} = \left(\frac{\lambda}{r_o} y_w + \frac{a\dot{\psi}_w}{V}\right) \tag{2.14}$$

$$\xi_{yr} = \frac{\dot{y}_w}{V} - \psi_w + \frac{\Gamma r_o \dot{y}_w}{Va} \tag{2.15}$$

$$\xi_{sr} = \frac{\dot{\psi}_w}{V} + \frac{\delta_r}{r_o} \tag{2.16}$$

The above expressions are used in equation (2.4) to calculate the creep forces for the linear stability model.

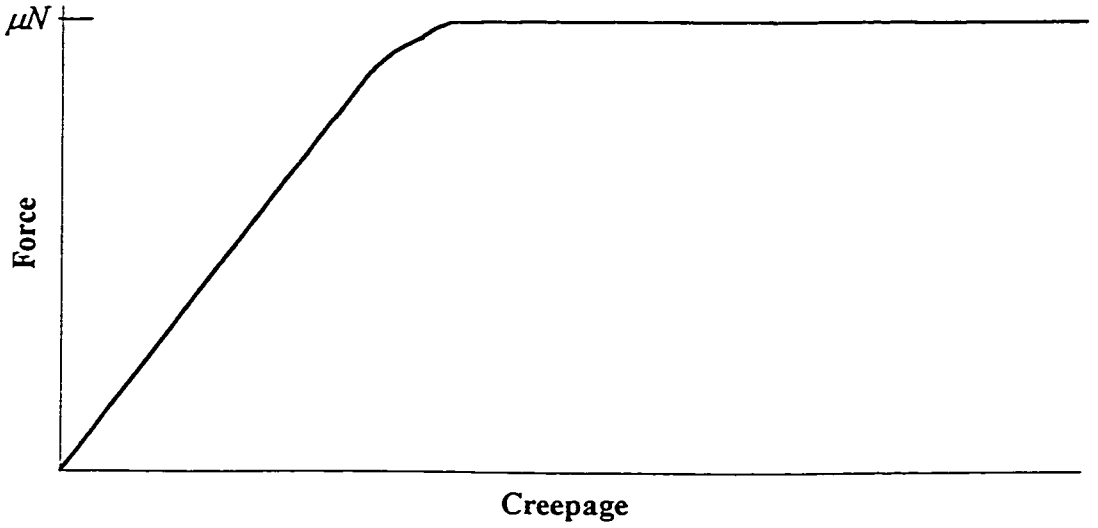

Non-Linear Creep Force Law

Figure 2.5

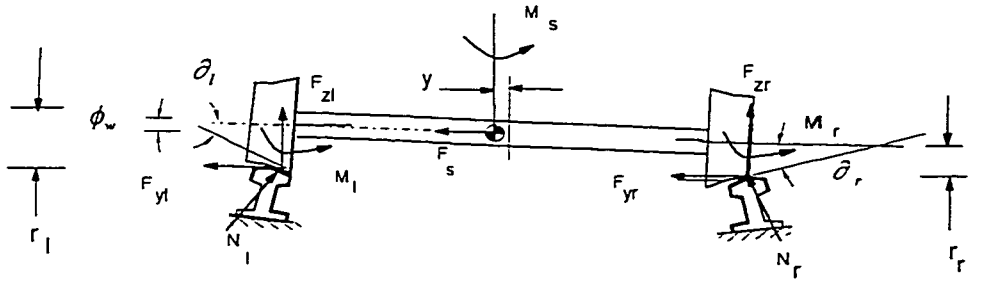

Free body diagram of wheelset

Figure 2.6

2.3.2 Creep Forces for Linear Curving Model

In curving wheel loads redistribute under the influence of cant deficiency as shown in Figure B-2. The expressions for vertical wheel forces at the left and right wheels with the load shift are derived in Section B.2.1 of Appendix B. The expression for the wheel load on the left wheel is

$$N_l = N_w(1+\frac{h_{cg}}{a}\phi_d) \tag{2.17}$$

$$N_r = N_w(1-\frac{h_{cg}}{a}\phi_d) \tag{2.18}$$

The offset of equilibrium positions between components and the redistribution of static loads lead to unequal vertical loads on the wheels. As wheel loads shift and redistribute in curving under the influence of curving forces, the creep coefficients are modified to calculate actual forces. Given the nominal wheel load N_w, the creep coefficients can be updated as a function of the actual wheel loads N_l and N_r, for the left and right wheels respectively as given by the following equations:

$$(f_{11})_{l/r} = f_{11}\left(\frac{N_{l/r}}{N_w}\right)^{2/3} \tag{2.19}$$

$$(f_{22})_{l/r} = f_{22}\left(\frac{N_{l/r}}{N_w}\right)^{2/3} \tag{2.20}$$

$$(f_{23})_{l/r} = f_{23}\left(\frac{N_{//r}}{N_w}\right) \tag{2.21}$$

$$(f_{33})_{l/r} = f_{33}\left(\frac{N_{//r}}{N_w}\right)^{4/3} \tag{2.22}$$

The creepage expressions for the linear curving model are derived in Appendix B.2.2. The equations for the left wheel are:

$$\xi_{xl} = -\frac{\lambda}{r_o}\left(y_w - \frac{r_o a}{\lambda R}\right)\left(1 - \frac{2h\phi_d}{3}\right) \tag{2.23}$$

$$\xi_{yl} = -\left(\psi_w + \frac{b^*}{R}\right) \tag{2.24}$$

$$\xi_{sl} = \frac{-\left(\frac{V}{R} + \frac{V}{r_o}\delta_l\right)}{V} \tag{2.25}$$

$$\xi_{xr} = \frac{\lambda}{r_o}\left(y_w - \frac{r_o a}{\lambda R}\right)\left(1 + \frac{2h\phi_d}{3}\right) \tag{2.26}$$

$$\xi_{yr} = -\left(\psi_w + \frac{b^*}{R}\right) \tag{2.27}$$

$$\xi_{sr} = \frac{-\left(\frac{V}{R} - \frac{V}{r_o}\delta_r\right)}{V} \tag{2.28}$$

The above creepage expressions are used in equation (2.4) to calculate creep forces for the linear curving model. In equations (2.24) and (2.27), b^* is $+b$ for the leading wheelset and $-b$ for the trailing wheelset in a truck. Linear creep forces that are calculated using equation (2.4) are then saturated according to the Vermuelen/Johnson saturation curve such that creep forces do not exceed the wheel/rail adhesion limit. This method is explained in Appendix D.

2.3.3 Creep Forces for Steady State Non-Linear Curving Model

For small creepages, the relationship is linear and the equation (2.4) can be applied to calculate creep forces. For large creepages, which are common in curving, the creep force laws are non-linear and non-linear wheel/rail geometry and non-linear creep force models have to be incorporated.

The creepage expressions (2.5) to (2.10) can be simplified by ignoring the velocity terms:

Longitudinal:

$$\xi_{lx} = \frac{r_l}{r_o} + \frac{r_l \beta}{V} - 1 - \frac{a}{R} \tag{2.29}$$

$$\xi_{rx} = \frac{r_r}{r_o} + \frac{r_r \beta}{V} - 1 + \frac{a}{R} \tag{2.30}$$

Lateral:

$$\xi_{ly} = \frac{\psi}{\cos\delta_l} \tag{2.31}$$

$$\xi_{ry} = \frac{\psi}{\cos\delta_r} \tag{2.32}$$

Spin:

$$\xi_{ls} = \frac{\sin\delta_l}{r_o} + \beta\frac{\sin\delta_l}{V} + \frac{\cos\delta_l}{R} \tag{2.33}$$

$$\xi_{rs} = \frac{\sin\delta_r}{r_o} + \beta\frac{\sin\delta_r}{V} + \frac{\cos\delta_r}{R} \tag{2.34}$$

The method explained in Section 2.2.2 is used to incorporate the effects of non-linear wheel-rail geometry in the calculation of the creepage terms above. For calculating non-linear creep forces, following three methods are normally used:

- Cubic saturation model proposed by Vermuelen and Johnson
- Simplified theory developed by Kalker and incorporated in his program FASTSIM
- Exact three-dimensional theory developed by Kalker and incorporated in the computer program DUVOROL [47]

The cubic saturation model which is explained in Appendix D is used in the non-linear steady state curving model developed in this thesis. This model is relatively simple and entails inexpensive numerical computation. But the calculation of creep forces may

be an approximation as compared to the latter two models.

Creep forces obtained with respect to the contact axes as shown in Figure 2.1, are then converted to the equilibrium axes by the following set of equations:

For the left wheel

$$F_{xl} = F'_{xl} \tag{2.35}$$

$$F_{yl} = F'_{yl}\cos(\partial_l + \phi_w) \tag{2.36}$$

$$F_{zl} = F'_{yl}\sin(\partial_l + \phi_w) \tag{2.37}$$

and for the right wheel

$$F_{xr} = F'_{xr} \tag{2.38}$$

$$F_{yr} = F'_{yr}\cos(\partial_r - \phi_w) \tag{2.39}$$

$$F_{zr} = F'_{yr}\sin(\partial_r - \phi_w) \tag{2.40}$$

2.4 Gravitational Stiffness Forces

At the wheel/rail interface, in addition to the creep forces, normal forces exist in a direction perpendicular to the contact plane. The term Gravitational Stiffness refers to the effective lateral force and yaw moment that exist between the wheelset and track, caused by the lateral components of these normal forces. For heavy axle loads, these forces have considerable effect on the dynamic behaviour of a railway vehicle. When a wheelset is centered on a uniform track, normal forces on the left and right wheels are equal in magnitude. The sum of vertical components of the normal forces are equal to the axle

load and lateral components have a zero resultant force. When the wheelset is displaced laterally by a small amount, the lateral component on the left wheel is,

$$N_{yl} = -N_l \sin(\partial_l + \phi_w) \tag{2.41}$$

and on the right wheel is,

$$N_{yr} = N_r \sin(\partial_r - \phi_w) \tag{2.42}$$

The net gravitational stiffness force is then,

$$\begin{aligned} N_y &= N_{yl} + N_{yr} \\ &= -N_l(\partial_l + \phi_w) + N_r(\partial_r - \phi_w) \end{aligned} \tag{2.43}$$

The yaw gravitational stiffness moment is written as

$$\begin{aligned} N_\psi &= (N_{yr} - N_{yl})a\psi_w \\ &= \left(N_l(\partial_l + \phi_w) + N_r(\partial_r - \phi_w)\right)a\psi_w \end{aligned} \tag{2.44}$$

The contact angles enter the equations of motion through the lateral components of normal wheel loads between the wheel and rail. For small contact angles, this force is approximately equal to the axle load multiplied by half the difference in contact angle plus the wheelset roll angle. This gravitational stiffness force acts in a direction to move the wheelset towards the centered position. If the gravitational stiffness is large, due to a large change in contact angle difference with lateral displacement, significant lateral restoring force is produced. Thus, gravitational stiffness gives a stabilizing effect to the vehicle motion. For new wheels with straight taper, the contact angle difference is zero until flange contact occurs.

2.4.1 Gravitational Stiffness for Linear Stability Model

The expression for lateral gravitational stiffness force (2.43) can be simplified using the equation (C-49) in Appendix C and the linearized equation is:

$$N_y = \frac{I_{wy} V \delta_o}{a r_o} \dot{\psi}_w - \frac{W_A(\Gamma + \Delta)}{a} y_w \tag{2.45}$$

The following simplified equation is obtained from the expression for the yaw gravitational stiffness moment in (2.44):

$$N_\psi = W_A a \delta_o \psi_w \tag{2.46}$$

2.4.2 Gravitational Stiffness for Linear Curving Model

Equation (2.46) can be written after linearizing as:

$$N_y = -(N_l - N_r)\delta_o - (N_l + N_r)\frac{(\Delta + \Gamma)}{a} y_w \tag{2.47}$$

Using equations (B-35) and (B-36) in the above expression, we get,

$$N_y = -W_A \frac{h_{cg}}{a} \phi_d \delta_o - \frac{W_A(\Gamma + \Delta) y_w}{a} \tag{2.48}$$

The yaw gravitational stiffness moment for the curved track is

$$N_\psi = a(-N_{yl} + N_{yr})\left(\psi_w + \frac{b^*}{R}\right)$$

$$= W_A a \delta_o \left(\psi_w + \frac{b^*}{R} \right) \tag{2.49}$$

In the above equation, b^* is $+b$ for the leading wheelset and $-b$ for the trailing wheelset in a truck.

2.5 Conventional Vehicle Model

2.5.1 Wheelset Force Balance

Figure 2.6 shows the free body diagram of a single wheelset. In the figure, δ_l and δ_r are the contact angles at the left and right wheels and ϕ_w is the roll angle of the wheelset. The equations for wheelset lateral and yaw force balance can be written from the free body diagram. The external forces and moments acting on the wheelset are:

F_s, M_s : Primary suspension force and moment

$F_{yr}, F_{xr}, M_{zr}, F_{yl}, F_{xl}, M_{zl}$: Creep forces and moment

N_r, N_l : Normal wheel-rail forces

Equilibrium equations are:

Lateral:
$$F_{yr} + F_{yl} + N_r \sin(\delta_r - \phi) - N_l \sin(\delta_l + \phi) + F_s = 0 \tag{2.50}$$

Yaw:

$$a(F_{xr} - F_{xl}) + a(F_{yr} - F_{yl})\psi + (N_r \sin(\delta_r - \phi) + N_l \sin(\delta_l + \phi))a\psi + M_{zl} + M_{zr} + M_{susp} = 0 \tag{2.51}$$

The equations of motion for a wheelset including inertia forces are derived in Appendix C.1.

2.5.2 Linear Stability Model

The equations for force balance in the truck and car body are derived in Sections C.2 and C.3 of Appendix C. In most conventional truck designs for passenger rail vehicles, an H-shaped frame is used and the wheelsets are directly connected to the frame through primary suspension elements. Figure 2.7 shows the suspension arrangement of a conventional truck. The primary suspension consists of a chevron shaped rubber element. The primary suspension allows the wheel-axle sets to move in relation to the truck frame and helps to isolate the truck frame from vibrations induced by rail irregularities.

The carbody is supported by the truck frame through a bolster and the softer secondary suspension elements. The purpose of the secondary suspension is to further isolate vibrations and to ensure a comfortable ride for the passengers. The bolster is connected to the car body by a large bearing. In reality, stiffness and damping properties of these suspension elements are non-linear. These non-linearities, coupled with the non-linear nature of wheel/rail force environment, make the prediction of rail vehicle performance difficult. In this thesis, each suspension element is modelled by a linear spring and damper element. Figure 2.8 is a schematic diagram of the carbody suspension model. Suspension force between any two rigid bodies is calculated by considering the relative displacement (velocity) between the bodies and the stiffness (damping coefficient) at the suspension connection. In Section C.4 of Appendix C, expressions for suspension forces on the wheelsets, trucks and carbody are given.

The linear equations of motions are derived for the stability analysis of the railway

vehicle by using terms derived for creep forces and moments, gravitational forces and moments, and suspension forces into the set of force balance equations obtained for each rigid body, i.e. wheelsets, trucks and carbody. These equations are listed for a single car model consisting of the following 17 degrees of freedom in Appendix C-5.

Lateral and yaw degrees of freedom for four wheelsets	..	8
Lateral, roll and yaw degrees of freedom for two trucks	..	6
Lateral, roll and yaw degrees of freedom for the car body	..	3

2.5.3 Linear Curving Model

The equations of static equilibrium for the linear curving model are obtained by including terms due to curvature and cant deficiency in the expressions for creep forces and normal forces derived in Sections 2.3.2 and 2.4.2 respectively . For the steady state curving model, velocity and acceleration terms are omitted from the force balance equations given in Sections C.1 to C.3 of Appendix C. The model used in the analysis has 8 degrees of freedom: lateral and yaw of two wheelsets, lateral and yaw of a truck and lateral and roll of car body. The complete set of equations of equilibrium for the linear curving model are listed in Section C.6 of Appendix C.

2.6 Summary

In this chapter, aspects of modelling a conventional truck has been discussed. The creepage expressions are derived in Appendix B. The suspension forces and the equations of motion are derived in Appendix C. In the next chapter, modified truck design models

will be developed. The stability behaviour of *C Truck*, *R Truck*, *US Truck* and *UW Truck* will be compared.

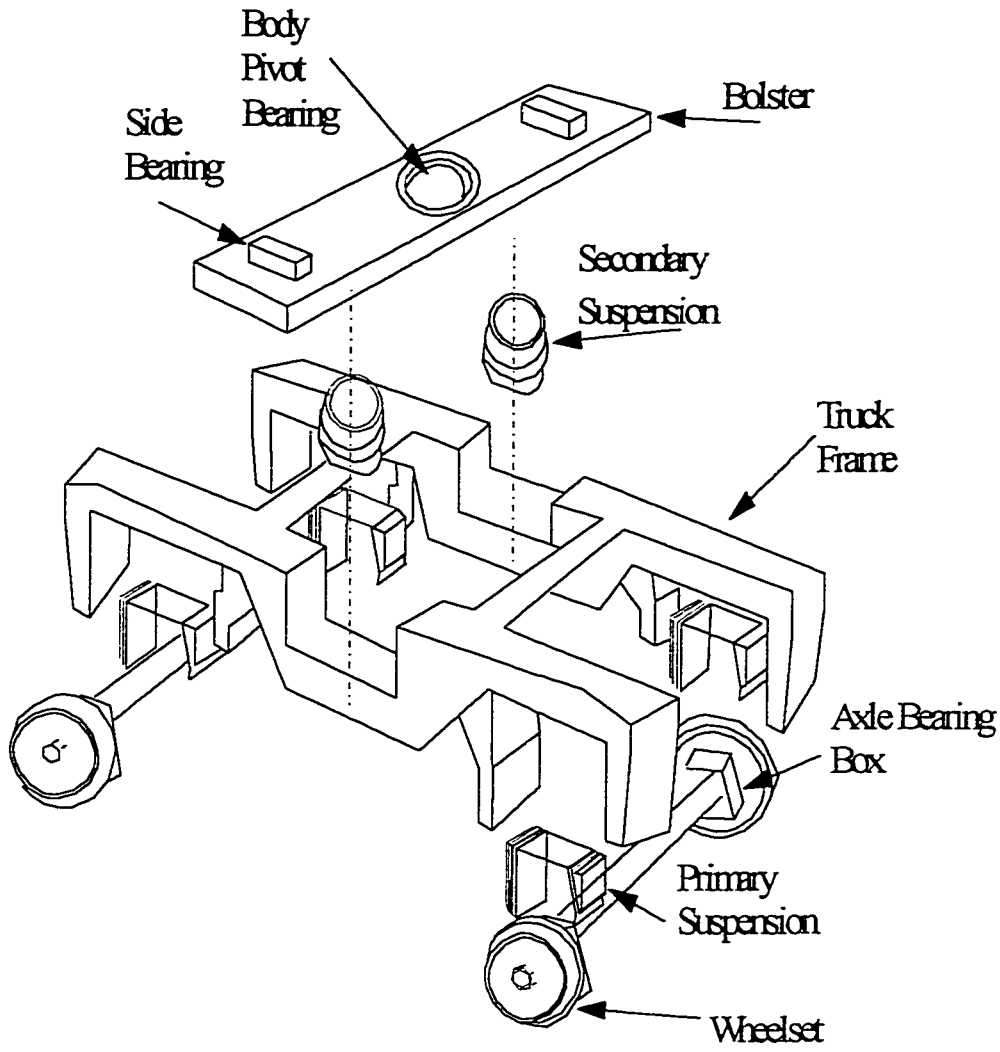

Suspension Arrangement of Conventional Truck

Figure 2.7

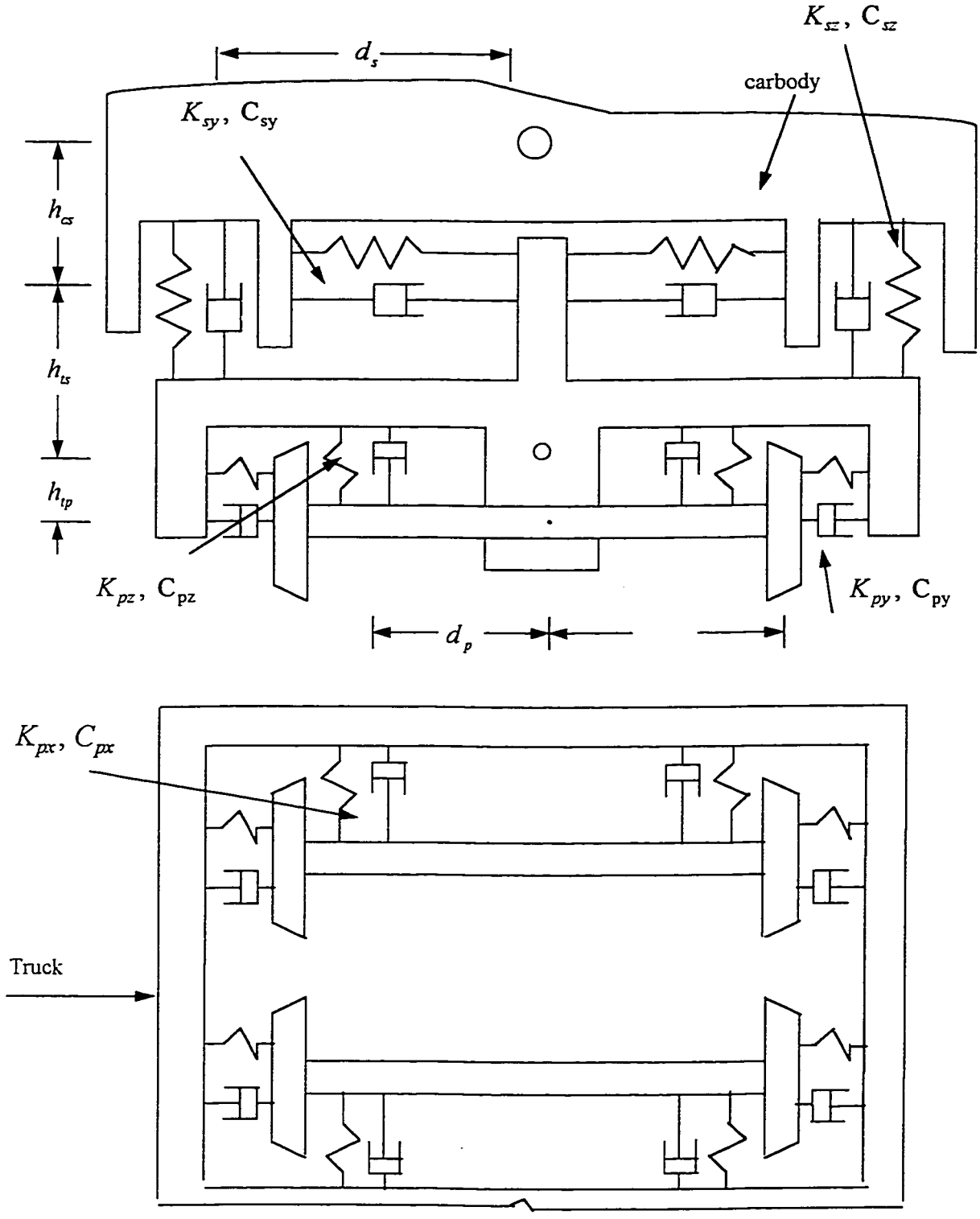

Carbody Suspension Model
Figure 2.8

Chapter 3

LATERAL STABILITY MODELS FOR MODIFIED TRUCK DESIGNS

3.1 Introduction

The modelling aspects of a conventional railway vehicle were considered in the previous chapter. The lateral stability model with a full carbody and two trucks interconnected with suspension elements is derived in Appendix C. The understanding of the lateral stability behaviour of such a complex system is made easier using a building block approach. In this chapter, lateral stability is evaluated using a simplified truck model with two wheelsets interconnected through suspension elements. Linear equations of motion are developed for the following alternative truck configurations: Radial Truck *(R Truck)*, Unsymmetric Suspension Truck *(US Truck)*, Unsymmetric Wheelset Truck (*UW Truck*), Conventional Truck with Primary Yaw Damper (*CD Truck*) and Unsymmetric Suspension Truck with Primary Yaw Damper (*USD Truck*). The stability behaviour of R truck, US truck and UW truck is evaluated and compared with the C truck. The results are presented as contours of constant linear critical speed on a generalized bending stiffness - shear stiffness plane.

3.2 Radial Truck

A conventional passenger truck is provided with primary suspension usually in the form of rubber chevrons between the wheelsets and the truck frame. A radial truck has an additional component, direct connection between the wheelsets which can take the form of

a steering arm mechanism or a cross bracing. This has the effect of increasing the inter axle shear stiffness.

The dynamics of a flexible truck are strongly affected by inter wheelset forces either through the truck frame as in the case of a conventional truck or through the inter connection elements as in the case of a radial truck. Any form of elastic inter wheelset structure can be represented by the generalized bending stiffness K_b and generalized shear stiffness K_s [6]. As shown in Figure 3.1, the inter-wheelset truck stiffnesses are defined by:

Shear Stiffness

$$K_s = \frac{\text{lateral force on leading wheelset due to lateral displacement of trailing wheelset}}{\text{lateral displacement of trailing wheelset}}$$

Bending Stiffness

$$K_b = \frac{\text{yaw moment on leading wheelset due to yaw displacement of trailing wheelset}}{\text{yaw displacement of trailing wheelset}}$$

Neglecting the dynamic effects due to truck frame inertia and primary suspension damping, the conventional stiffness K_{px} & K_{py} and the inter axle bending and shear stiffness k_b & k_s can be transformed into generalized stiffness.

The equations are [6]:

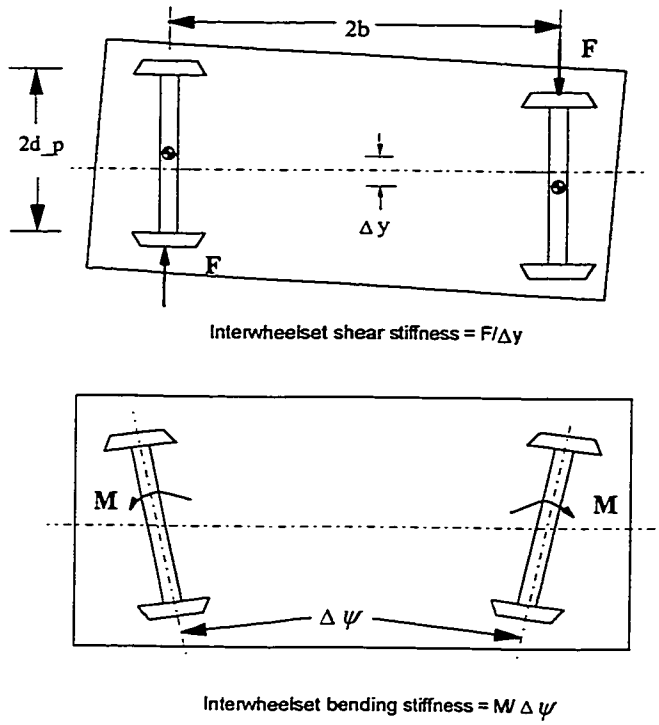

Inter-Wheelset Stiffnesses

Figure 3.1

$$K_b = K_{px} d_p^2 + k_b \tag{3.1}$$

$$K_s = \frac{K_{py} K_{px} d_p^2}{b^2 K_{py} + d_p^2 K_{px}} + k_s \tag{3.2}$$

A schematic diagram of a radial truck with generalized stiffnesses is shown in Figure 3.2. For a conventional truck with elastic connections at the primary suspension, $k_b = 0$ and $k_s = 0$. From equations (3.1) and (3.2), it can be shown for a conventional truck that

$$K_s \leq \frac{K_b}{b^2} \tag{3.3}$$

In this thesis, contours of vehicle performance indices are presented on plots of generalized shear stiffness K_s and generalized bending stiffness K_b. Thus the conventional truck is limited to values of shear stiffness that satisfy the constraint (3.3) as shown in Figure 3.3. Point 1 in the figure represents a typical conventional truck with a bending stiffness of $5x10^6$ Nm/rad, the optimum value for a prototype passenger railway vehicle reported in reference [7]. The corresponding value of the linear stiffness is $K_{px} = 1.5x10^7$ N/m. This truck was designed with the wheelset conicity of 0.15 for a critical speed of 78 m/s and would negotiate a 1 degree curve without flanging. To achieve a similar performance, a radial truck would be designed with a bending stiffness of $2.5x10^6$ Nm/rad as given by point 2. For the radial truck, K_s can be greater than

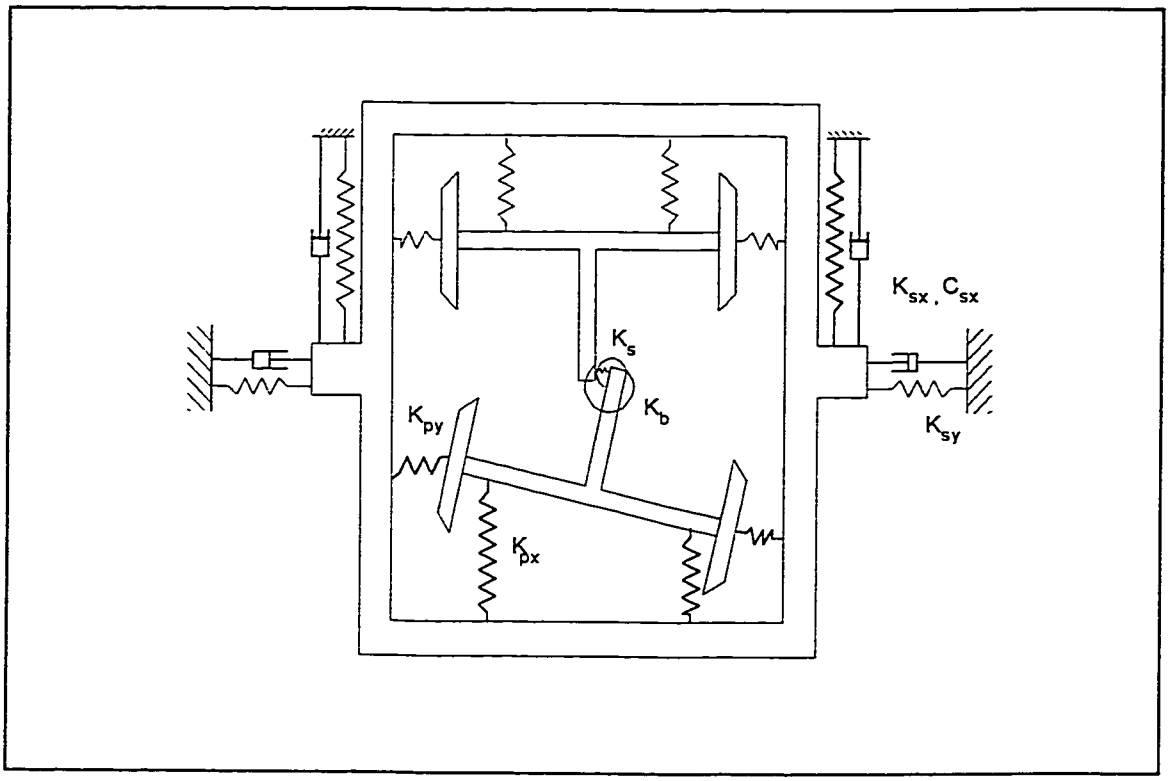

Schematic of a radial truck

Figure 3.2

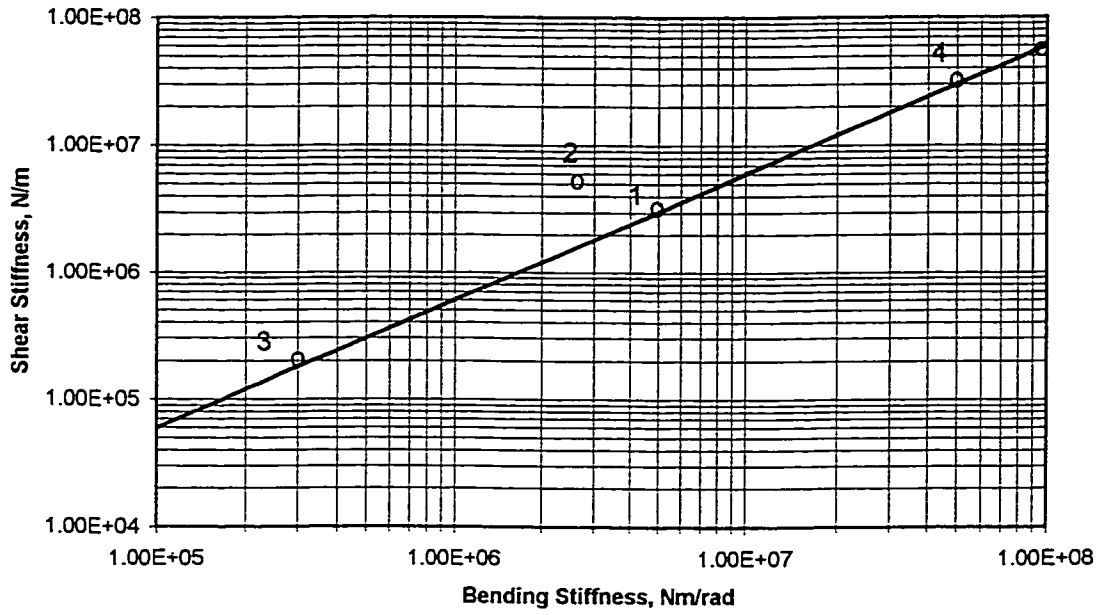

Stiffness values that characterize different truck designs

Figure 3.3

$\frac{K_b}{b^2}$ due to the effect of inter axle stiffnesses k_b and k_s. Point 3 in the figure represents soft values of total shear and bending stiffnesses which allow the wheelsets in the truck to behave almost like unrestrained free wheelsets and point 4 represents a rigid truck with stiff values of K_b and K_s [22].

3.3 Unsymmetric Suspension Truck

A modified design considered for performance evaluation is a truck with an asymmetry in the primary suspension. Wickens has reported that a particular configuration of two-axle articulated vehicle with elastic restraint can have static and dynamic stability and perfect steering on curves [48, 49]. A longitudinal asymmetry is introduced in the truck according to the direction of motion, by making the primary stiffness in the leading axle of a conventional truck different from the trailing axle. This truck is referred as an Unsymmetric Suspension truck (*US truck*).

The US truck makes use of different primary stiffness between leading and trailing wheelsets, thus introducing a longitudinal asymmetry. The unsymmetric parameter a_s as defined in Figure 3.4 is given by [50]

$$a_s = -b\frac{K_{x1} - K_{x2}}{K_{x1} + K_{x2}} \tag{3.4}$$

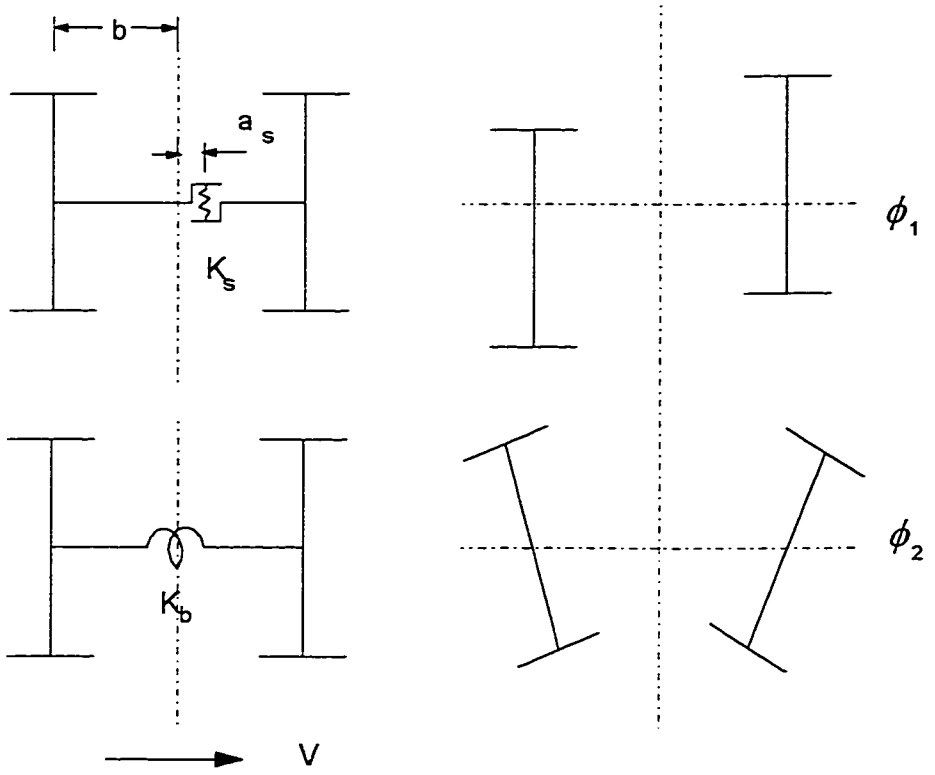

Definition of US Index and generalized coordinates for

US Truck

Figure 3.4

where K_{x1} and K_{x2} are the primary longitudinal suspension stiffnesses for leading and trailing axle of an unsymmetric truck. Referring to Figure 2.4, the chevron shaped rubber elements are typically designed to provide a symmetric longitudinal and lateral primary stiffnesses, K_{px} and K_{py}, in the case of a conventional truck. For the US truck, the stiffness properties of the chevron elements only in the longitudinal direction have to be modified so that the leading wheelset has a softer primary suspension of K_{x1} and the trailing wheelset has a primary stiffness K_{x2} which is greater than K_{x1}.

The equivalent bending stiffness is obtained in the case of US truck, referring to figure 3.5 and figure 3.1, from the following equation:

$$\frac{M}{K_b} = \frac{M}{2K_{x1}d_p^2} + \frac{M}{2K_{x2}d_p^2}$$

$$K_b = \frac{2K_{x1}K_{x2}d_p^2}{K_{x1}+K_{x2}} \qquad (3.5(a))$$

The equivalent shear stiffness can be expressed as (refer to figure 3.6)

$$K_s = \frac{K_{py}(K_{x1}+K_{x2})d_p^2}{2b^2K_{py}+(K_{x1}+K_{x2})d_p^2} \qquad (3.5(b))$$

Equation (3.4) can be rearranged to express the longitudinal stiffness of the leading axle in terms of the longitudinal stiffness of the trailing axle as

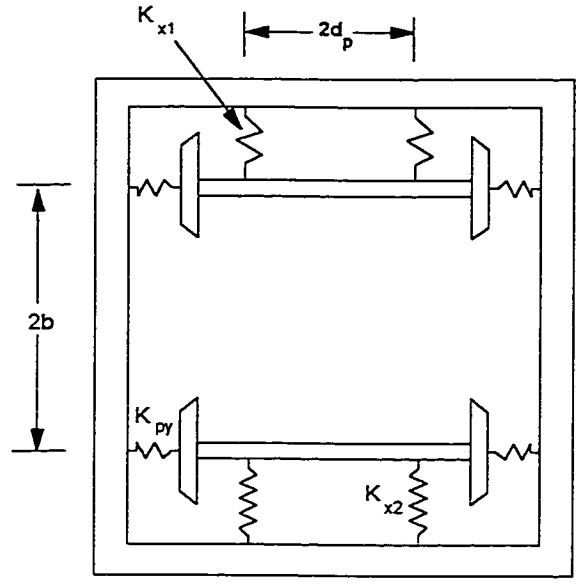

Schematic of Unsymmetric Suspension Truck

Figure 3.5

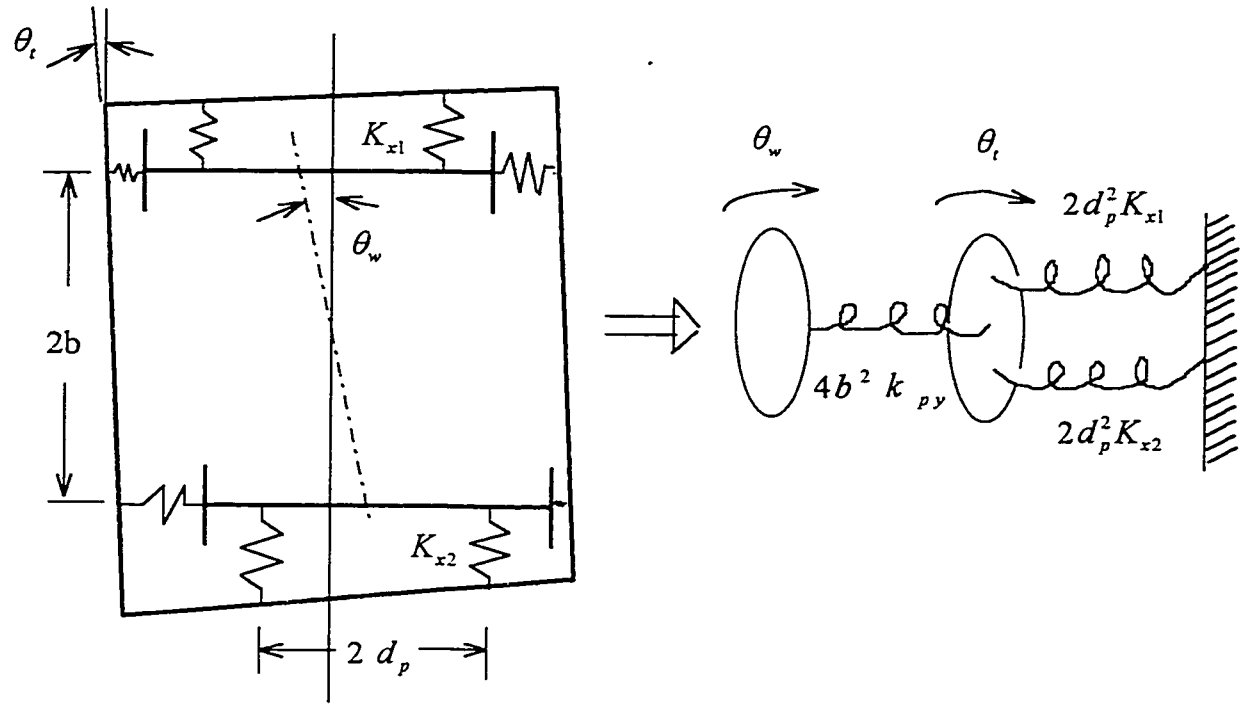

Equivalent Shear Stiffness for US Truck

Figure 3.6

$$K_{x1} = K_{x2}\left(\frac{b-a_{ps}}{b+a_{ps}}\right) \tag{3.6}$$

Using the above equation in equation (3.5(a)), we can eliminate K_{x2} to get,

$$K_{x1} = \frac{bK_b}{d_p^2(b+a_s)} \tag{3.7a}$$

Similarly, we can write

$$K_{x2} = \frac{bK_b}{d_p^2(b-a_s)} \tag{3.7b}$$

and

$$K_{x1}+K_{x2} = \frac{2b^2K_b}{d_p^2(b^2-a_s^2)} \tag{3.8}$$

From equation (3.5(b)), we can write,

$$K_{py} = \frac{K_s(K_{x1}+K_{x2})d_p^2}{(K_{x1}+K_{x2})d_p^2-2b^2K_s} \tag{3.9}$$

Using (3.8) in the above equation, we get,

$$K_{py} = \frac{2b^2K_sK_b}{2b^2(K_b-K_s(b^2-a_s^2))} \tag{3.10}$$

For $K_{py} \geq 0$, $K_b \geq K_s(b^2-a_s^2)$ from the above equation. Rearranging this, we get,

$$K_s \leq \frac{K_b}{(b^2 - a_s^2)} \qquad (b > a_s) \tag{3.11}$$

Equation (3.11) gives the value of maximum possible shear stiffness realizable by the US truck and is similar to the criteria (3.3) for the conventional truck.

The generalized coordinates in Figure 3.4 are the interaxle lateral displacement (shear) and interaxle yaw (bending). The stiffness matrix for the inter-wheelset structure of the US truck can be expressed as [50]

$$K_{us} = \begin{bmatrix} a_s^2 K_s + K_b & a_s K_s \\ a_s K_s & K_s \end{bmatrix} \tag{3.12}$$

The stiffness matrix for the conventional coordinates, in terms of lateral and yaw degrees of freedom of the two wheelsets $(y_1, \psi_1, y_2, \psi_2)$ can be obtained from the following transformation [51].

$$K = P^T K_{us} P \tag{3.13}$$

where

$$P = \begin{bmatrix} 0 & 1 & 0 & -1 \\ 1 & -b & -1 & -b \end{bmatrix} \tag{3.14}$$

$$K = \begin{bmatrix} K_s & a_s K_s - bK_s & -K_s & -(a_s K_s + bK_s) \\ a_s K_s - bK_s & a_s^2 K_s + K_b - 2ba_s K_s + b^2 K_s & -a_s K_s + bK_s & -a_s^2 K_s + b^2 K_s - K_b \\ -K_s & -a_s K_s + bK_s & K_s & a_s K_s + bK_s \\ -(a_s K_s + bK_s) & -a_s^2 K_s + b^2 K_s - K_b & a_s K_s + bK_s & a_s^2 K_s + K_b + 2ba_s K_s + b^2 K_s \end{bmatrix} \tag{3.15}$$

The equations of motion for a four degree of freedom "frameless" model with unsymmetric suspension is given below. In this model, the truck frame mass is decoupled from the wheelset pair and the total shear and bending stiffness is provided entirely through direct inter wheelset connections.

The equations of motion for the US truck are:

Leading wheelset lateral

$$m_w\ddot{y}_1 + \left(K_s + \frac{W(\Gamma+\Delta)}{a} - \frac{2f_{23}\Delta}{r_o a}\right)y_1 + \left(a_s K_s - bK_s - 2f_{22}\right)\psi_1 - K_s y_2 - \left(a_s K_s + bK_s\right)\psi_2 + \left(\frac{2f_{22}}{V} + \frac{2f_{22}r_o\Gamma}{Va}\right)\dot{y}_1 + \left(\frac{2f_{23}}{V} - \frac{I_{wy}V\partial_o}{ar_o}\right)\dot{\psi}_1 = 0 \tag{3.16}$$

Leading wheelset yaw

$$I_{wz}\ddot{\psi}_1 + \left(\frac{I_{wy}V\Gamma}{ar_o} - \frac{2f_{23}}{V} - \frac{2f_{23}r_o\Gamma}{Va}\right)\dot{y}_1 + \left(a_s K_s - bK_s + \frac{2f_{33}a\lambda}{r_o} - \frac{2f_{33}\Delta}{ar_o}\right)y_1 + \left(\frac{2f_{11}a^2}{V} + \frac{2f_{33}}{V}\right)\dot{\psi}_1 + \left(K_b + 2f_{23} + b^2K_s + a^2K_s - 2ba_sK_s - Wa\partial_o\right)\psi_1 + \left(bK_s - a_sK_s\right)y_2 + \left(b^2K_s - K_b - a_s^2K_s\right)\psi_2 = 0 \tag{3.17}$$

Trailing wheelset lateral

$$m_w\ddot{y}_2 + \left(K_s + \frac{W(\Gamma+\Delta)}{a} - \frac{2f_{23}\Delta}{r_o a}\right)y_2 + \left(a_s K_s - bK_s - 2f_{22}\right)\psi_2 - K_s y_1 - \left(a_s K_s - bK_s\right)\psi_1 + \left(\frac{2f_{22}}{V} + \frac{2f_{22}r_o\Gamma}{Va}\right)\dot{y}_2 + \left(\frac{2f_{23}}{V} - \frac{I_{wy}V\partial_o}{ar_o}\right)\dot{\psi}_2 = 0 \tag{3.18}$$

Trailing wheelset yaw

$$I_{wz}\ddot{\psi}_2+\left(\frac{I_{wy}V\Gamma}{ar_o}-\frac{2f_{23}}{V}-\frac{2f_{23}r_o\Gamma}{Va}\right)\dot{y}_2+\left(a_sK_s-bK_s+\frac{2f_{33}a\lambda}{r_o}-\frac{2f_{33}\Delta}{ar_o}\right)y_2+\left(\frac{2f_{11}a^2}{V}+\frac{2f_{33}}{V}\right)\dot{\psi}_2$$
$$+\left(K_b+2f_{23}+b^2K_s+a^2K_s+2ba_sK_s-Wa\partial_o\right)\psi_2-\left(bK_s+a_sK_s\right)y_1+\left(b^2K_s-K_b-a_s^2K_s\right)\psi_1=0 \tag{3.19}$$

When the unsymmetric index a_s is zero, the above equations will simulate a radial truck. The radial truck is simulated by providing inter-wheelset shear stiffness k_s such that K_s is greater than $\frac{K_b}{b^2}$.

The conventional truck is simulated by using values of K_b and K_s from equations (3.1) and (3.2) in which inter wheelset stiffness values (k_b and k_s) are zero. Also conventional trucks do not permit total decoupling of truck frame mass.

3.4 Unsymmetric Wheelset Truck

The Unsymmetric Wheelset is a configuration of a conventional truck in which the trailing axle has an Independently Rotating Wheelset (IRW). This configuration is referred to as an *UW truck*. The UW truck model is simulated by assuming the value of longitudinal creep coefficient of the trailing axle to be zero. This assumption is valid for single point contact of the wheels.

3.5 Conventional Truck with Yaw Damper

To improve the dynamic stability, stiff primary suspension is used in the conventional truck which deteriorates the curving performance. The curving performance

can be improved by providing softer primary suspension. Yaw dampers can then be introduced in the primary suspension to compensate the loss of restraint and maintain dynamic stability. As shown in Figure 3.7, yaw dampers are fitted between the wheelset and truck frame as part of the primary suspension. This type of truck with damper in the primary suspension is referred to as *CD truck*. If the primary yaw dampers are used, the longitudinal restraint is removed for low velocity steering motions; for higher frequency motions the damper resistance increases and the higher restraint helps to achieve desired critical speeds. Yaw dampers provided in the primary suspension helped achieve a better performance for the British Rail Class 37 locomotive as was reported by Pennington et al [52]. In this thesis, linear characteristics for the primary yaw damper are used. The yaw damper is characterized by the yaw damper coefficient $C_{p\psi}$ (Ns/m) and the series damper stiffness $K_{d\psi}$ (N/m). The damper series stiffness comes from the damper end mounting and bulk modulus of the damper working medium.

3.6 Unsymmetric Suspension Truck with Yaw Damper

This truck configuration is schematically shown in Figure 3.8. This type of truck has an unsymmetric suspension. Yaw dampers are provided in the primary suspension to improve the high speed performance of the US truck. This design configuration is referred to as an *USD truck*.

In Appendix C, the equations of motion for a passenger railway vehicle with *C trucks* are derived. The full carbody model has 17 degrees of freedom and the equations

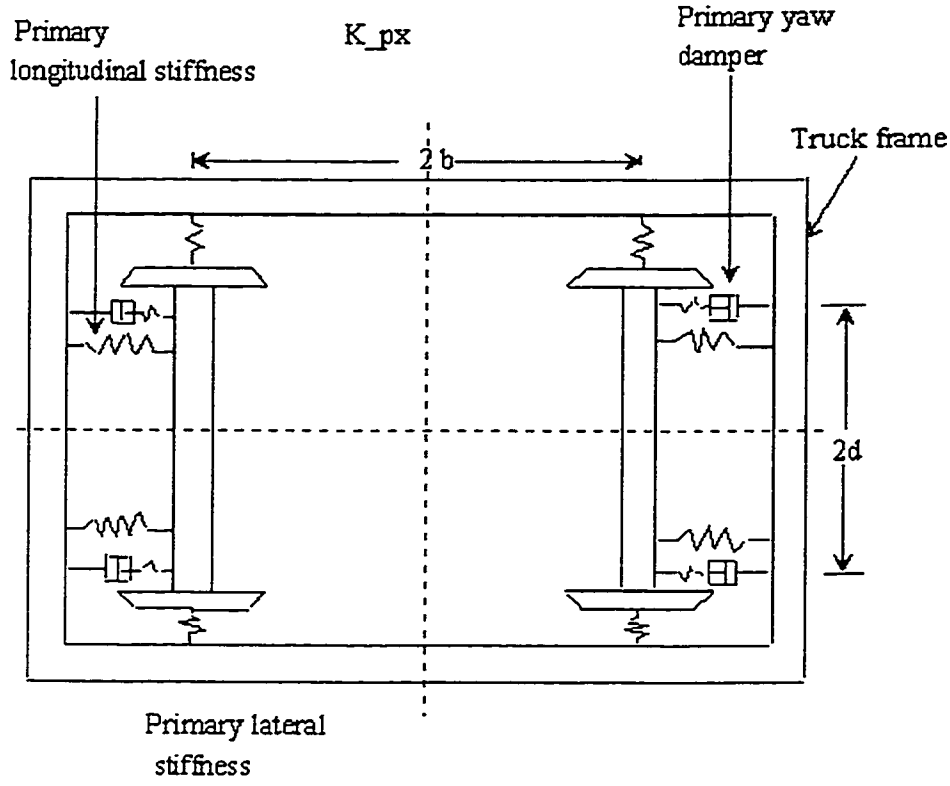

CD Truck Model
Figure 3.7

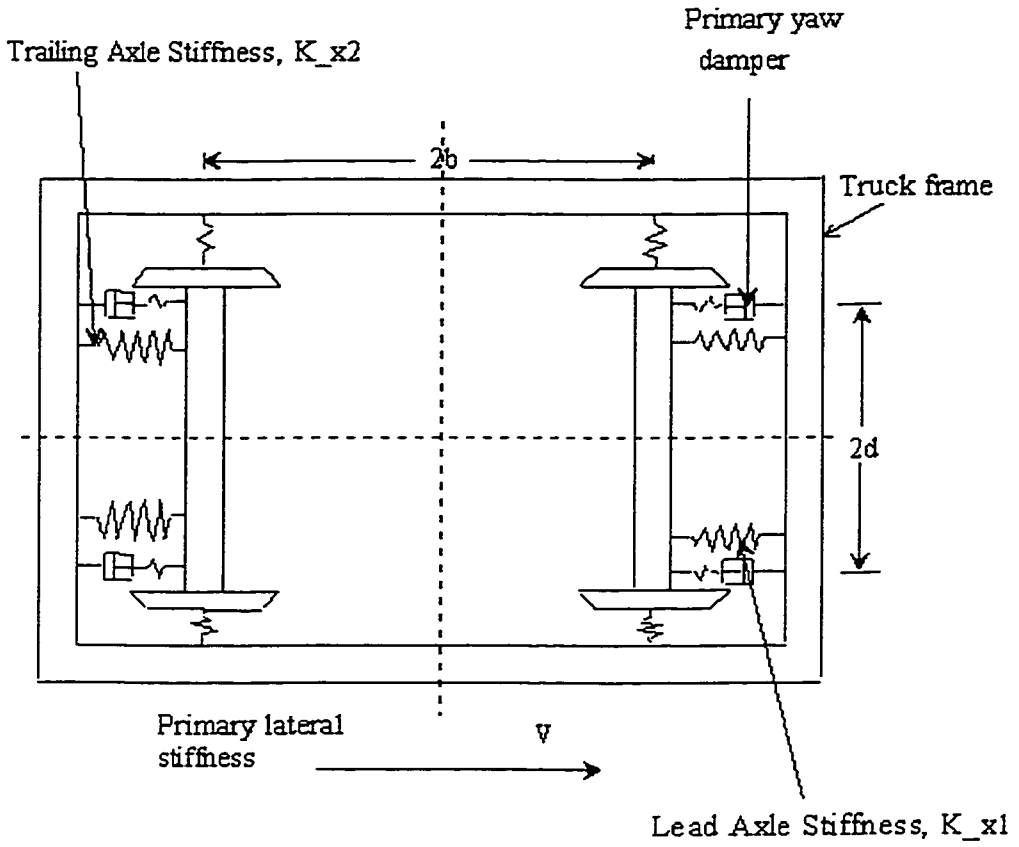

USD Truck Model
Figure 3.8

of motion are given in Appendix C.6. For stability analysis of a truck with yaw damper, effect of the primary yaw dampers has to be included. The degree of freedom for the yaw damper can be modelled by the following equation of quasi-static equilibrium:

$$C_{p\psi}(\dot{\psi}_d - \dot{\psi}_t) + K_{d\psi}(\psi_d - \psi_w) = 0 \tag{3.20}$$

The equations of motion for wheelsets given in the Appendix C-6 are modified for the USD truck to include the unsymmetric index a_s and the damper parameters. The equation for yaw motion of the leading wheelset can then be written as

$$\begin{aligned} & I_{wz}\ddot{\psi}_{w1} + \left(\frac{I_{wy}V\Gamma}{ar_o} - \frac{2f_{23}}{V} - \frac{2f_{23}r_o\Gamma}{Va}\right)\dot{y}_1 + \left(a_sK_s - bK_s + \frac{2f_{33}a\lambda}{r_o} - \frac{2f_{33}\Delta}{ar_o}\right)y_1 + \left(\frac{2f_{11}a^2}{V} + \frac{2f_{33}}{V}\right)\dot{\psi}_1 \\ & + \left(2K_{x1}d_p^2 + K_{d\psi} + 2f_{23} + b^2K_s + a^2K_s - 2ba_sK_s - Wa\partial_o\right)\psi_1 + \left(bK_s - a_sK_s\right)y_2 + \left(b^2K_s - a_s^2K_s\right)\psi_2 \\ & - 2K_{x1}d_p^2\psi_{t1} - K_{d\psi}\psi_d \quad = \quad 0 \end{aligned} \tag{3.21}$$

The yaw motion of the truck frame is given by

$$\begin{aligned} & I_{tz}\ddot{\psi}_{t1} - C_{s\psi}\dot{\psi}_c + \left(C_{p\psi} + C_{s\psi} + 4C_{py}b^2\right)\dot{\psi}_{t1} - 2C_{py}b(\dot{y}_{w1} - \dot{y}_{w2}) - K_{s\psi}\psi_c + \\ & (K_{s\psi} + 2K_{x1}d_p^2 + 2K_{x2}d_p^2 + 4K_{py}b^2)\psi_{t1} - 2K_{py}b(y_{w1} - y_{w2}) - 2K_{x1}d_p^2\psi_{w1} - 2K_{x2}d_p^2\psi_{w2} - C_{p\psi}\dot{\psi}_d = 0 \end{aligned} \tag{3.22}$$

For easier bi-directional operation of the train, Suda suggested the use of switched primary yaw dampers [53]. Referring to Figure 3.9, the switch of the longitudinal stiffness is realized by changing the damping coefficient of the longitudinal dampers which is in

series with the hard longitudinal stiffness K_{x2} . The soft longitudinal stiffness K_{x1} for the leading wheelset is set in parallel with this series damper-stiffness arrangement. For a given direction of vehicle travel, damping coefficient of the dampers in the trailing wheelset is made very high so that the longitudinal stiffness of the trailing wheelset is K_{x2}. On the other hand, the damping coefficient of the leading wheelset is kept at a designed value to achieve the required critical speed and its longitudinal stiffness retains a softer value of K_{x1}.

3.7 Tangent Track Stability Analysis

The interesting problem of railway vehicle lateral stability is studied through the eigen value analysis associated with the unforced response of the vehicle. The dynamic equations of motion can be expressed in the following matrix form:

$$[\mathrm{M}]\{\ddot{Y}\}+[\mathrm{C}]\{\dot{Y}\}+[\mathrm{K}]\{Y\}=\{0\} \tag{3.23}$$

In the above equation, [M] is the mass matrix, [C] is the damping matrix and [K] is the stiffness matrix. In order to analyze the various modes of vibration of the railway vehicle system defined by the above equations, their eigen values and eigen vectors must be investigated. This is done by converting equation (3.17) into an equivalent first order form by letting

$$\{X\}=\begin{Bmatrix}\dot{Y}\\ Y\end{Bmatrix}$$

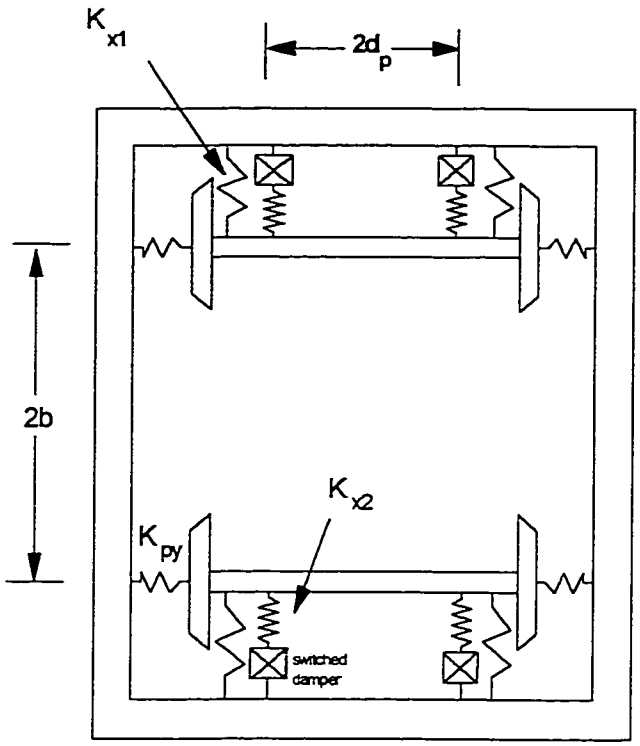

USD Truck with Switched Damper

Figure 3.9

so that

$$\{\dot{X}\} = [A]\begin{Bmatrix}\dot{Y}\\ Y\end{Bmatrix} \tag{3.24}$$

where

$$[A] = \begin{bmatrix}-\mathrm{M}^{-1}C & -M^{-1}K\\ I & 0\end{bmatrix} \tag{3.25}$$

The solution of the eigen value problem in equation (3.24) for an N degree-of-freedom rail vehicle model results in a set of N complex conjugate pairs of roots. These eigen values, ζ 's, take the form:

$$\zeta_i = \alpha_i \pm i\beta_i \tag{3.26}$$

where

ζ_i = i^{th} eigen value
j = $\sqrt{-1}$
α_i = real part of i^{th} eigen value
β_i = imaginary part of i^{th} eigen value

From these eigen values, natural frequencies of the vibration modes ω_{ni} and their damping ratios, ξ_{di}, can be obtained as:

$$\omega_{ni} = \sqrt{\alpha_i^2 + \beta_i^2} \tag{3.27}$$

$$\xi_{di} = \frac{-\alpha_i}{\omega_{ni}} \tag{3.28}$$

As the rail vehicle velocity increases, damping ratio of one of the lateral modes of the vibration system will decrease to zero and cross into the negative region at a critical velocity V_c. Thus, V_c denotes a stability boundary for vehicle operation without the lateral instability or hunting. In the design of railway vehicles, it is important to ensure that the critical speed of the vehicle is comfortably above the maximum operating speed. For this reason, sometimes velocity for which the damping ratio $\xi_d = 0.1$ in the least damped mode is also used in the stability analysis. This indicator, referred to as 10% modal velocity, is used in Chapter 5.

The equations (3.10) to (3.13) are used for stability analysis of the different truck configurations. The results of the computer simulations, discussed in the next section, will be presented as contours of constant critical speed in the $K_b - K_s$ plane. As will be shown, this simple model helps to achieve understanding of the stability characteristics of the US truck and UW truck and compare them with the stability behaviour of C truck and R truck.

The stability analysis is extended to a full carbody model with 17 degrees of freedom based on the equations of motion given in Chapter 5. The critical velocities are obtained through the eigen value analysis for the following four configurations: (1) C truck (2) R truck (3) CD truck (4) USD truck. The damper characteristics as given in equations (3.14) to (3.16) are incorporated in the models for CD truck and USD truck.

3.8 Stability Properties

The results of computer simulation of the stability behaviour of different truck configurations are reported in reference [54]. The contours of constant critical speed in the $K_b - K_s$ plane for a C truck, as shown in Figure 3.10, are obtained through a typical eigen value analysis. As bending and shear stiffnesses are increased from low values, the critical speed of the truck increases. Thus increasing the truck flexibility helps to stabilize the truck. The numbers given in the plots adjacent to the lines are the critical speed in m/s. The figure shows that to achieve a critical speed of 70 m/s the C truck has to be designed with $5x10^6$ Nm/rad and $3x10^6$ N/m. The line given by the equation $K_s = \frac{K_b}{b^2}$ gives the maximum possible shear stiffness in the case of the C truck and above this line an infeasible region is shown.

Figure 3.11 shows the critical speed plot for the R truck. In this case, due to truck frame decoupling, to achieve the same critical speed lower values of K_b and K_s are required. This is because, inter wheelset forces do not pass through the truck frame in a radial truck. The critical speed is inversely proportional to the square root of the hunting mass as given by the following equation developed by Wickens [6]:

$$V_{cr}^2 = \left(\frac{r_o}{2M\lambda a}\left(K_b + \left(a^2 + b^2\right)K_s - \sqrt{(K_b + (a^2 + b^2)K_s)^2 - 4b^2 K_s K_b}\right)\right) \quad (3.29)$$

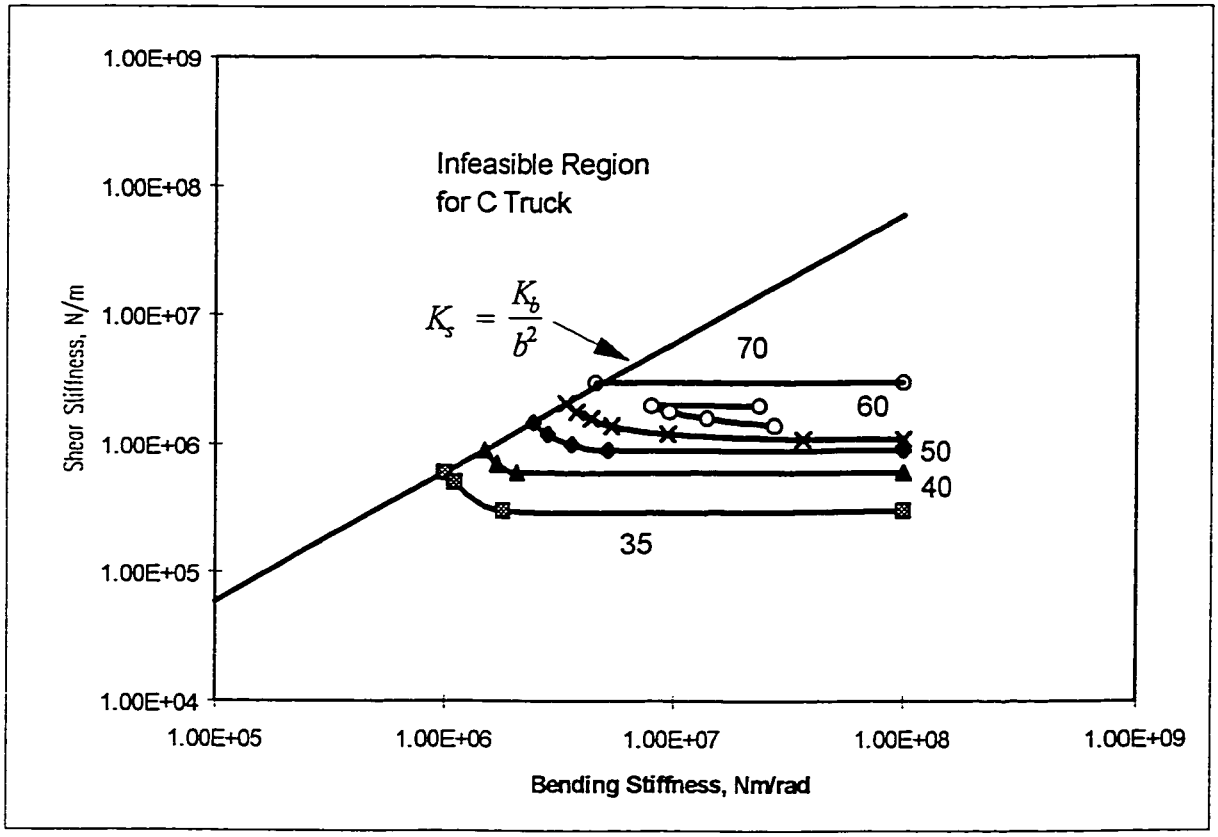

Stability plot for C Truck

Figure 3.10

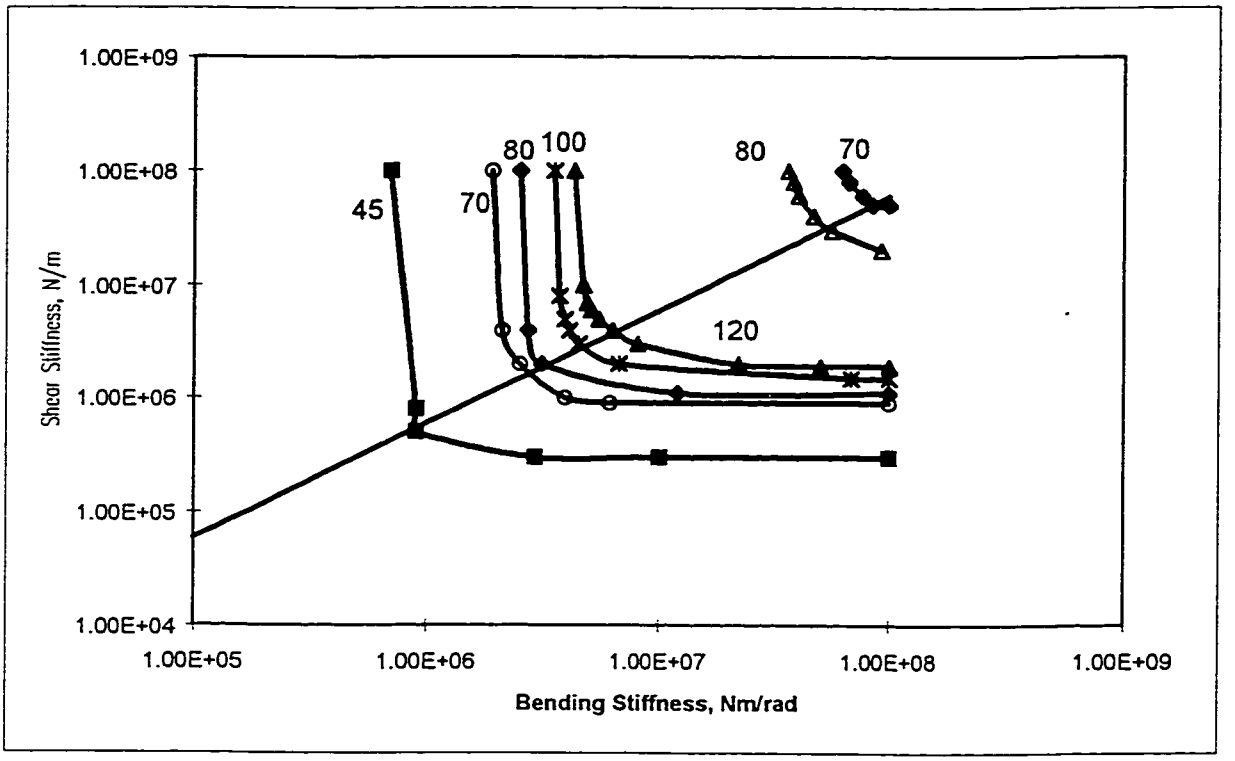

Stability plot for R Truck

Figure 3.11

where V_{cr} is the critical velocity and M is the truck hunting mass.

Since the hunting mass is decreased in the case of the R truck, the critical speed is higher compared to a C truck. Scheffel showed that a truck suspension using self steering wheelsets and diagonal constraints had better stability characteristics compared to a conventional truck [16]. For the critical speed of 70 m/s, the required parameters are $K_b = 1.75x10^6$ Nm/rad and $K_s = 1x10^7$ N/m. Because of the higher inter-wheelset stiffness in shear achievable in the R truck, lower bending stiffness is required in comparison to the C truck to achieve a given critical speed. The plot in Figure 3.11 has an approximate line of symmetry. It is seen that both K_b and K_s are equally important for stability for stiffness values around the line of symmetry. For higher values of the stiffness, K_b & K_s are not inter dependent.

The critical speed plots for the US truck are shown in Figure 3.12. The critical speed of 70 m/s is achieved for the values of $K_b = 4x10^6$ Nm/rad and $K_s = 5x10^6$ N/m. The plot also shows a line corresponds to equation (3.25) and gives the maximum possible shear stiffness for a US truck without inter wheelset connections. A comparison of stability performance of the three truck designs for a critical velocity of 70 m/s is shown in Figure 3.13. The performance of the US truck is in between the fully decoupled radial truck and a conventional truck. It is found that introduction of asymmetry reduces the stability of the truck in comparison to an ideal radial truck. The soft longitudinal stiffness in the leading wheelset K_{x1} in the US truck, designed to provide better curving

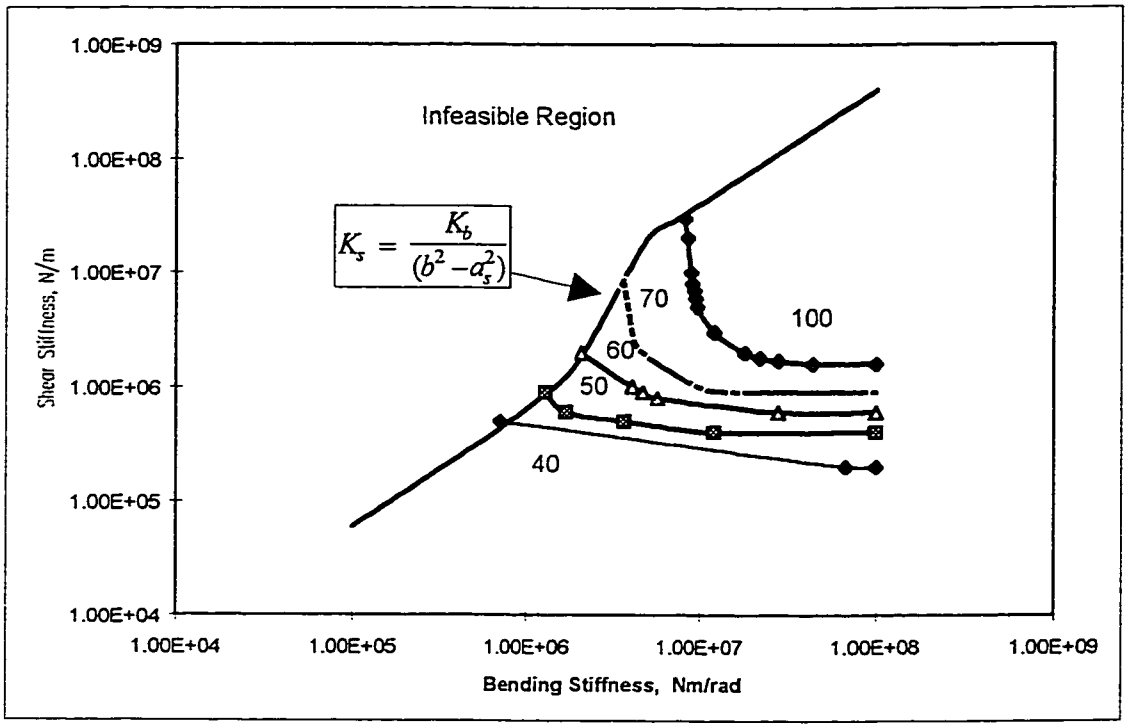

Stability plot for US Truck

Figure 3.12

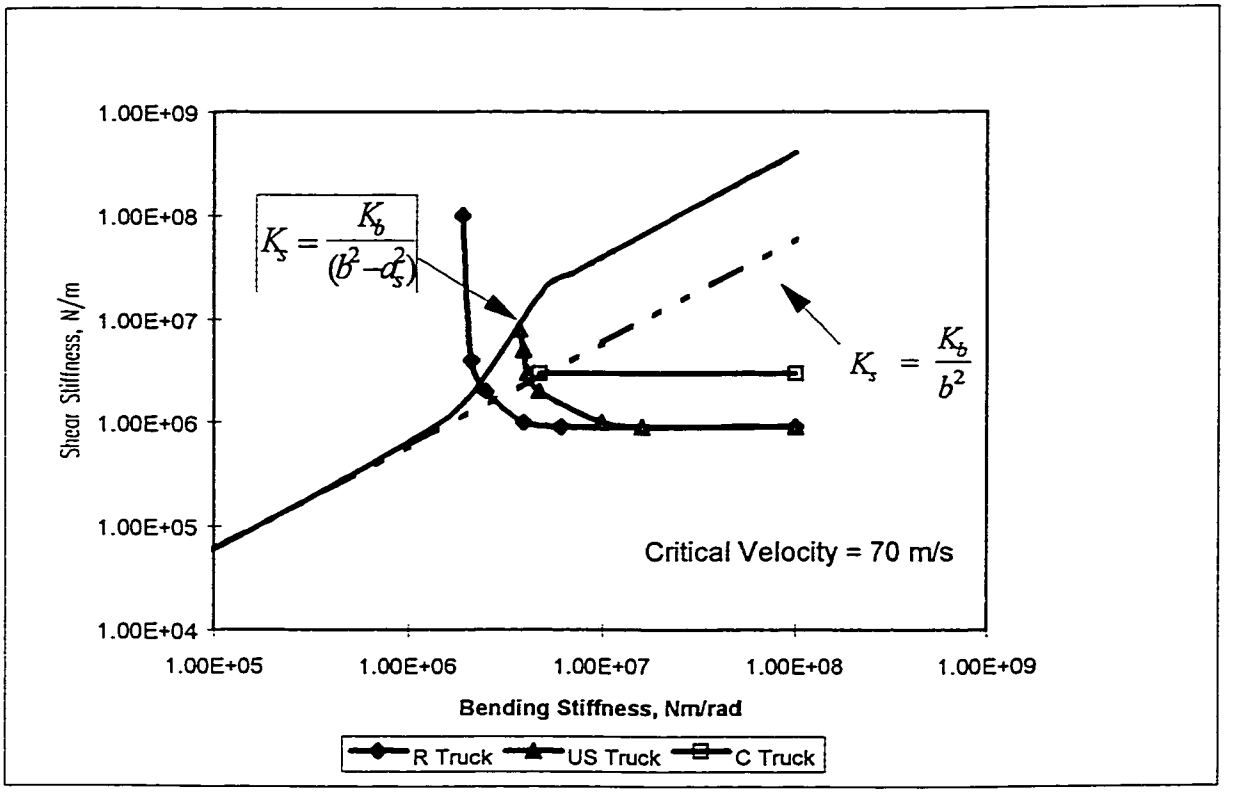

Comparison of Stability for Different Truck Designs

Figure 3.13

performance, has contributed to the lower critical speed.

In the case of an UW truck, there is a low speed instability zone for low values of shear stiffness as seen from Figure 3.14. The motion of the trailing wheelset is unstable in the case of lower values of shear stiffness because IRW has no restoring action towards the centerline of the track. Above the values of shear stiffness of $K_s = 1x10^7$ N/m, the variation of critical speed is seen to be independent of K_s and depends only on K_b. The variation of critical speed with bending stiffness is shown in Figure 3.15 for $K_s = 1x10^7$ N/m. To achieve a critical speed of 70 m/s, a bending stiffness of $1.75x10^6$ Nm/rad is required.

The UW truck can achieve a given critical speed with lowest value of bending stiffness in comparison to other truck configurations. This is probably due to the reduction of hunting phenomenon in the UW truck because of the independently rotating wheels in the rear axle.

3.9 Summary

In this chapter, lateral stability of the following truck configurations were evaluated using simplified truck models: Radial Truck *(R Truck)*, Unsymmetric Suspension Truck *(US Truck)* and Unsymmetric Wheelset Truck (*UW Truck)*. The stability properties of these models were compared with the conventional truck.

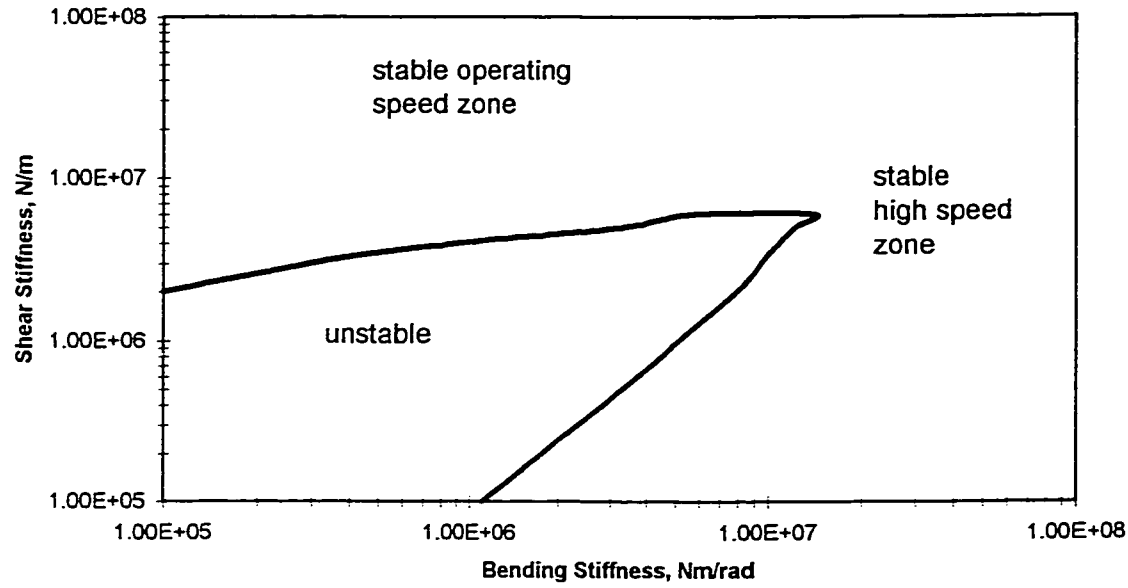

Stability zone for UW Truck

Figure 3.14

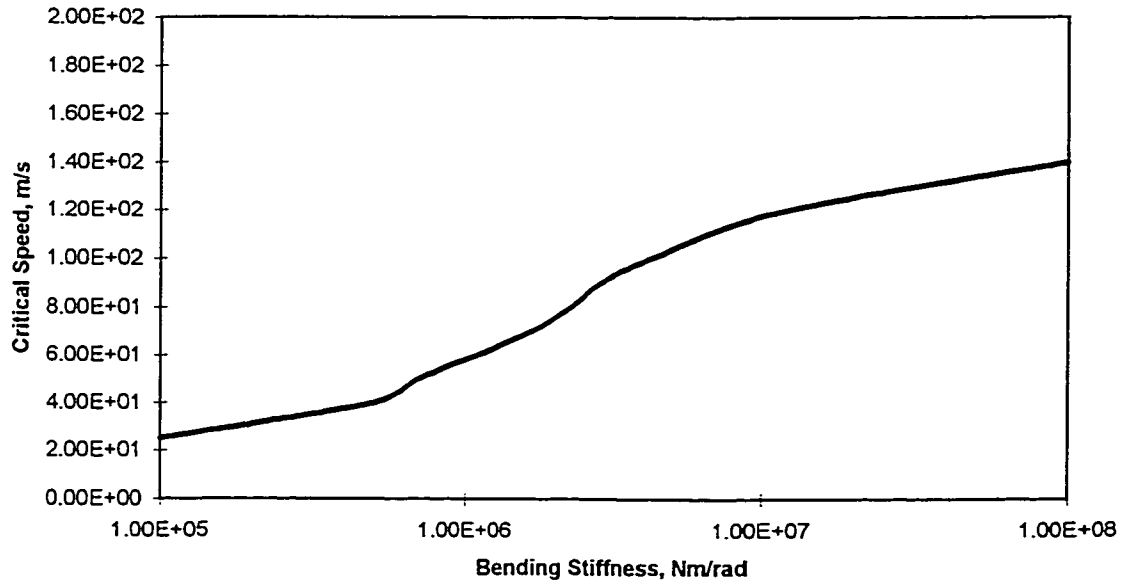

Variation of critical speed for UW truck

Figure 3.15

The inter axle shear stiffness in the C truck and US truck are limited to values given by equations (3.3) and (3.25) respectively. Introduction of asymmetry in the case of the US truck deteriorated the stability behaviour of the US truck. The critical speed for a given value of stiffness parameters K_b & K_s achieved by the US truck was less than that of the R truck. The R truck achieves higher critical speed because of the higher shear stiffness and lower hunting mass in comparison to the C truck. The UW truck is unstable for lower values of shear stiffness. But for values of $K_s > 1x10^7$ N/m, critical speed for UW truck is higher in comparison to other truck configurations. This is due to the stabilizing effect of the independently rotating wheels in the rear axle of the truck.

In the next chapter, the off flange curving performance of these designs will be evaluated in detail. Stability-curving trade-off plots will be developed for the different truck configurations in order to optimize the stiffness parameters.

Chapter 4

LINEAR CURVING MODELS AND CURVING/STABILITY TRADE-OFF

4.1 Introduction

The lateral stability of railway vehicles on tangent track for high speed operation have been traditionally achieved by designers through the use of stiff primary suspension elements. A railway vehicle truck designed with stiff primary suspension elements has poor curving ability. A number of modified truck designs have been proposed over the years to resolve this inherent conflict in the design of railway vehicle suspension. Wickens has reviewed recent progress in the development of suspension design in railway vehicle trucks that addressed the conflict between stability and curving [55].

In this chapter, linear curving models are developed for the *R truck*, *US truck* and *UW truck*. The curving analysis of these truck designs are carried out to evaluate their off-flange and on-flange curving characteristics which are then compared with the performance of the *C truck*. The off-flange curving behaviour is evaluated in terms of the maximum curvature for which the lead wheelset lateral excursion is equal to the available flange clearance. A trade-off analysis is made by plotting together the lines of constant critical speed and curving performance in the $K_b - K_s$ plane to determine the optimum values of the stiffness parameters.

4.2 Linear Curving Model

The curving behaviour of a railway vehicle exhibits effects that are quite different from tangent track dynamics. In the linear model for lateral stability on tangent track

discussed in the previous chapter, it was assumed that all wheels have equal vertical load between wheel and rail, creep forces are linear functions of creepages and wheel/rail contact conditions are independent of wheelset position. In curving, change in the track centre line position and the angular orientation of the tangent to the centre line result in relative displacements between components that must be properly accounted for in the calculation of suspension forces. The offset of equilibrium positions between components and the redistribution of static loads lead to unequal vertical loads on the wheels. Linear creep forces that are calculated using equation (2.4) are then saturated according to the Vermuelen/Johnson saturation curve such that creep forces do not exceed the wheel/rail adhesion limit.

4.2.1 *C Truck* and *R Truck*

The equilibrium equations for steady state curving can be written in the form

$$[K]\{X\} = [\mathrm{E}]\begin{Bmatrix} 1/R \\ \phi_d \end{Bmatrix} \tag{4.1}$$

where K is the stiffness matrix and X is the displacement vector. Two independent forcing functions describe the curving conditions to which the vehicle is exposed: track curvature 1/R and cant deficiency ϕ_d (lateral unbalance). An expression for cant deficiency is derived in Appendix B.2.1. In North America, track curvature is often expressed in terms of degree curve, D. It is defined as the angle subtended at the center of the curve due to a 100 ft chord, as shown in Figure 4.1. For a conventional or a radial truck, [K] consists

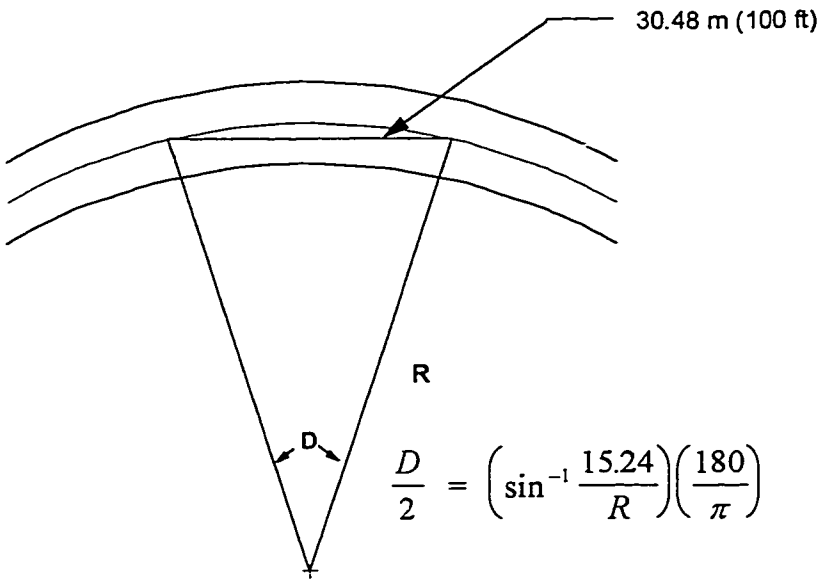

Definition of Degree Curve

Figure 4.1

of primary and interconnection stiffnesses and the equations for static equilibrium is given by the following equation [6].

$$\begin{bmatrix} K_s & -bK_s - 2f_{22} & -K_s & -bK_s \\ \frac{2f_{11}a\lambda}{r_o} - bK_s & K_b + b^2K_s & bK_s & b^2K_s - K_b \\ -K_s & bK_s & K_s & bK_s - 2f_{22} \\ -bK_s & b^2K_s - K_b & \frac{2f_{11}a\lambda}{r_o} + bK_s & K_b + b^2K_s \end{bmatrix} \begin{Bmatrix} y_1 \\ \psi_1 \\ y_2 \\ \psi_2 \end{Bmatrix} = \begin{Bmatrix} -F_f + \frac{F_c}{2} + \frac{2f_{22}b}{R} \\ \frac{2f_{11}a^2}{R} \\ \frac{F_c}{2} - \frac{2f_{22}b}{R} \\ \frac{2f_{11}a^2}{R} \end{Bmatrix} \tag{4.2}$$

The wheelset in a conventional truck with high bending stiffness K_b will not be able to align radially in a curve. The wheelset balances the yaw moment applied to it by the primary suspension by moving further laterally in order to generate equal and opposite longitudinal creep forces. The wheelset balances the lateral force by yawing more. For a given curvature and cant deficiency, the attitude of the truck in a curve and a set of forces acting on it are obtained by solving the equations of equilibrium given above.

As pointed out by Wickens, perfect steering for which the lateral creep is zero, can be achieved only when the bending stiffness is zero in the case of a conventional or radial truck [6].

4.2.2 *US Truck*

The equilibrium equations for an US truck is written using equations (3.15) and (4.1) as

$$\begin{bmatrix} K_s & a_sK_s - bK_s - 2f_{22} & -K_s & -(a_sK_s + bK_s) \\ \frac{2f_{11}a\lambda}{r_o} + a_sK_s - bK_s & a_s^2K_s + K_b - 2ba_sK_s + b^2K_s & -a_sK_s + bK_s & -a_s^2K_s + b^2K_s - K_b \\ -K_s & -a_sK_s + bK_s & K_s & a_sK_s + bK_s - 2f_{22} \\ -(a_sK_s + bK_s) & -a_s^2K_s + b^2K_s - K_b & \frac{2f_{11}a\lambda}{r_o} + a_sK_s + bK_s & a_s^2K_s + K_b + 2ba_sK_s + b^2K_s \end{bmatrix}$$

$$\begin{Bmatrix} y_1 \\ \psi_1 \\ y_2 \\ \psi_2 \end{Bmatrix} = \begin{Bmatrix} -F_f + \frac{F_c}{2} + \frac{2f_{22}b}{R} \\ \frac{2f_{11}a^2}{R} \\ \frac{F_c}{2} - \frac{2f_{22}b}{R} \\ \frac{2f_{11}a^2}{R} \end{Bmatrix} \qquad (4.3)$$

Adding the first and third equation in (4.3),

$$-2f_{22}(\psi_1 + \psi_2) = F_c$$

For balanced curving, the cant deficiency is zero and hence, $\psi_1 = -\psi_2$.

Manipulating the first and second equations and the first and fourth equations to eliminate y_1, we can obtain two equations in terms of y_2, ψ_1 & ψ_2. These two equations can again be combined to get the following equations in terms of ψ_1 & ψ_2.

$$\left(\frac{2f_{11}a\lambda}{r_o}(a_sK_s - bK_s) - \frac{4f_{22}f_{11}a\lambda}{r_o} - 4f_{11}a_sK_s - 2K_bK_s\right)\psi_1 + \left(2K_bK_s - \frac{2f_{11}a\lambda}{r_o}(a_sK_s + bK_s)\right)\psi_2$$
$$= \left(\frac{f_{11}a\lambda}{r_o} + a_sK_s\right)F_c + \frac{4f_{22}f_{11}ab\lambda}{Rr_o} + \frac{4f_{22}ba_sK_s}{R} \qquad (4.4)$$

For $F_c = 0$, we have $\psi_2 = -\psi_1$ and the above equation is simplified as

$$\psi_1 = 4\frac{f_{22}b}{R}\left(a_s K_s + \frac{f_{11}a\lambda}{r_o}\right) \tag{4.5}$$

As explained in Appendix A when the truck achieves perfect steering in a curve (refer Fig.(A-3)), the leading wheelset yaw angle equals $-\frac{b}{R}$. Using this we can arrive at the condition for perfect steering for an US truck from equation (4.5). This is given by,

$$a_{ps} = \frac{K_b r_o}{f_{11}a\lambda} \tag{4.6}$$

The unsymmetric index for perfect steering, a_{ps}, is proportional to the bending stiffness and is inversely proportional to the wheel conicity. The index does not depend on the radius of curve. Thus it is seen that for reasonable values of K_b & λ, perfect steering is possible for an US truck.

An expression for the unsymmetric index for perfect steering can be derived in terms of rear axle stiffness K_{x2} for an *US truck*. By using equation (3.6) in (3.5a), we can get an expression for K_b in terms of K_{x2} and a_s. By using equation (4.6) in the resulting expression, we get,

$$a_{ps} = \frac{bK_{x2}d_p^2 r_o}{bf_{33}a\lambda + K_{x2}r_o d_p^2}. \tag{4.7}$$

Then from equations (3.6) and (3.5(a)), values of K_{x1} and K_b can be calculated. This is

plotted in figure 4.2 from where it is seen that K_{x1} and K_b initially increase as K_{x2} increases and saturate. From figure 4.3, it is seen that the unsymmetric index for perfect steering tends to b, the value of the half wheel base. In a conventional truck with unsymmetric configuration, it is not possible to increase the asymmetry beyond the value of half the wheel base.

4.2.3 *UW Truck*

The equilibrium equations for the UW truck are obtained from equations (4.2) by setting the longitudinal creep coefficient f_{11} for the rear axle to be zero. The resulting equations can be manipulated to obtain the following expressions for the lateral displacement and yaw rotation for the leading and trailing wheelsets.

$$\frac{y_1}{\left(\frac{ar_o}{\lambda R}\right)} = 1 + \frac{2b^2 K_b f_{22}}{f_{11} a^2 (K_b + b f_{22})} \tag{4.8}$$

$$\frac{y_2}{\left(\frac{ar_o}{\lambda R}\right)} = 1 + \frac{2bK_b f_{22}(br_o K_s - f_{11} a\lambda)}{K_s r_o f_{11} a^2 (K_b + b f_{22})} \tag{4.9}$$

$$\frac{\psi_{w1} + (b/R)}{(b/R)} = \frac{K_b}{bf_{22} + K_b} \tag{4.10}$$

$$\frac{\psi_{w2} - (b/R)}{(b/R)} = \frac{-K_b}{bf_{22} + K_b} \tag{4.11}$$

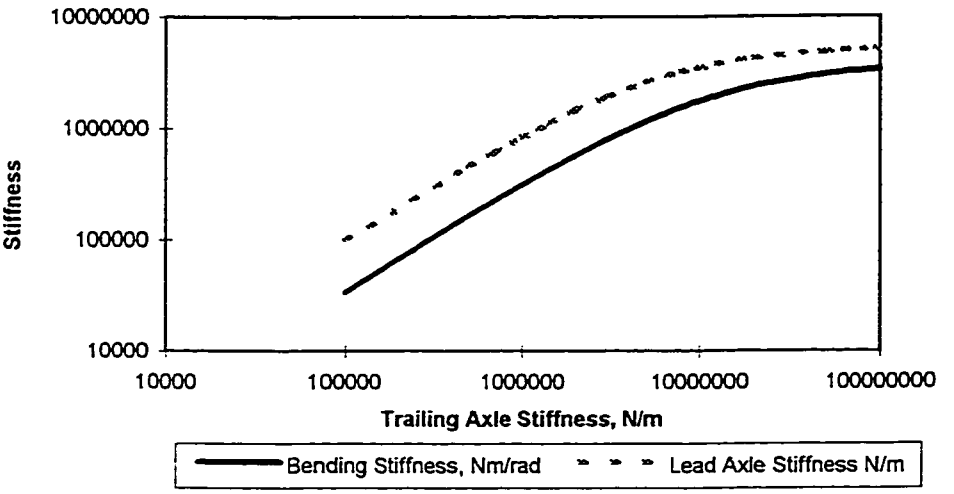

Stiffness Relationships for US Truck

Figure 4.2

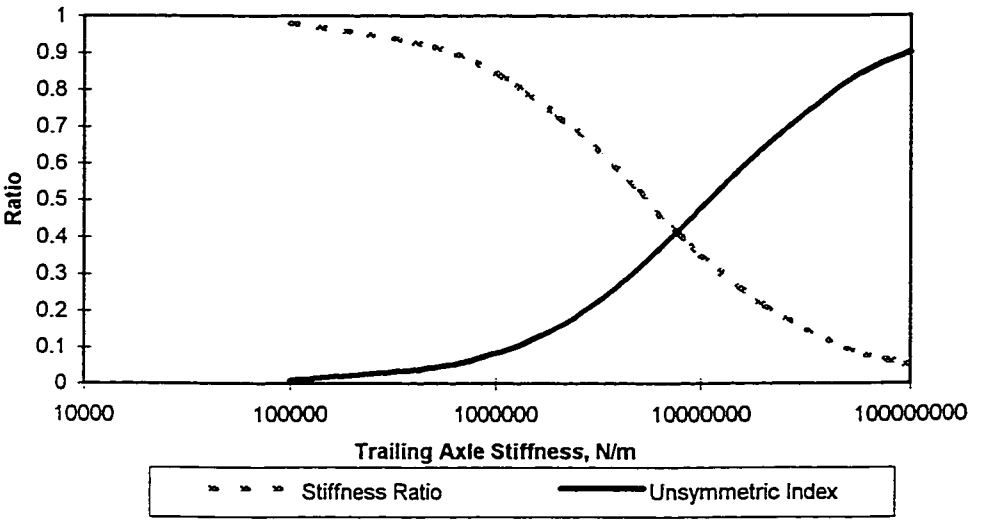

Stiffness Ratio and Unsymmetric Index for US Truck

Figure 4.3

Unlike the US truck, the UW truck can not achieve perfect steering for non-zero values of bending stiffness as seen from equation (4.10).

4.3 Off-flange curving/stability trade-off

The off-flange curving performance is measured in terms of the degree curve for which the lead wheelset lateral excursion is equal to the available flange clearance. In the analysis, flange clearance is assumed to be 10 mm. The model used is a steady state curving single truck model with a simulated half car body. The total degrees of freedom is eight viz. lateral and yaw displacements of two wheelsets and a truck, and lateral and roll displacements for the car body. The derivation for the equations of static equilibrium were discussed in Chapter 2 and listed in Appendix C-7 (equations C-70 to C-77). The steady state model computes non-linear creep forces according to a modified Vermuelen/Johnson approximation, using linear wheel and rail geometry [56]. The Vermuelen/Johnson method is described in Appendix D.

In the case of a free wheelset the offset of pure rolling line towards the outside of a curve is given by [2,3]

$$y_w = \frac{ar_o}{\lambda R} \tag{4.12}$$

In the case of a rigid truck, the lateral displacement of the wheelset is given by [2,3]

$$y_{w1} = y_{w2} = \frac{ar_o}{\lambda R}\left(1+\left(\frac{b}{a}\right)^2\right) \tag{4.13}$$

The off-flange curving performance of practical trucks fall between these two extreme cases.

Figure 4.4 shows the lateral displacement of lead wheelset as the degree curve is varied for the various configurations. The K_b and K_s values chosen for each type is such that a critical velocity of 70 m/s is achieved. A conicity value of 0.15 is assumed. A condition of balanced running is simulated.

The UW truck has the best off-flange curving performance followed by the radial truck. The UW truck can negotiate a 4.5 degree curve before flanging action occurs. In comparison, the radial truck negotiates a 3.6 degree curve, the US truck negotiates 3.4 degree curve and a conventional truck negotiates a 2 degree curve.

Figure 4.5 shows the tread wear index for the different configurations. The tread wear index is defined as the product of the normal wheel load and the resultant creepage at the wheel. Even though the index may not predict the actual wear occurring on a wheel, it serves as an indicator of comparative performance of different trucks. It is seen that the UW truck experiences lower tread wear compared to a radial truck for a given

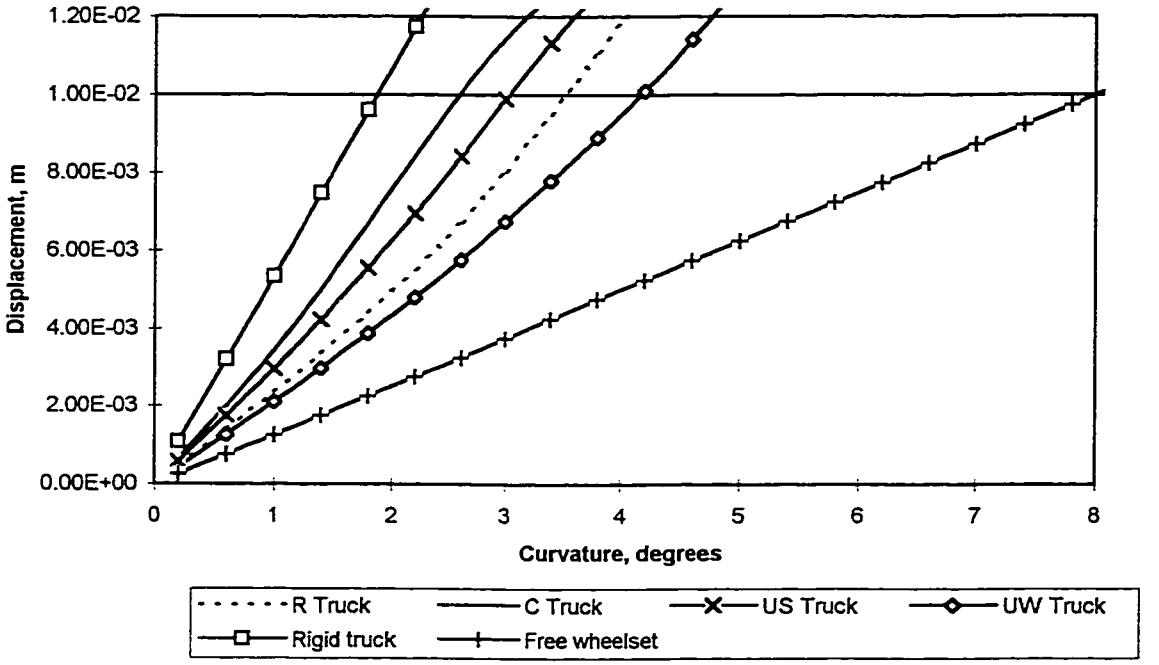

Lateral displacement of lead wheelset

Figure 4.4

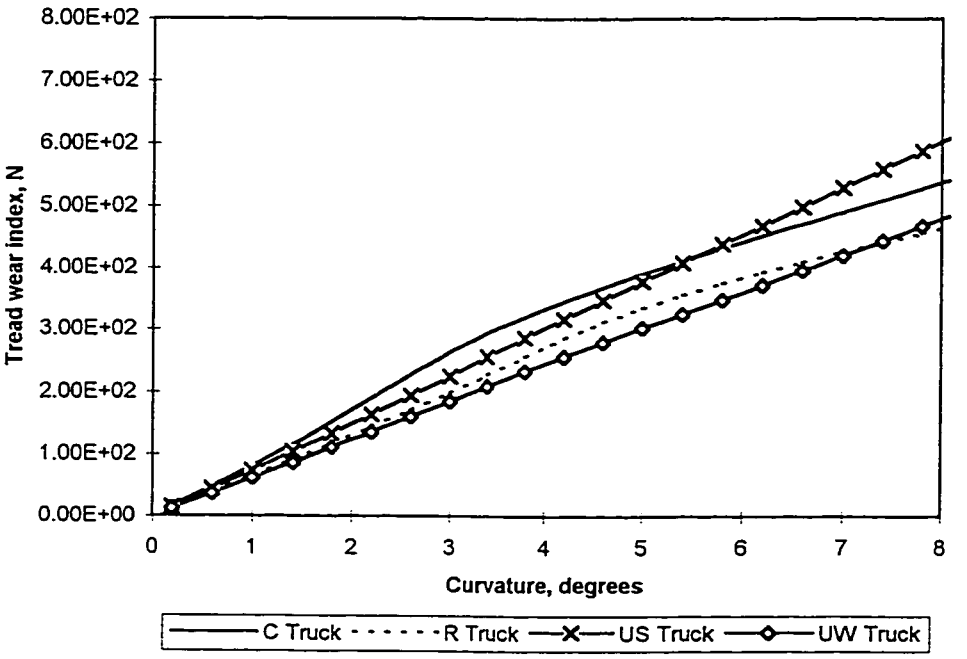

Tread wear index on lead outer wheel

Figure 4.5

degree curvature. The performance of an US truck is better than a conventional truck.

For determining the off-flange curving trade-off, lines of constant curving performance and critical speed are plotted together in the plane in order to find the optimum curving stability tradeoff.

The following steps are involved:

1. For different sets of $K_b - K_s$, degree curvature at which flange contact is initiated, is determined.

2. Curves of constant curvature for initial flange contact in $K_b - K_s$ plane are constructed

3. This chart is used in conjunction with chart for critical speed to trade-off stability and curving performance in the choice of K_b and K_s.

Figure 4.6 shows a trade-off plot for the C truck for a conicity of 0.15. The constant critical velocity lines are shown together with contours of curvatures for which the flanging is initiated. The plot shows that increasing the bending stiffness increases the critical speed of the truck. But high stiffness value decreases the curvature at which flange contact is initiated and result in poor curving performance. Assume a critical velocity of 70 m/s is desired. The stiffness values required to achieve the speed of 70 m/s are $K_b = 6x10^6$ Nm/rad and $K_s = 3.5x10^6$ N/m for $\lambda = 0.15$. The truck so designed

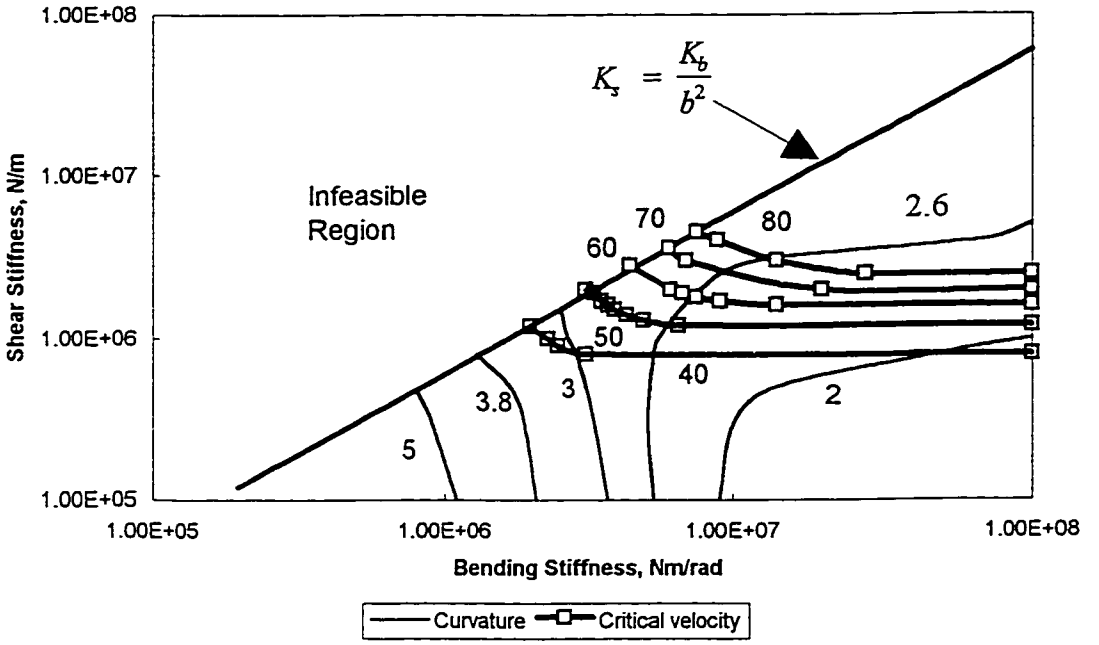

Trade Off Plot for C Truck, $\lambda = 0.15$

Figure 4.6

will negotiate a 2.6 degree curve (671 m radius) without flanging. Figures 4.7 shows the trade-off for the C truck for $\lambda = 0.25$.

The results of simulation for the R truck are shown in Figure 4.8 for $\lambda = 0.15$. The stiffness values required for the R truck is less compared to a C truck since it achieves full truck frame decoupling. The radial truck can negotiate a 3.6 degree curve without flanging by choosing K_b and K_s values near the point of minimum separation between the two curves of constant curvature and constant critical speed.

The results of the trade-off study for the US truck are given in figures 4.9 and 4.10 for the wheel conicity of 0.15 and 0.25 line respectively. The dash-dot line in the figure satisfies the equation (3.25) which gives the maximum possible value of shear stiffness realized by this configuration. An US truck can be designed to achieve a critical speed of 70 m/s and negotiate a 3.4 degree curve without flanging by choosing proper values of bending and shear stiffness from the trade-off plot in Figure 4.9.

In the case of the UW truck, the curving performance does not depend on the value of K_s. Simulations were done for $K_s = 1x10^7$ N/m. The variation of degree curve with the bending stiffness is shown in figures 4.11 and 4.12 respectively for conicities of 0.15 & 0.25. It is seen that a truck designed to achieve a critical speed of 70 m/s can negotiate a 4.6 degree curve without flanging for the case of $\lambda = 0.15$.

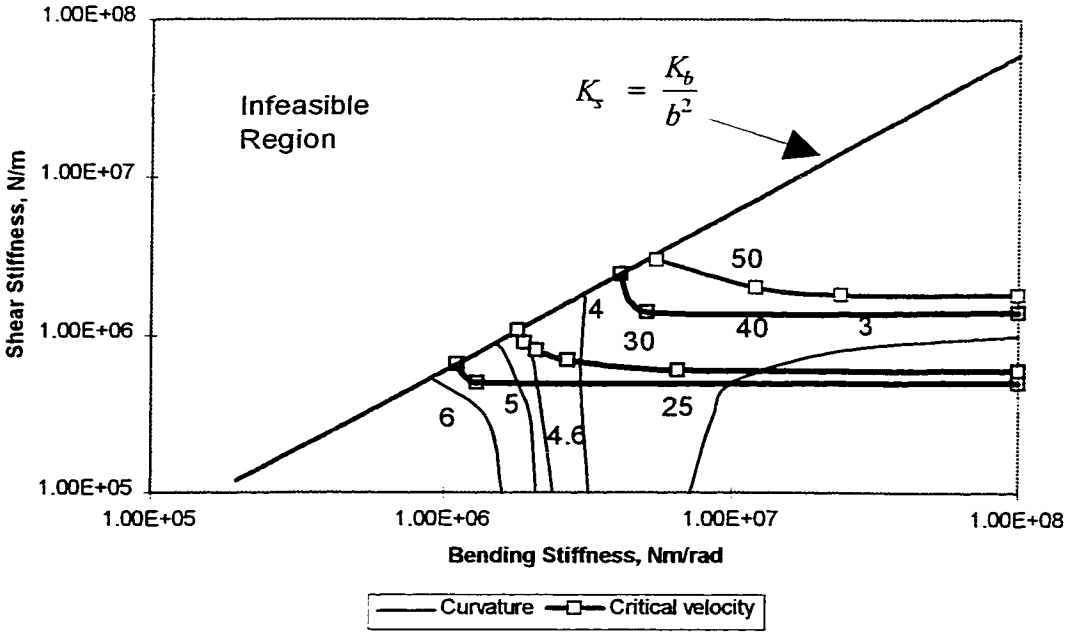

Trade Off Plot for C Truck, $\lambda = 0.25$

Figure 4.7

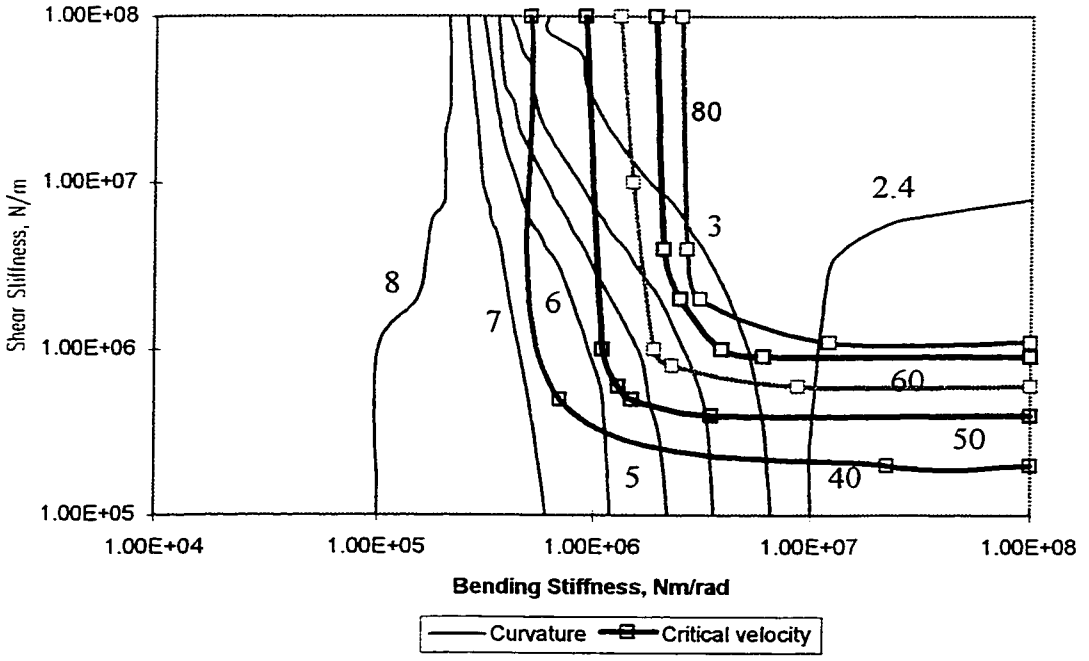

Trade Off Plot for R Truck, $\lambda = 0.15$

Figure 4.8

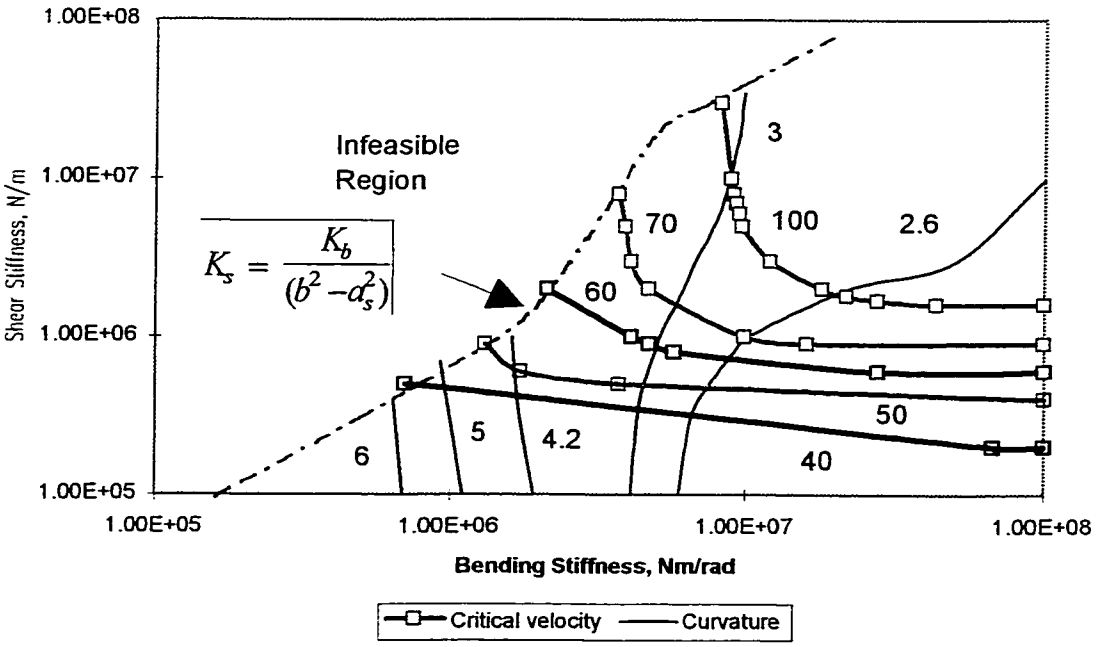

Trade Off Plot for US Truck, $\lambda = 0.15$

Figure 4.9

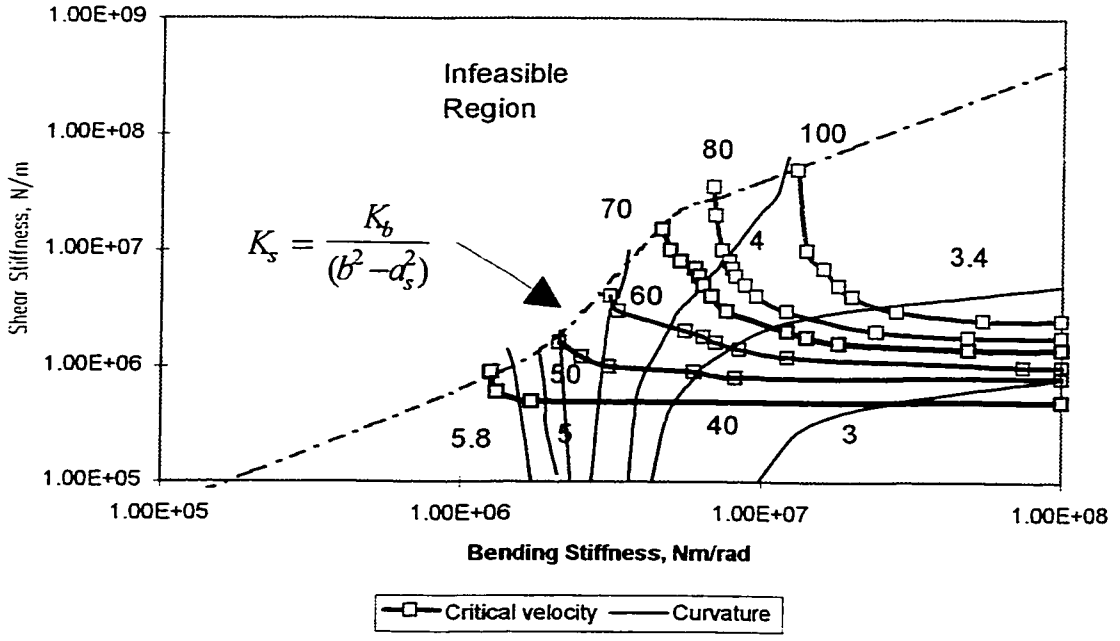

Trade Off Plot for US Truck, $\lambda = 0.25$

Figure 4.10

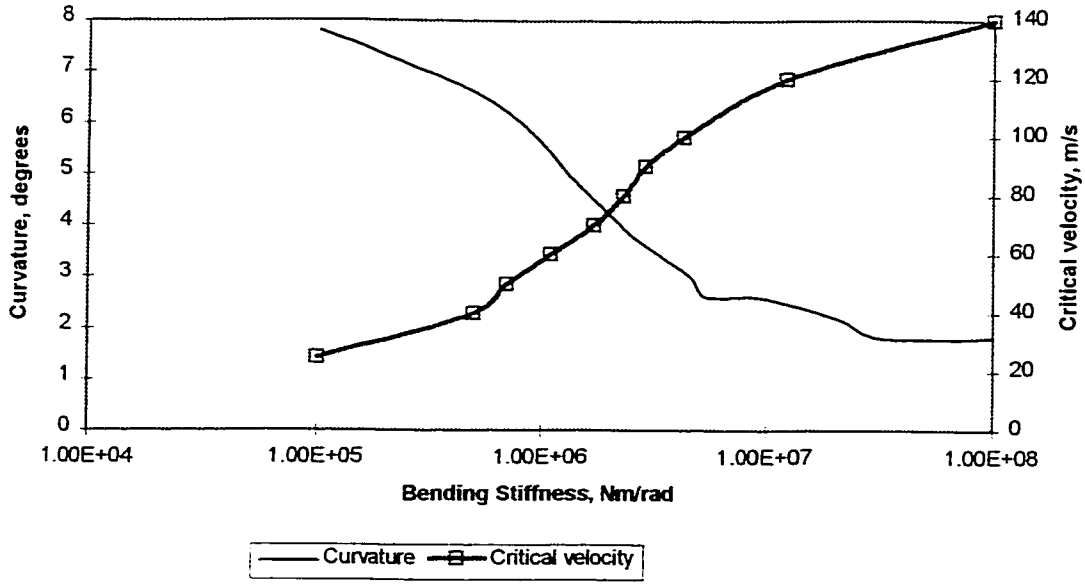

Trade Off Plot for UW Truck, $\lambda = 0.15$

Figure 4.11

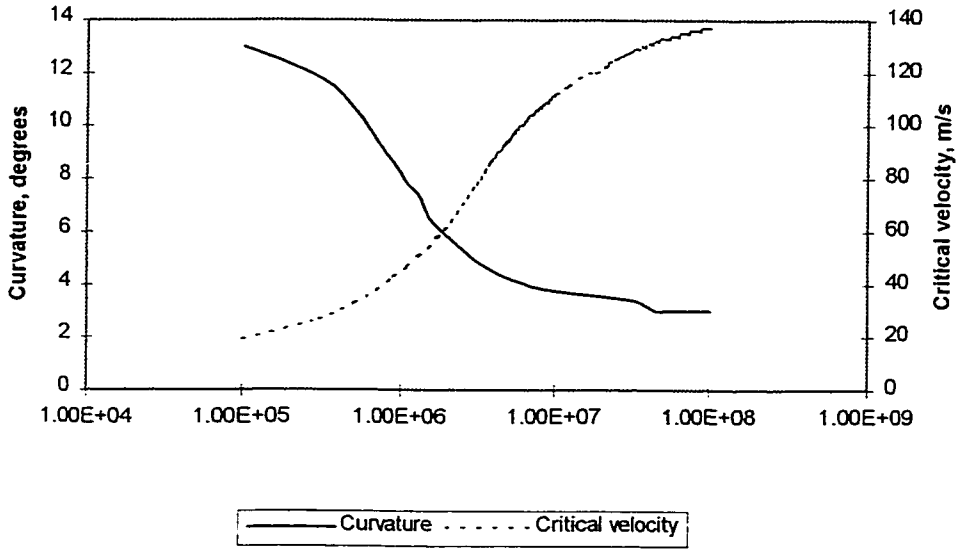

Trade-off plot for UW truck, $\lambda = 0.25$

Figure 4.12

The results of the off-flange trade-off for different truck configurations are summarized in Figure 4.13 for the wheel conicity of 0.15. The plot shows the maximum degree curve that can be negotiated by optimal designs as a function of critical speed for the different truck types. The vehicle is assumed to negotiate the curve at a balanced speed and run on a smooth track with no geometric perturbations.

The plot shows that the conventional vehicle designed to negotiate a 4 degree curve without flanging can achieve a speed of 36 m/s. For the same curving performance, the US truck can achieve a critical speed of 55 m/s (an improvement of 52%) and the radial truck can achieve a critical speed of 67 m/s (an improvement of 86%). The UW truck achieves the highest speed of 79 m/s which is an improvement of 119%.

Alternatively, there is a 1.5 degree improvement in off-flange curving of the US truck for a given critical speed of 60 m/s over the conventional truck. The US truck designed for a critical speed of 60 m/s could negotiate a 3.8 degree curve compared to a 2.3 degree curve for the conventional truck - an improvement of 65%. The introduction of asymmetry helps to achieve better off-flange curving performance in the case of the US truck. The radial truck can negotiate a 4.4 degree curve (an improvement of 91%) and the UW truck can negotiate a 5.2 degree curve (an improvement of 126%).

Figures 4.14 compares the trade-off performance of the different truck types for the conicity of 0.25. The trend observed is the same, but the trucks are now able to

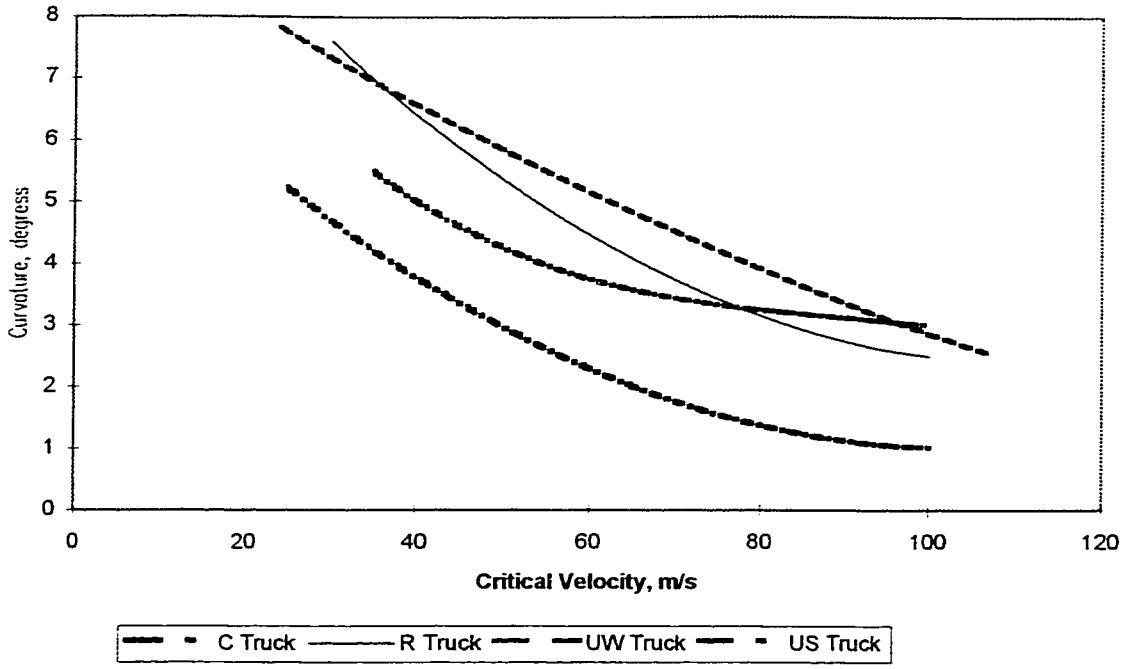

Trade Off Comparison for Different Truck Types, $\lambda = 0.15$

Figure 4.13

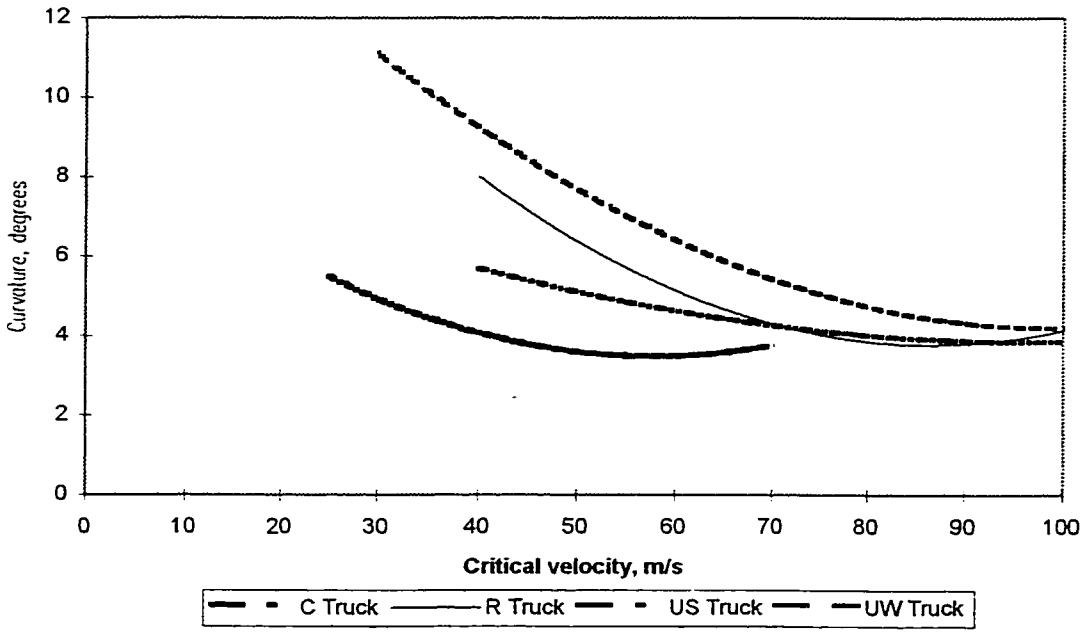

Trade-off comparison for different truck types, $\lambda = 0.25$

Figure 4.14

negotiate sharper curves without flanging. Table 4.1 shows the optimized suspension values to achieve a critical speed of 70 m/s and the corresponding curvature for no flanging.

4.4 On-flange curving

The on-flange curving are examined in terms of angle of attack and the flange wear index. The angle of attack is the yaw angle of the wheelset from its radial position as the truck negotiates a curve. The flange wear index is obtained as the product of the flange force developed and the angle of attack. Flanging action is approximated by pinning the lateral excursion of wheelset from exceeding the flange clearance, the lateral force which develops thereby accounting for the flange force.

Figure 4.15 shows the variation of angle of attack (AOA) of the leading wheelset for different degree curvature. For negotiating a 6 degree curve, that is a curve radius of 290 m, the angle of attack developed in the leading wheelset of the conventional truck is 7 mrad. For the leading wheelset of the UW truck, it is 2 mrad, an improvement of 71%. The values of angle of attack for the radial truck is 4.6 mrad and for the US truck is 6.5 mrad. Figure 4.16 shows the variation of the flange wear index with degree curve.

The angle of attack and the flange wear index for the *UW truck* increase dramatically in comparison to the *R truck* for curvatures greater than 7 degrees. The trend

Conicity	Type	K_b x 10^6 Nm/rad	K_s x 10^6 N/m	Curvature, degrees
0.1	C Truck	4.0	2.4	1.8
	R Truck	1.25	1	3.3
	US Truck	2.6	5	2.8
	UW Truck	1.25	10	3.6
0.15	C Truck	6.0	3.5	2.6
	R Truck	1.75	2	3.6
	US Truck	3.8	7	3.4
	UW Truck	1.75	10	4.5
0.25	C Truck	10.0	6	3.8
	R Truck	4.0	3	4.6
	US Truck	4.6	15	4.4
	UW Truck	2.5	10	5.4

Optimized stiffness parameters for different truck configurations

Table 4.1

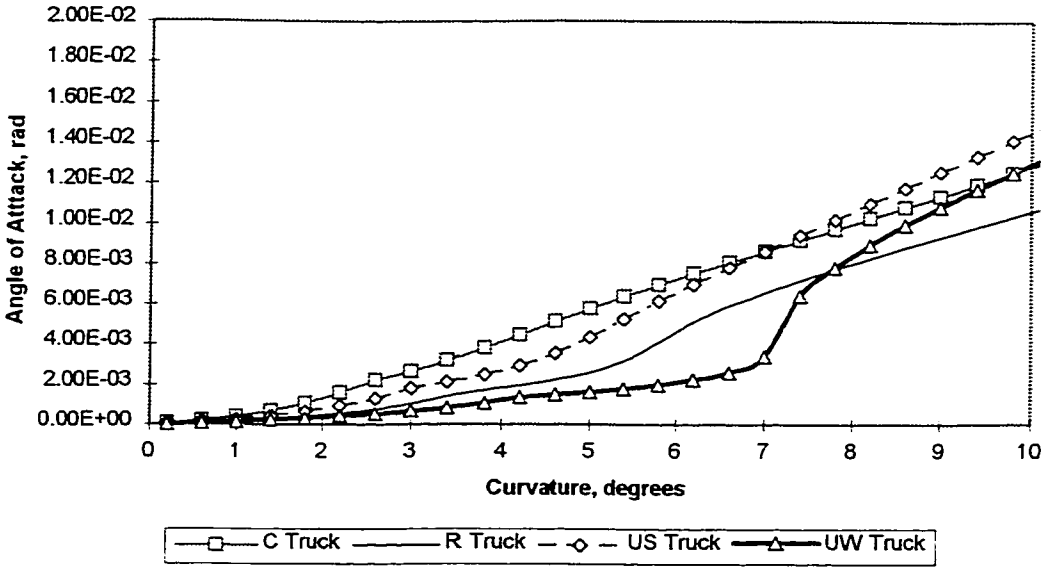

Variation of AOA for different truck types, λ = 0.15

Figure 4.15

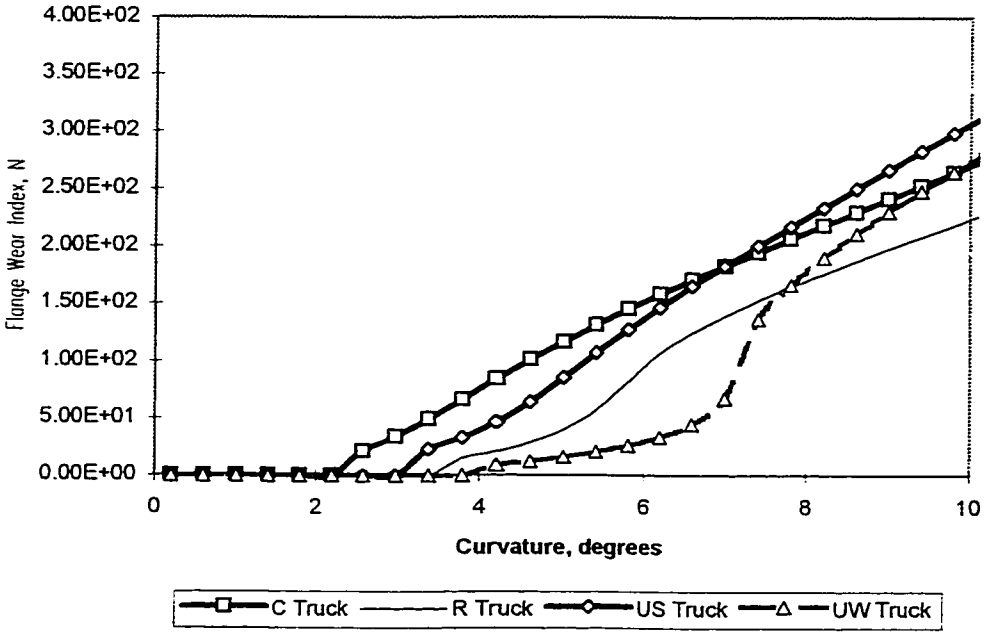

Variation of Flange Wear for Different Truck Types, λ = 0.15

Figure 4.16

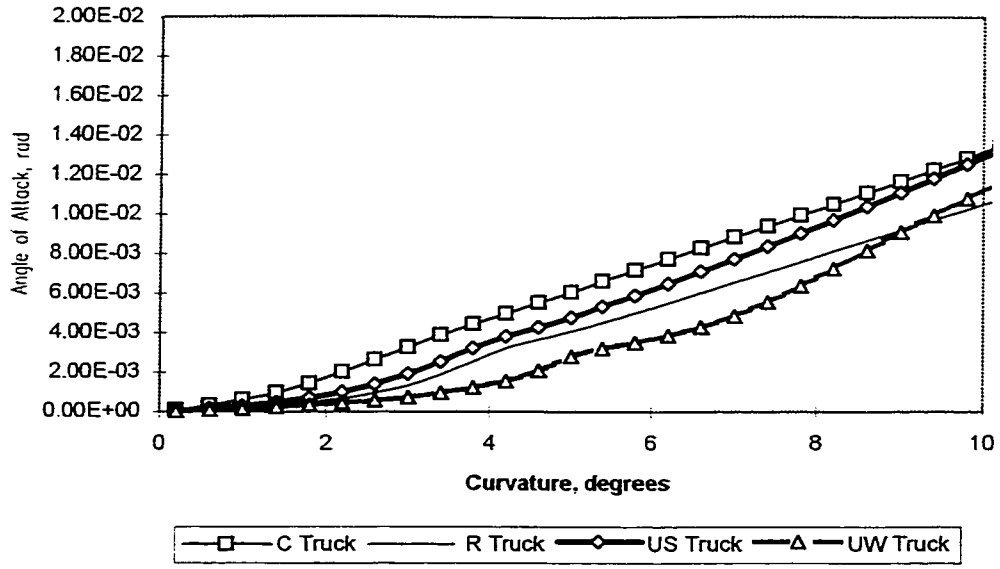

Variation of AOA for Different Truck Types, λ = 0.25

Figure 4.17

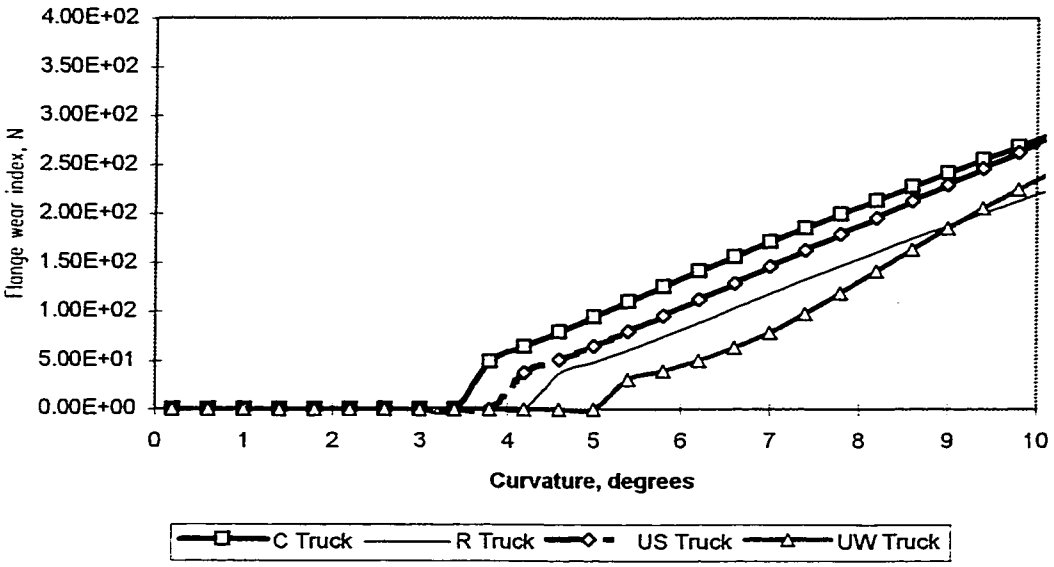

Variation of flange wear for different truck types, λ = 0.25

Figure 4.18

appears to be the same for the wheel conicity of 0.25 (Figures 4.17 and 4.18). This is due to the fact that independently rotating wheels in the rear axle of the UW truck do not contribute to steering the truck through sharp curves leading to the loss of curving performance.

Curvatures in the range of 8 degrees to 12 degrees are common on most main line tracks in North America. Over this range of curvatures, the *UW trucks* show increased angle of attack and flange wear, and hence potentially increased track maintenance and wheel and rail replacement costs in comparison to the *R truck*. From the results of on-flange curving analysis, it appears there will be little benefit in equipping the railway vehicles with *UW trucks*.

4.5 Summary

In this chapter, linear curving models were developed for the C truck, R truck and US truck. The introduction of asymmetry in the US truck improves its curving performance in comparison to the C truck. The analysis of off-flange curving and stability trade-off showed that the performance of the US truck is in between the C truck and the R truck, and the UW truck has a potential for achieving improved performance in comparison to other truck types.

However, the analysis of on-flange curving behaviour revealed that the performance of UW truck deteriorates on curvature greater than 7 degrees in comparison

to the R truck. This is because the independently rotating wheels in the rear axle of the UW truck do not contribute to proper steering of the truck through sharp curves.

Chapter 5

LATERAL STABILITY BEHAVIOUR OF MODIFIED TRUCK DESIGNS

5.1 Introduction

The lateral stability characteristics of passenger railway trucks having primary yaw dampers are evaluated in this chapter. The results of stability/curving trade-off were discussed in the previous chapter using a single truck, half car body model. It was concluded that the introduction of suspension asymmetry reduced the critical speed of the *US truck*. To improve the stability characteristics, analysis of trucks provided with yaw dampers in the primary suspension, *CD truck* and *USD truck*, are discussed in this chapter. For the analysis, a full car body model with two trucks having 17 degrees-of-freedom is considered. The development of this model with conventional trucks was discussed in Chapter 2. The equations of motion are given in Appendix C.6, equations (C-62) to (C-69). Values of design parameters for the railway passenger vehicle is given in Appendix E [7].

Creep coefficients for the tread region measured in field tests are usually lower than the theoretical value of creep coefficients observed in the laboratory controlled environment [56]. Because of the uncertainty about predicting accurate values of creep coefficients, sensitivity of truck performance to changes in creep coefficients, in addition to parameters like bending stiffness K_b and wheel conicity λ, is evaluated [57].

5.2 Conventional truck

From the eigen value analyses, critical speed as a function of bending stiffness is plotted in figure 5.1 for the conventional truck. As the bending stiffness increases, the critical speed initially increases. The critical speed increases as the effective conicity is decreased. Increasing the truck flexibility or decreasing the effective conicity results in wheel/rail creep forces in directions that reduce amplitude of kinematic oscillations. As seen from the figure, critical speed decreases for higher values of bending stiffness. This is probably because at high K_b, the amplitude of wheelset oscillation remains constant as it is disturbed from equilibrium until inertial forces cause wheel/rail creepages in directions which increase the amplitude of kinematic oscillations.

The bending stiffness to achieve a critical speed of 80 m/s is found to be 5×10^6 Nm/rad for the conicity of 0.15. If the design critical speed is 60 m/s, the value of bending stiffness required is 2.5×10^6 Nm/rad. The velocity corresponding to 10% modal damping (referred to as 10% model velocity) for the C truck is plotted in figure 5.2. The 10% modal velocity is 60 m/s for 5×10^6 Nm/rad and 45 m/s for 2.5×10^6 Nm/rad.

Figure 5.3 shows the variation of critical speed as the bending stiffness is varied for different creep coefficients. The wheel conicity is 0.15. For low values of bending stiffness, the reduction of Kalker's creep coefficient value from 100% to 50% has a stabilizing influence resulting in slightly higher critical speed. But as the bending

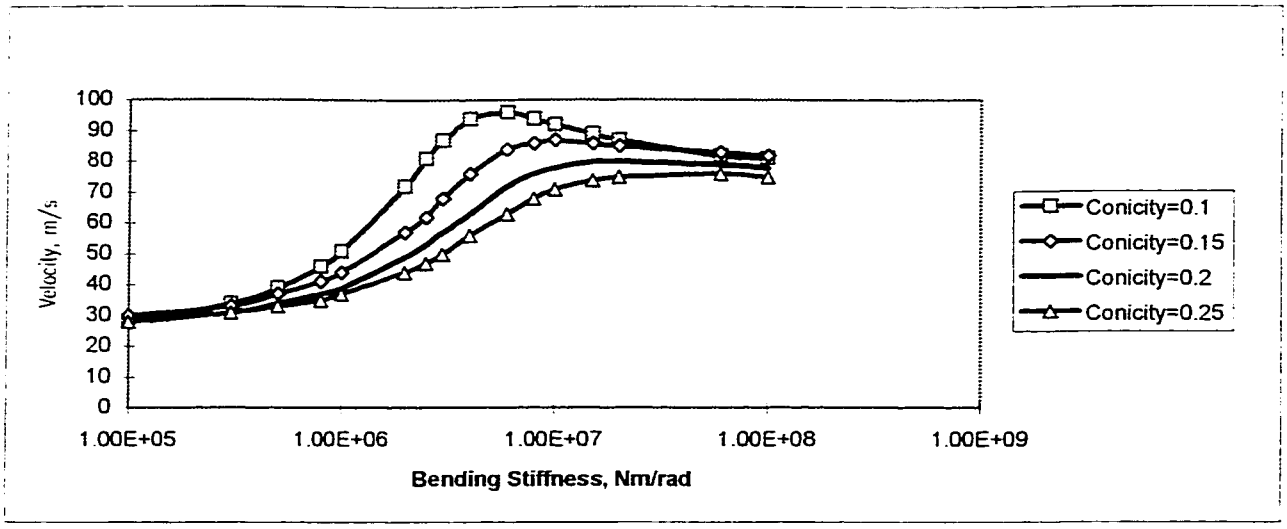

Critical Velocity for C Truck

Figure 5.1

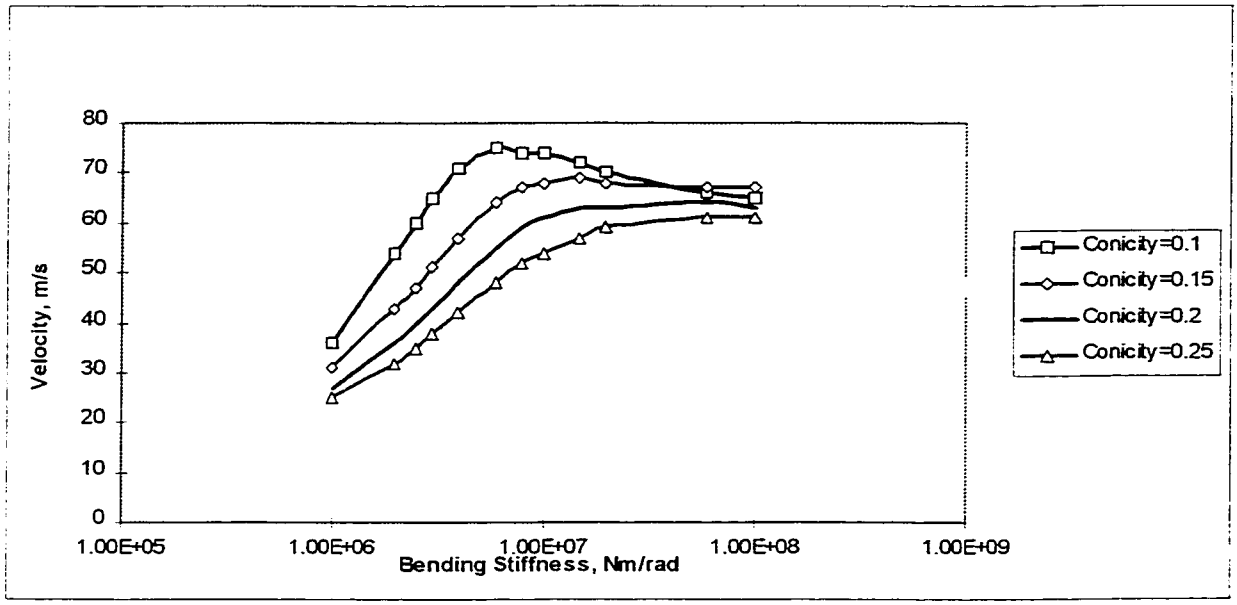

10% Modal Velocity for C Truck

Figure 5.2

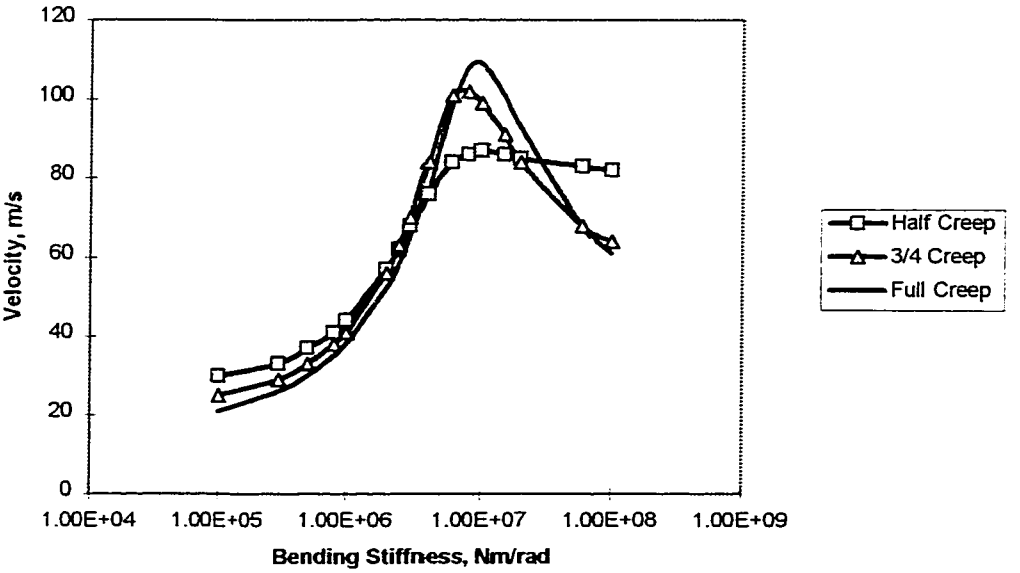

Effect of Creep Coefficient on the C Truck Stability

Figure 5.3

stiffness is increased, decreasing the creep coefficient from 100% to 50% has a destabilizing influence as the critical speed now reduces dramatically. The shift of the peak in the plot indicates that correct balance between creep forces and suspension forces influence the maximum critical speed. The reduction in the peak for the case of 50% creep coefficients indicate that inertial forces begin to dominate as creep forces are reduced.

5.3 Conventional truck with primary yaw damper

To improve the dynamic stability, stiff primary suspension is used in the conventional truck which deteriorates the curving performance. One method to improve the trade-off is by providing primary yaw dampers as shown in Figure 3.7. The yaw dampers are fitted between the wheelset and truck frame as part of the primary suspension. If the primary yaw dampers are used, the longitudinal restraint is removed for the low velocity steering motions; for higher frequency motions the damper resistance increases and the higher restraint helps to achieve desired critical speeds. Yaw dampers provided in the primary suspension helped achieve a better performance for the British Rail Class 37 locomotive as was reported by Pennington et al [52]. In this thesis, linear characteristics for the primary yaw damper are used. In reference [58], equations of motion for a single wheelset with a non-linear damper is derived.

The eigen value analysis is carried out for the CD truck with a linear yaw damper in the primary suspension. The yaw damper is characterized by the yaw damper

coefficient $C_{p\psi}$ (Ns/m) and the series damper stiffness $K_{d\psi}$ (N/m). The damper series stiffness comes from the damper end mounting and bulk modulus of the damper working medium. As the yaw damper coefficient increases, the increase in critical speed is only gradual for low values of the damper series stiffness (figure 5.4). As the damper series stiffness is increased to $2x10^6$ Nm/rad, the yaw damping coefficient has much more stabilizing influence on the truck. Accordingly, values of $C_{p\psi} = 2x10^5$ Nms/rad and $K_{d\psi} = 2x10^6$ Nm/rad are chosen. Figure 5.5 shows the variation of critical speed for different bending stiffness for the CD truck. For 50% Kalker creep values, primary bending stiffness of 1.5 million Nm/rad will achieve a critical speed of 120 m/s and 300,000 Nm/rad , a speed of 65 m/s. The velocity for 10% modal damping for 1.5 million Nm/rad is 70 m/s and for 300,000 Nm/rad is 49 m/s, as seen from Figure 5.6. Figure 5.7 shows the effect of Kalker's creep coefficient on the stability of CD truck.. For 100% Kalker creep values, bending stiffness value of $3.5x10^6$ Nm/rad will achieve a critical speed of 90 m/s and the corresponding velocity for 10% modal damping is 62 m/s. The CD truck with bending stiffness of $1.5x10^6$ Nm/rad will be stable up to a speed of 70 m/s and the corresponding velocity for 10% modal damping is 42 m/s. From figure 5.7, it is seen that 50% Kalker creep coefficient values have a stabilizing effect on CD truck. A comparison plot of critical speed for the conventional truck and CD truck for 50% Kalker creep coefficient and a conicity of 0.15, are shown in Figure 5.8. The maximum 10% modal velocity of 69 m/s achieved by C Truck when $K_b = 1.5x10^7$ Nm/rad. The CD truck attains a speed of 103 m/s when the bending stiffness is $5x10^6$

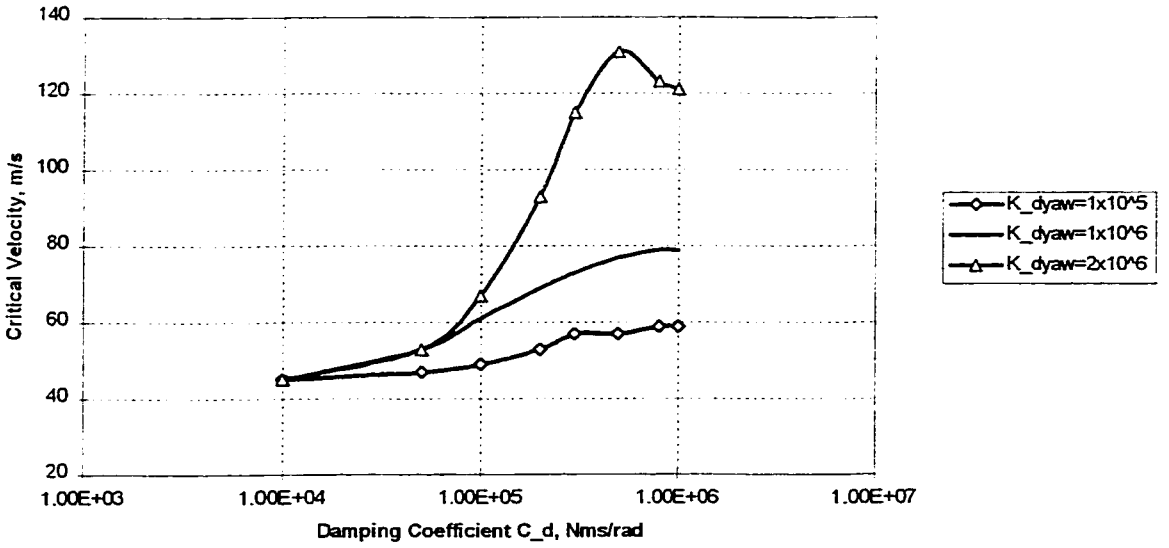

Effect of Damper Parameters for CD Truck

Figure 5.4

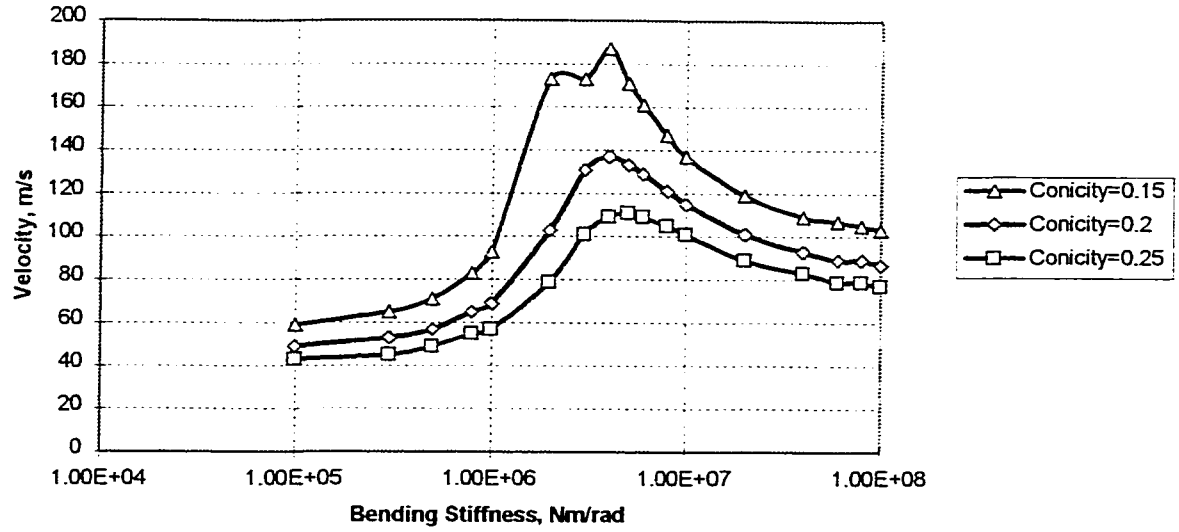

Critical Velocity for CD Truck

Figure 5.5

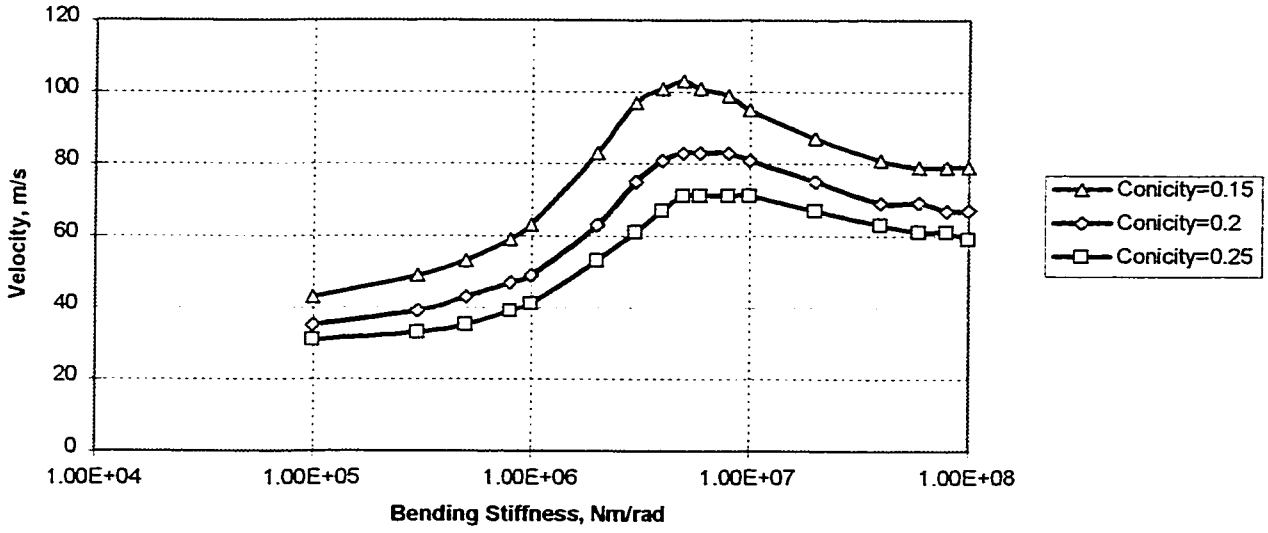

10% Modal Velocity for CD Truck

Figure 5.6

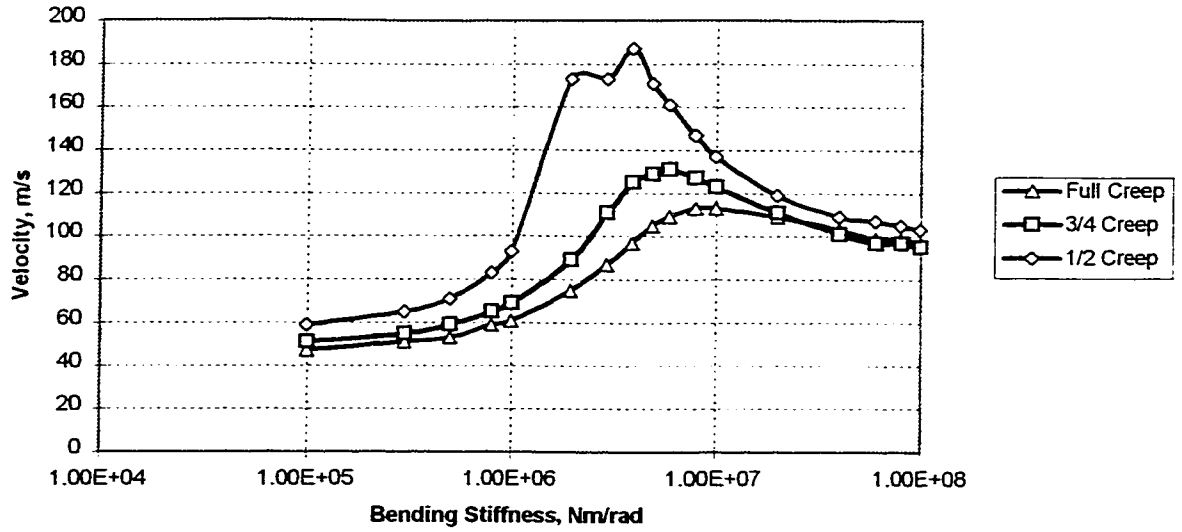

Effect of Creep Coefficient for CD Truck
Figure 5.7

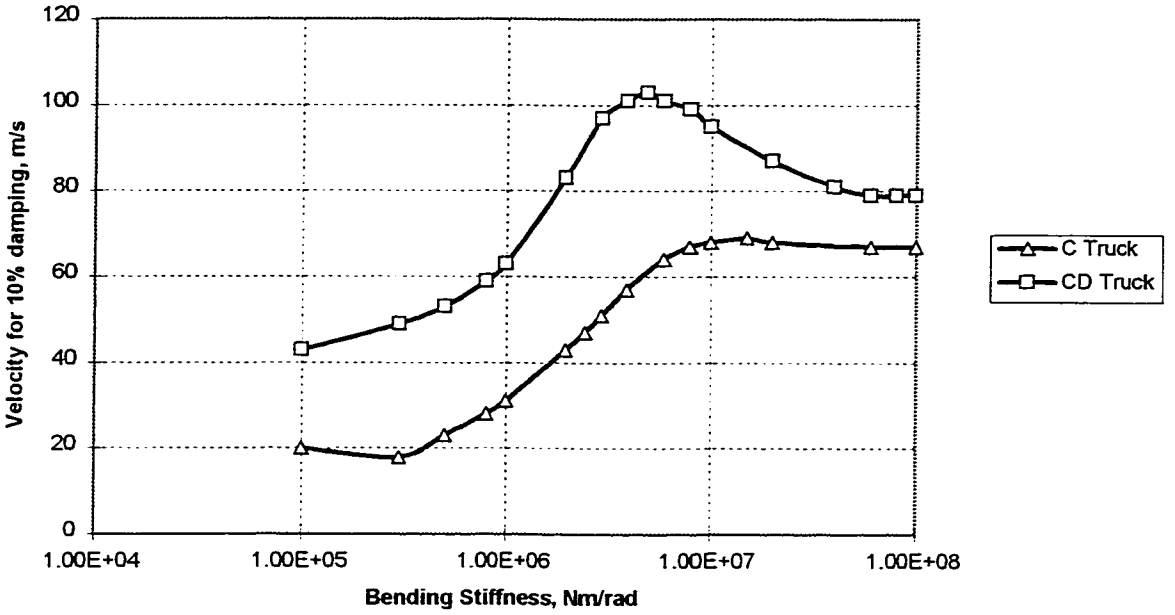

Comparison of critical velocity for C and CD Trucks
Figure 5.8

Nm/rad. The 10% modal velocity increases by 49% in the case of the CD truck in comparison to the conventional truck.

5.4 Radial Truck

The variation of critical speed with bending stiffness for the case of radial truck is shown in Figure 5.9. The radial truck shows improved stability performance compared to the conventional truck due to the influence of inter-axle shear stiffness. For the case of $\lambda = 0.15$, bending stiffness is chosen to be $1.75x10^6$ Nm/rad for the critical speed of 80 m/s and $1.25x10^6$ Nm/rad for the critical speed of 60 m/s. From figure 5.10, the corresponding 10% modal velocities are 60 m/s and 50 m/s respectively. The effect of bending stiffness on the critical speed for different Kalker creep coefficients is shown in Figure 5.11. The lower values of creep coefficient again has stabilizing effect on critical. speed for low values of bending stiffness.

5.5 Unsymmetric Suspension Truck with Yaw Damper

The variation of critical velocity with the damping coefficient of the primary yaw damper of the USD truck is shown in figure 5.12. Based on this, the damping coefficient of $C_{pw} = 2x10^5$ Nms/rad and the damper series stiffness of $K_{d\psi} = 2x10^6$ Nm/rad are selected. The variation of critical speed with bending stiffness for various values of λ, is shown in figure 5.13. From the figure, which shows the variation of critical velocity for 50% Kalker creep values, a bending stiffness of $7.43x10^5$ Nm/rad

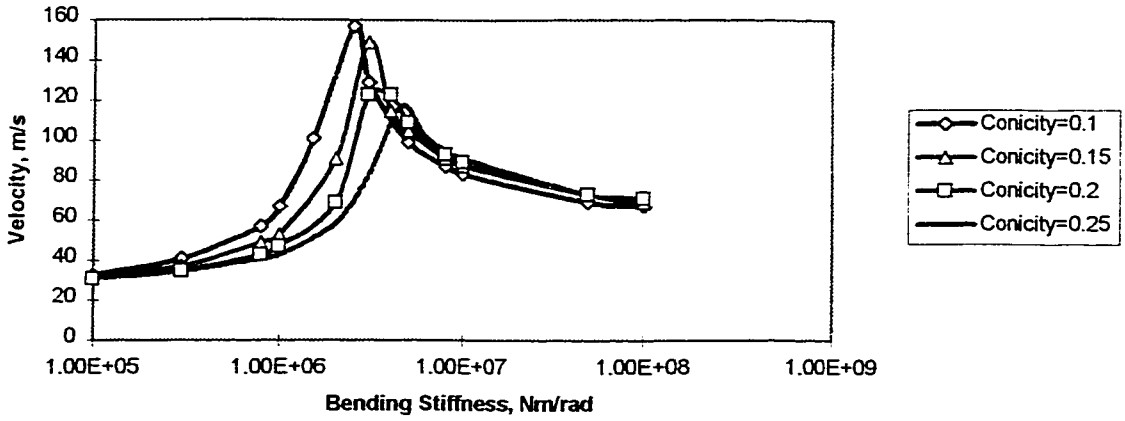

Critical Velocity for R Truck

Figure 5.9

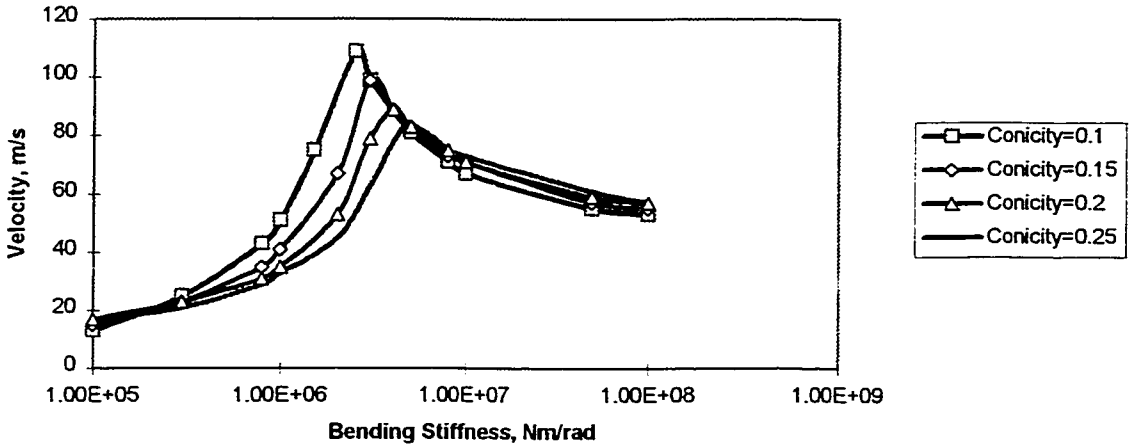

10% Modal Velocity for R Truck

Figure 5.10

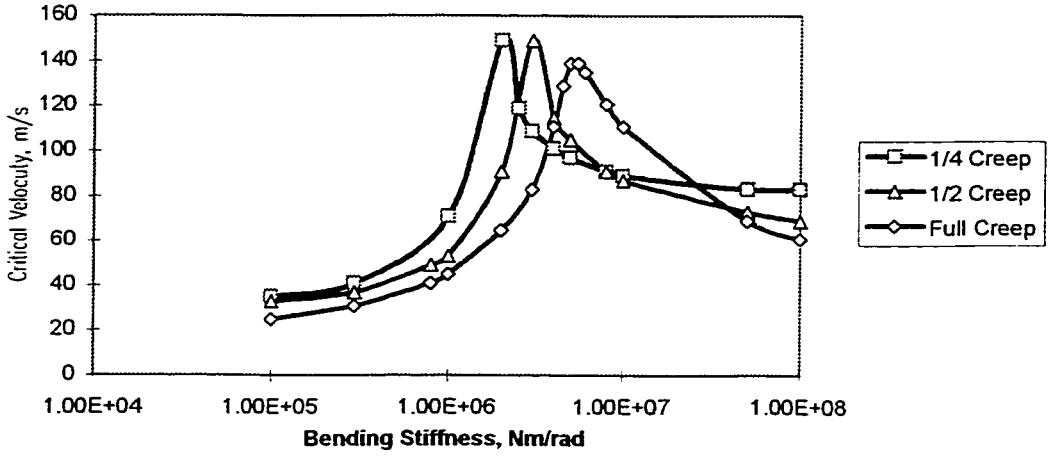

Effect of Creep Coefficients in R Truck

Figure 5.11

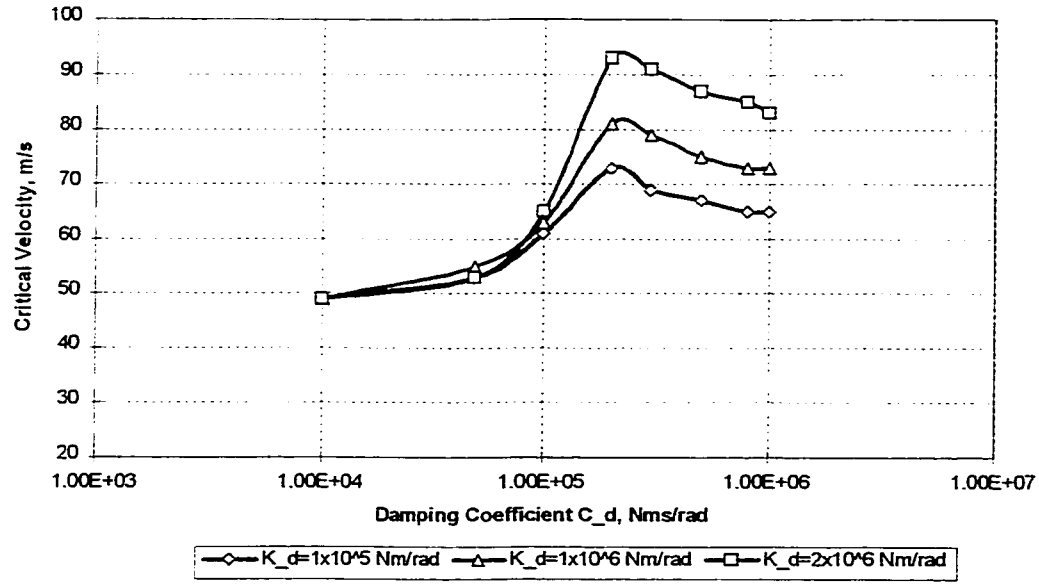

Variation of Critical Velocity with Damper Coefficient

Figure 5.12

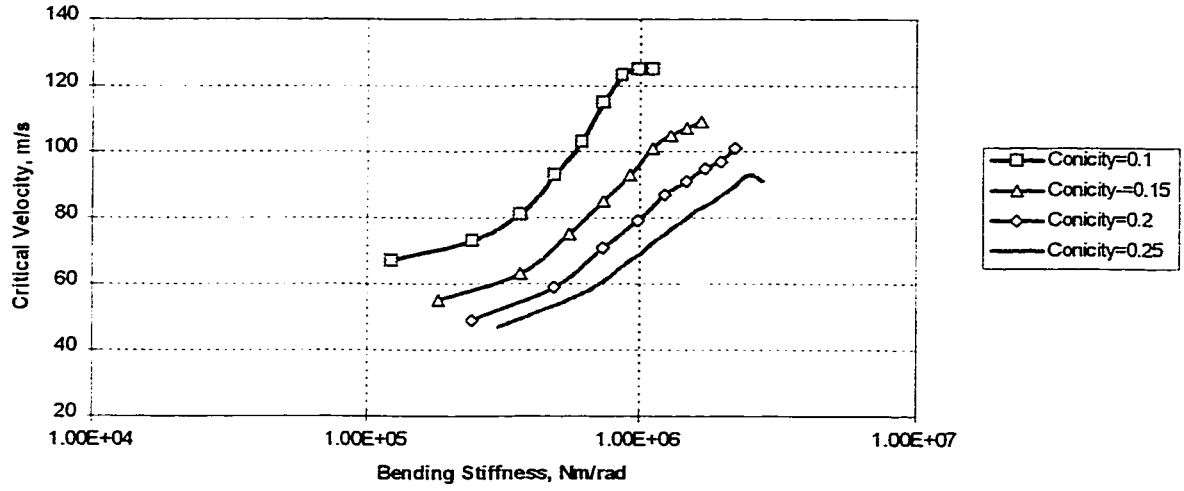

Critical Velocity for USD Truck – Half Creep

Figure 5.13

for the wheelset conicity of 0.15 is required to achieve a critical speed of 85 m/s and $3.71x10^5$ Nm/rad is required to achieve a critical speed of 63 m/s. If the USD truck is designed with $K_b = 1.11x10^6$ Nm/rad, the critical velocity will be 101 m/s and the corresponding velocity for 10% modal damping will be 81 m/s. The critical velocity for 100% creep coefficient is plotted in figure 5.14 . The critical velocity of 103 m/s and 10% modal velocity of 89 m/s will be attained using full Kalker creep values when the bending stiffness is $2.23x10^6$ Nm/rad. Table 5.1 summarizes the values of bending stiffness parameter required to achieve minimum critical velocities of 80 m/s and 60 m/s for various truck designs.

5.6 Summary

As seen from results of the stability analysis discussed in this chapter, the stability of a railway vehicle truck is influenced by the dynamic balance of suspension forces, wheel/rail creep forces and inertia forces. Suspension forces, which increase with bending stiffness, stabilize the truck by reducing the amplitude of wheelset kinematic oscillations and help to achieve higher critical speeds. Inertia forces destabilize the truck by increasing the amplitude of wheelset kinematic oscillations.

A full car body model with 17 degrees of freedom was used to analyze the stability behaviour of modified truck designs. A model with primary yaw damper was developed to improve the stability behaviour of the conventional truck and unsymmetric suspension truck. Suitable values of yaw damper parameters were chosen through the analysis. The

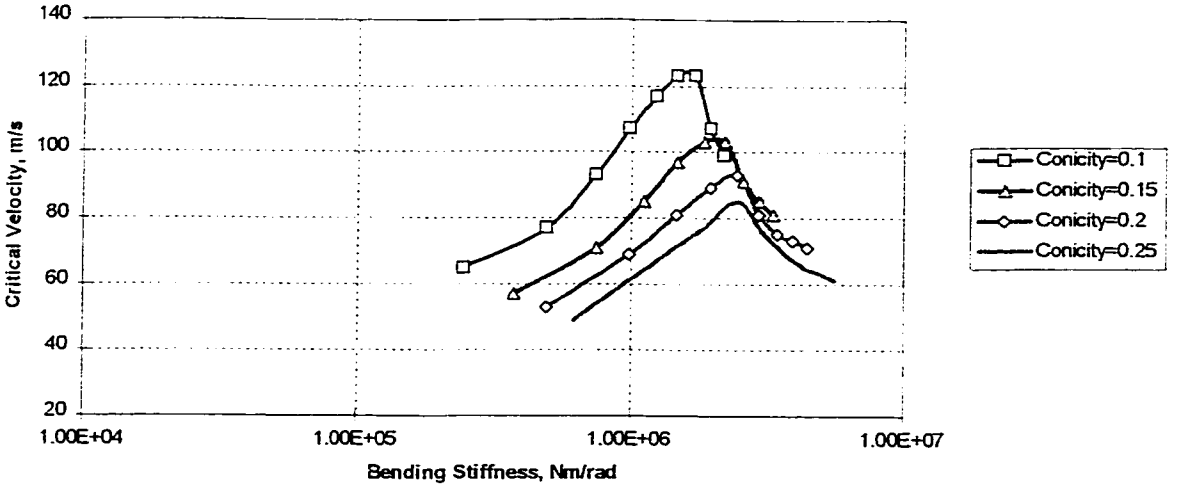

Critical Velocity for USD Truck - Full Creep

Figure 5.14

Truck type	Kalker's Creep Value	Bending Stiffness Nm/rad CV 80 m/s	CV 60 m/s	Remarks
C truck	50%	$5.0x10^6$	$2.5x10^6$	
	100%	$4.5x10^6$	$3.0x10^6$	
R truck	50%	$1.75x10^6$	$1.25x10^6$	
	100%	$3.0x10^6$	$2.0x10^6$	
CD truck	50%	$1x10^6$	$3x10^5$	
	100%	$3.5x10^6$	$1.5x10^6$	
USD truck	50%	* $7.43x10^5$	** $3.71x10^5$	* asymmetric ratio = 0.4
	100%	* $1.49x10^6$	** $7.43x10^5$	** asymmetric ratio = 0.2

Bending Stiffness for different truck configurations

Table 5.1

values of primary suspension stiffnesses, K_b and K_s, were selected for design critical speeds of 60 m/s and 80 m/s. In the next chapter, steady state curving behaviour of these truck designs will be analyzed using a steady state, non-linear model.

CHAPTER 6

Steady State, Non-Linear Curving Analysis and Comparison with NUCARS

6.1 Introduction

In this chapter, the curving analysis of different truck configurations is carried out using a steady state, non-linear curving model. In this model, effects of wheel/rail geometric non-linearities as described in Section 2.2.2 and creep force saturation as described in Section 2.3.3 in Chapter 2 are included. The equations of force and moment equilibrium for a single wheelset were derived in Section 2.5.1. The vehicle model includes a truck and has the same eight degrees of freedom used in Chapter 4 for the steady state, linear curving model.

The displacement vector is calculated by solving the following steady-state non-linear equation:

$$KY = F(y) \tag{6.1}$$

where K is the suspension stiffness matrix, Y is a vector of vehicle displacements and $F(y)$ are the external forces and moments acting on the vehicle. The analytical technique is a multi-step iteration on the simultaneous equations of motion for which the IMSL subroutine is used.

6.2 Analysis of simulation results

The performance of different truck designs are compared using the Steady State

(SS) curving program. The simulation results will be presented in terms of wheelset yaw angle or the angle of attack (AOA), wheel lateral force and wear index.

One of the objectives for the present investigation is to reduce wheel and rail wear in curves. The wear index suggested by Elkins and Allen is used [12]. It is based on the premise that rates of wheel and rail wear can be related to the forces and creepages between the wheels and the rail. Mathematically, the work done in the contact patch is equal to the dot product of the resultant creep force vector with the resultant creepage:

$$W = F_c \bullet \xi_c \tag{6.2}$$

In the above equation, W is the work done in the contact patch, F_c is the resultant creep force vector and ξ_c is the resultant creepage. The wear index is not necessarily indicative of the actual wear in wheel-rail contact patch. But a comparison of wear index for different truck configurations could be done as a means of measuring their curving performance.

The trucks considered for evaluation are the Conventional Truck (*C Truck*), Radial Truck *(R Truck*), Conventional Truck provided with Yaw Damper (*CD Truck*), and Unsymmetric Suspension Truck with Yaw Damper (*USD truck*). The suspension parameters, bending stiffness and shear stiffness, are chosen for two critical speeds, 80 m/s and 60 m/s from the results presented in Chapter 5.

Figures 6.1 and 6.2 present the equilibrium free body diagrams obtained from the computer simulation results as the trucks negotiate a 10 degree curve (175 m radius). The figures show all the creep and suspension forces and the moments generated during steady state curving for the C Truck and USD Truck. A constant centre plate moment input of 7702 N-m is assumed for each case. The figures shown are for 50% Kalker creep coefficients. The trucks have a design critical speed of 80 m/s.

The centre plate yaw moment is reacted by wheel/rail lateral forces and wheelset yaw moments. The moment balance is given by the equation,

$$M_{cp} + 2f_{lw}b + M_{w1} + M_{w2} = 0 \tag{6.3}$$

where

M_{cp} = Centre plate yaw moment

M_{w1}, M_{w2} = Wheelset yaw moments on axles 1 & 2

f_{lw} = Wheelset lateral force

b = Truck wheelbase

In order for the wheelset to achieve equilibrium on curved track, a positive angle of attack is required, which results in a positive lateral creep force on the leading wheel on the inside rail (refer to Figure 6.1). The lateral creep force pushes the wheelset into the flange at the outside rail, causing the outside wheel to develop an increased rolling radius. The magnitude of the angle of attack is determined by the magnitude of the lateral creep force balance. The yaw moment applied on the wheelset by the suspension is reacted by

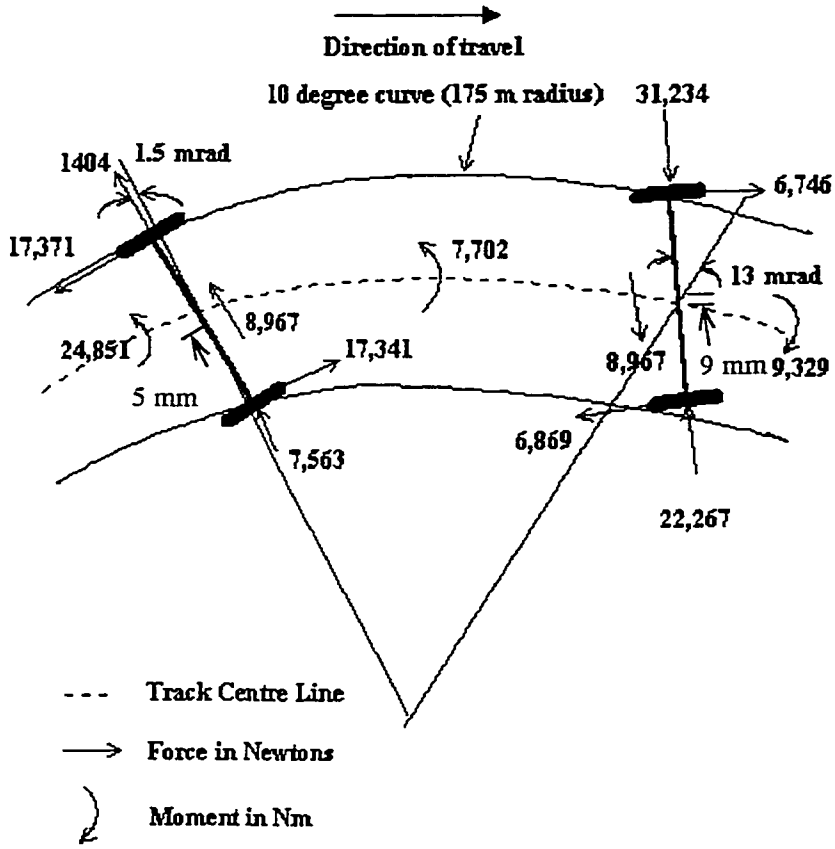

Steady State Curving Attitude of C Truck

Figure 6.1

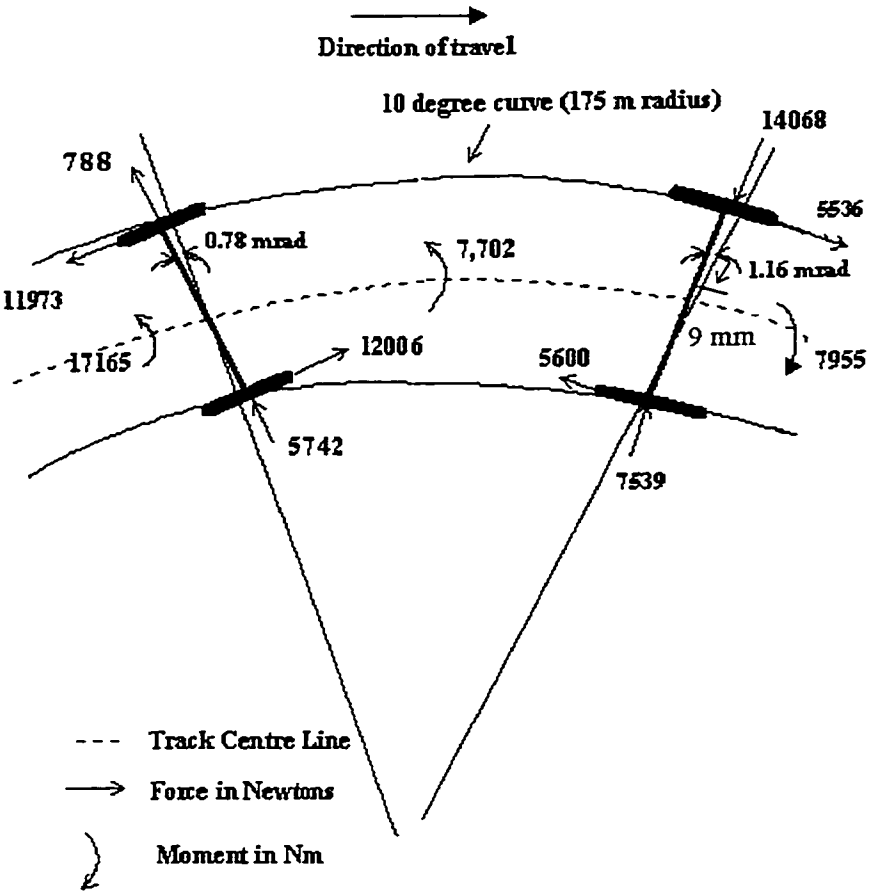

Steady State Curving Attitude of USD Truck

Figure 6.2

the longitudinal creep forces, generated from the rolling radius difference.

Referring to figure 6.1, for the C truck, 31,234 N of lateral force is generated on the leading, high rail wheel with an angle of attack of 13 mrad. For the USD truck (figure 6.2), 14068 N of lateral force is generated with an AOA of 1.16 mrad in the leading wheelset. It is seen that better steering capability of the USD truck reduces the AOA and the resulting lateral force.

In the following sections, results of the simulation are given in terms of Angle of Attack (AOA), lateral force on lead high rail wheel and wear index. These parameters are analyzed for 100% and 50% Kalker creep coefficients. Creep coefficients in reality could vary over a wide range of values, due to contamination of the rail surface, work hardening etc. The 100% Kalker creep values would represent a clean, uncontaminated and dry surface. From Table 5.1 it is seen that trucks in general need higher primary bending stiffness for 100% creep coefficient values to achieve the same critical speed as compared to the case of 50% creep coefficient values.

6.2.1 Angle-of-Attack of Leading Axle

Figure 6.3 compares the leading wheelset AOA for 100% Kalker creep values. The trucks are designed to achieve a critical speed of 80 m/s. For the C truck, the angle of attack rapidly increases as the curvature is increased. The angle of attack of 15.6 mrad is developed in the lead axle as the truck negotiates a 12 degree curve (146 m radius). The AOA is 13.1 mrad for the R truck, 14.3 mrad for the CD truck and 7.63 mrad for the

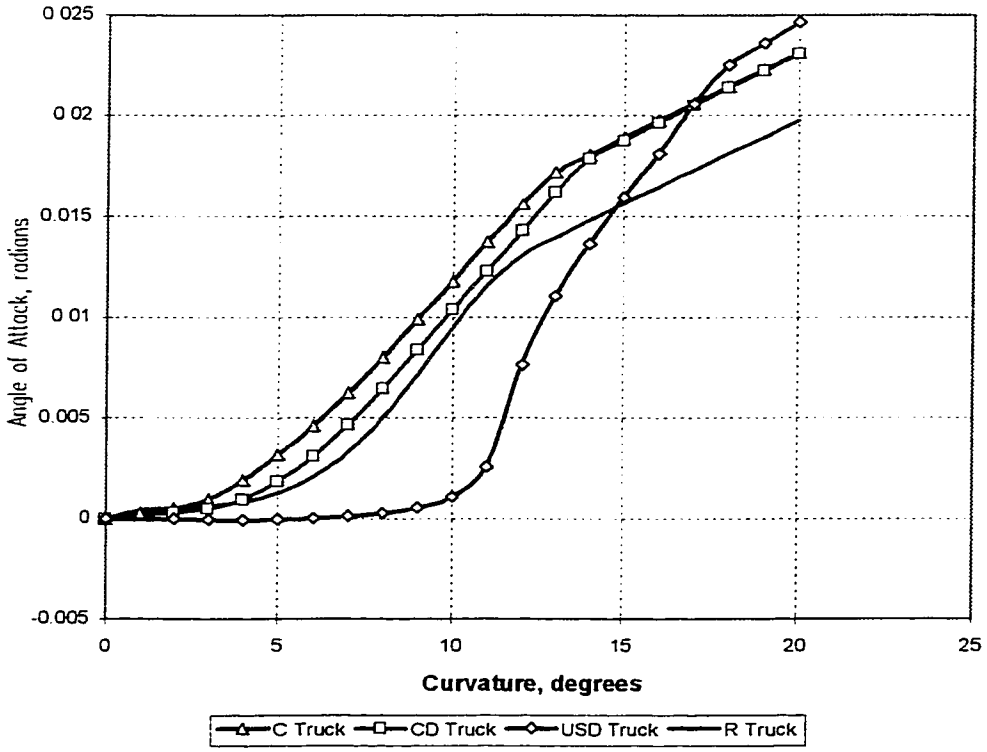

Angle of Attack for Leading Axle (100% Kalker Creep Coefficient)

Figure 6.3

USD truck. The USD truck provides the lowest buildup of angle of attack up to a curvature of 12 degrees. This is because the truck is designed to achieve perfect steering with an unsymmetric index a_{ps} as given by the equation (4.6). The lower value of bending stiffness provided in the USD truck also helps it to achieve better steering through the curve. Beyond this curvature, the angle of attack for the USD truck increases dramatically and the AOA is higher than the R truck for curvatures beyond 15 degrees. This is probably because the R truck is designed with high shear stiffness helping it achieve lower flange forces on tight curves.

The variation of angle of attack shown in Figure 6.4 is for the case of 50% Kalker creep coefficient. On a 12 degree curve, the angle of attack is 16.4 mrad for the C truck, 8.7 mrad for the R truck, 3.7 mrad for the CD truck and 1.85 mrad for the USD truck. In general, the AOA is higher for 100% Kalker creep values compared to the case of 50% Kalker creep value. The performance of the CD truck deteriorates most rapidly as the Kalker creep value increases from 50% to 100%. The values of AOA for half creep and full creep values are tabulated for two design critical speeds of 80 m/s and 60 m/s in Table 6.1. It is seen that USD truck achieves superior performance compared to other truck designs on the 12 degree curve.

6.2.2 Lateral Force on the Leading Axle

The lateral forces exerted on the high rail wheel are shown in Figures 6.5 and 6.6 for the case of full and half creep values respectively. The direction of forces on the rails

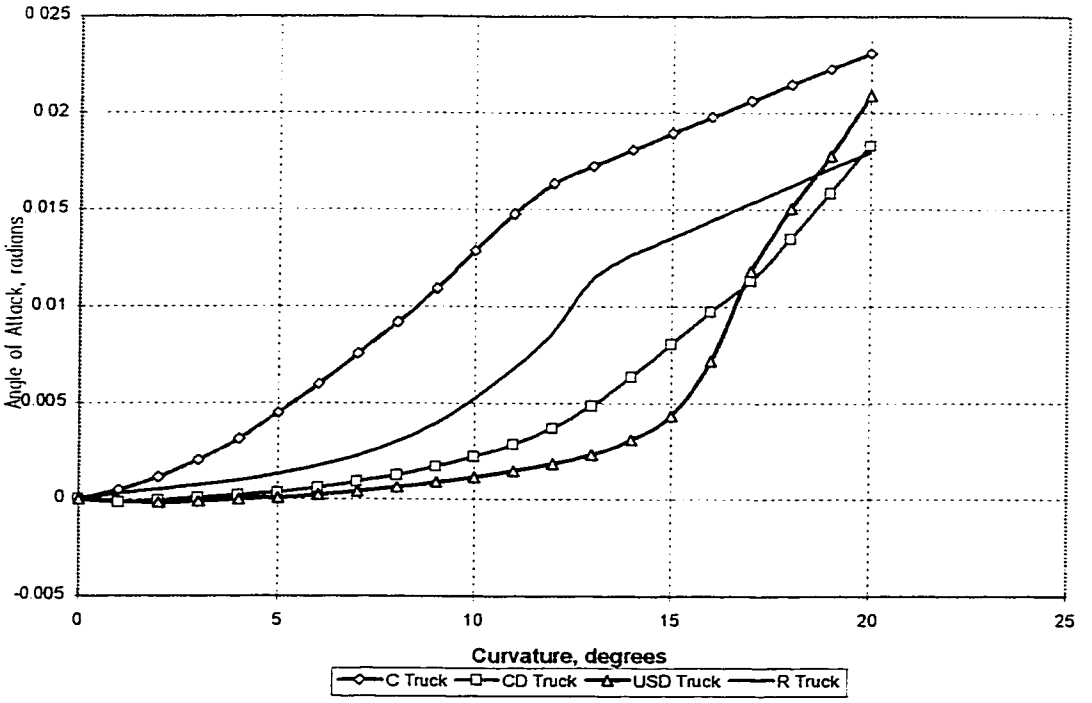

Angle of Attack for Leading Axle (50% Kalker Creep Coefficient)

Figure 6.4

Truck type	Design Critical Speed 80 m/s				Design Critical Speed 60 m/s			
	Full Creep		Half Creep		Full Creep		Half Creep	
	Front	Rear	Front	Rear	Front	Rear	Front	Rear
C Truck	15.6	1.67	16.4	1.95	13.2	1.4	12.5	1.5
R Truck	13.1	1.3	8.66	1.39	1.6	0.54	4.25	1.17
CD Truck	14.3	1.54	3.7	1.0	4.85	0.83	1.8	1.6
USD Truck	7.63	1.1	1.85	0.95	0.84	0.75	1.62	1.54

Angle of Attack of front and rear wheelsets in mrad on a 12 degree curve

Table 6.1

Truck type	Design Critical Speed 80 m/s				Design Critical Speed 60 m/s			
	Full Creep		Half Creep		Full Creep		Half Creep	
	High	Low	High	Low	High	Low	High	Low
C Truck	-33483	22566	-33476	22629	-32928	22403	-32105	22461
R Truck	-32966	22380	-30612	21708	-20134	12986	-24104	16744
CD Truck	-33203	22486	-21343	15783	-28163	20658	-13903	10324
USD Truck	-30877	21770	-18032	10297	-13127	8423	-14415	9658

Lead wheelset lateral forces in Newton on a 12 degree curve

Table 6.2

exerted by the wheels cause gauge widening of the track. As the track curvature increases, the lateral flange force required to keep the lateral displacement of the lead wheelset exceeding the available flange clearance increases and approaches the adhesion limit between wheel and rail. The unsymmetric truck configuration, USD truck, provides the lowest rate of buildup of flange contact force in comparison to the other configurations in the curvature range of 1 - 12 degrees. Table 6.2 compares the lateral force on the high rail wheel on a 12 degree curve.

The ratio of lateral force to vertical force on a wheel, more commonly referred as L/V ratio, gives an indication of the derailment potential of a truck. Typically, a value of L/V ratio larger than 1.0 is not desirable and all the trucks analyzed have ratios below this threshold during steady state curving.

6.2.3 Truck Wear Index

One major objective in the evaluation of curving behaviour is to reduce wheel and rail wear in curves. The variation of wear index for the different truck designs are shown in Figures 6.7 and 6.8 for 100% and 50% Kalker creep values. The trucks are designed for a critical speed of 80 m/s. The wear index for the conventional truck increases sharply as curvature increases. The wear index for the USD truck is less than other designs in the curvature range. Table 6.3 compares the wear index for different truck designs on a 12 degree curve.

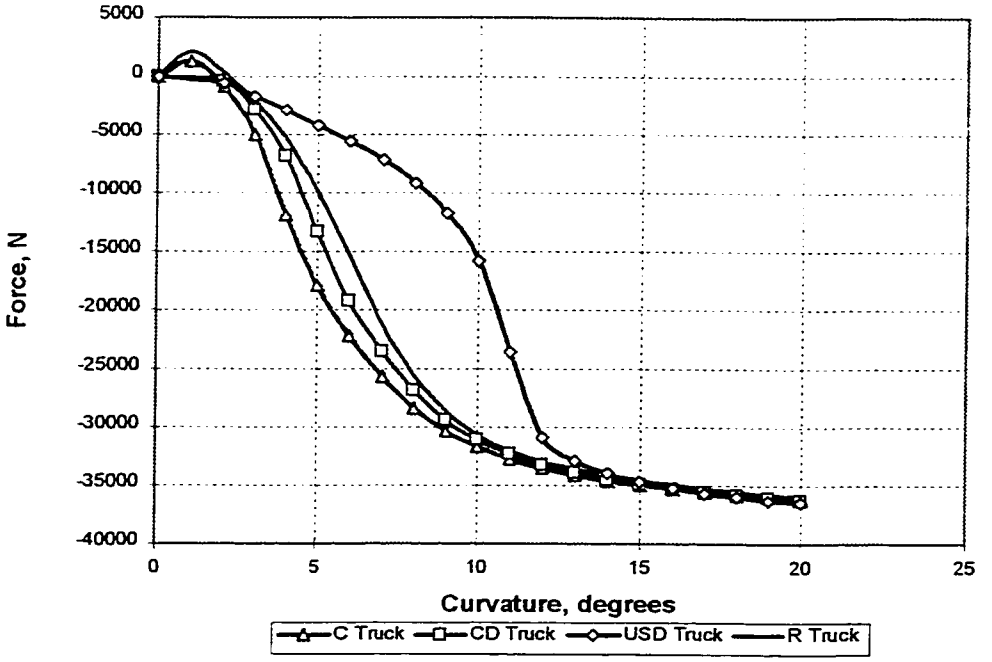

Lateral Force on Lead High Rail Wheel (100% Kalker Creep Coefficient)

Figure 6.5

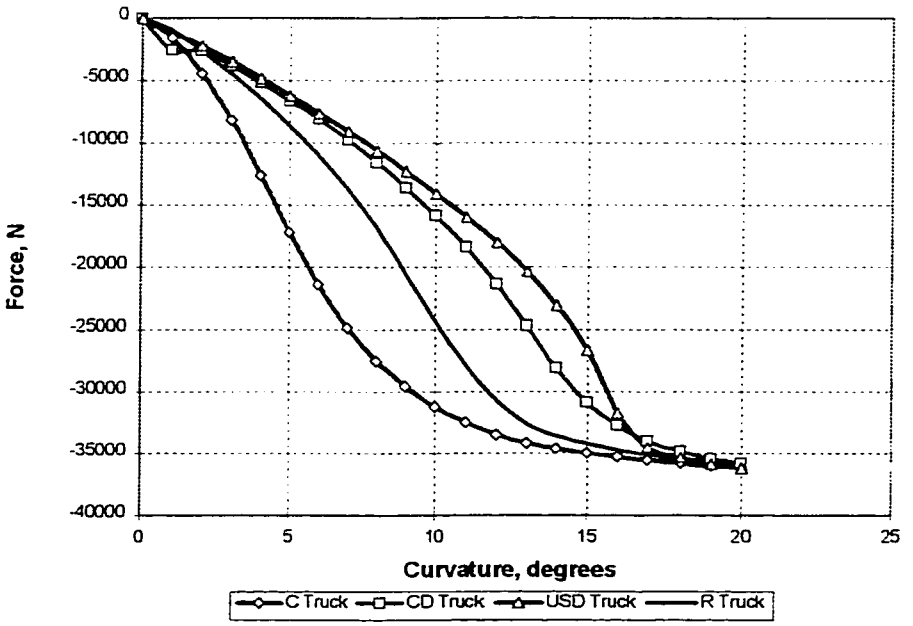

Lateral Force on Lead High Rail Wheel (50% Kalker Creep Coefficient)

Figure 6.6

6.2.4 Summary of Simulation Results

The curving performance indices used in the steady state curving program are angle of attack, wheel lateral force and truck wear index. The analysis has shown that USD truck achieves better curving performance in comparison to other truck designs on curvatures up to 12 degrees. On most main line tracks in the North American Railways, the curvatures are in the range of 1 to 12 degrees. Thus it is seen that the curving performance of the USD truck would be superior to the other truck configurations for main line operations. In the next section, the results obtained here will be validated using a commercially available software program.

6.3 Curving Analysis using NUCARS

NUCARS (New and Untried Car Analytic Regime Simulation) is a general purpose, multi-body dynamic program used in the modeling and simulation of railway vehicles [59]. This program was developed by Association of American Railroads (AAR). This program has undergone extensive validation since its development and is an industry-wide standard in North America.

NUCARS models a rail vehicle system as a collection of interconnected lumped masses. Each rigid body can have multiple connections and each connection is defined by a resilient and dissipative element that is configured properly to represent the physical connections between the bodies. A variety of connections in a series or parallel

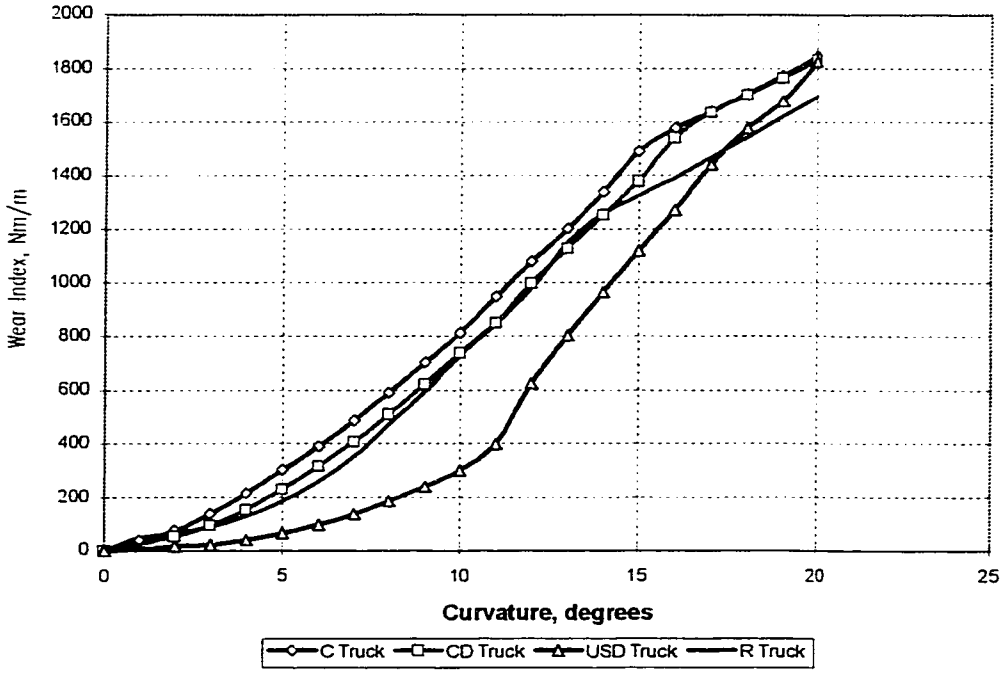

Wear Index per Truck (100% Kalker Creep Coefficients)

Figure 6.7

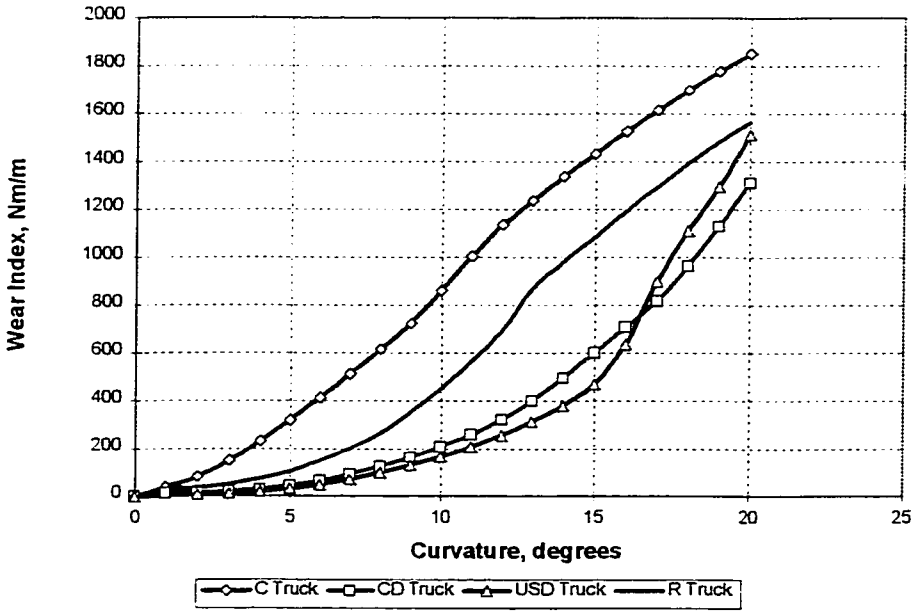

Wear Index per Truck (50% Kalker Creep Coefficients)

Figure 6.8

	Design Critical Speed 80 m/s		Design Critical Speed 60 m/s	
Truck type	Full Creep	Half Creep	Full Creep	Half Creep
C Truck	1079	1137	920	857
R Truck	976	695	577	437
CD Truck	996	322	462	177
USD Truck	624	257	242	173

Wear Index per Truck in Nm/m on a 12 degree curve

Table 6.3

arrangement can be modelled with either linear or nonlinear properties as discussed in [60].

In the following sections, curving performance of different truck designs are evaluated using NUCARS. The objective is to compare the results of the steady state curving analysis obtained earlier with results from NUCARS. Thus an indirect validation of the steady state curving analysis program has been carried out.

6.3.1 Angle of Attack

The leading axle angles of attack for C truck, CD truck and USD truck predicted by NUCARS are shown in figures 6.9 and 6.10. As seen from Table 5.1, the CD truck requires a bending stiffness in the range of $3x10^5$ N/m to $1.5x10^6$ N/m, depending on the creep coefficient considered, to achieve a critical speed of 60 m/s. For half Kalker creep values, the CD truck has a softer primary suspension compared to the USD truck. As the creep coefficient is increased, much higher primary bending stiffness is required for CD truck to maintain the same critical speed compared to the USD truck. The result is improved steering for the entire curvature range for the USD truck as seen in figure 6.10. Figures 6.11 and 6.12 show a similar trend when the trucks are designed for a critical speed of 80 m/s.

6.3.2 Lateral force on the Leading Axle

The lateral force on the high rail wheel obtained from NUCARS simulations are plotted in figures (6.13) and (6.14). The design critical speed is 80 m/s. The trend is similar to the plots in figure 6.5 and 6.6 obtained from the steady state curving program. The absolute values of lateral force obtained from NUCARS simulation for the USD truck are higher compared to the steady state program. Still the USD truck achieves the lowest lateral force compared to the C truck and CD truck.

6.3.3 Wheel/Rail Resistance

The wear index developed in NUCARS is similar to the one defined earlier by equation 6.1. It relates the energy dissipated in the contact patch to the wheel wear. By summing the wear indices for all wheel/rail contact points on a vehicle the total rolling resistance of the vehicle due to wheel on rail contact is obtained in NUCARS. This is a measure of the drag induced in the wheel/rail contact area. The rolling resistance obtained from NUCARS is different from the wear index used earlier in the steady state curving analysis in that it takes into account wheel/rail wear of two trucks.

Figures 6.15 and 6.16 compare the total wheel/rail resistance values for the different truck designs for the critical speed of 80 m/s. The trend is similar to the wear index plot shown in figures 6.7 and 6.8.

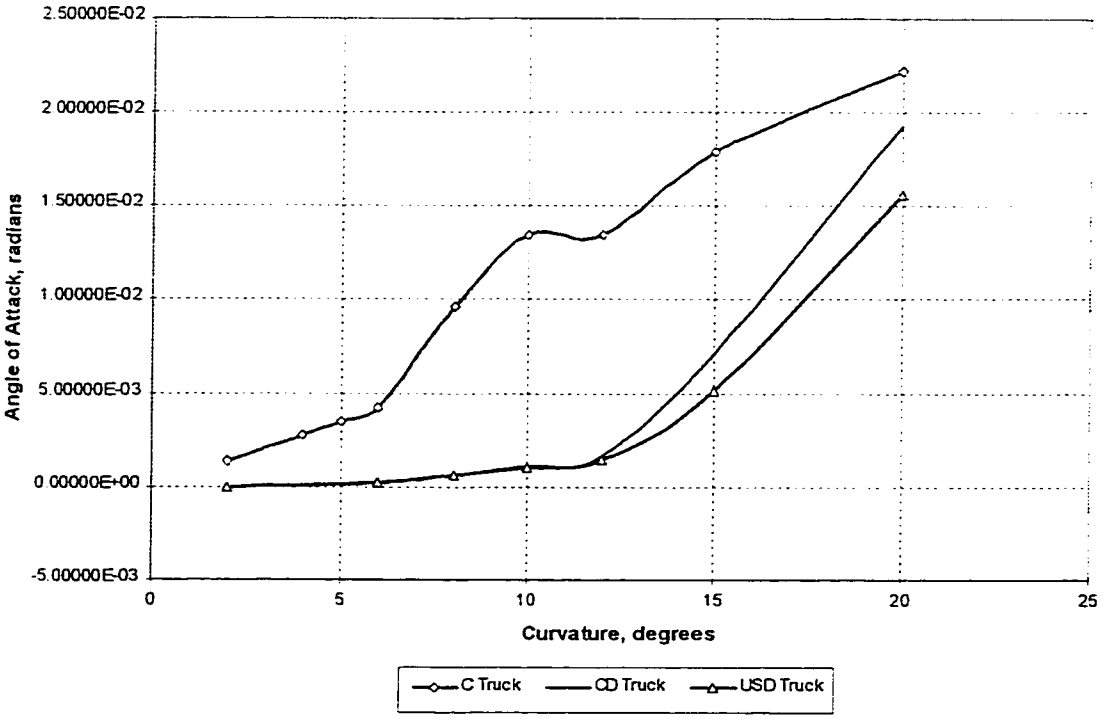

Angle of Attack from NUCARS, Critical Speed 60 m/s

(K_b values correspond to half creep)

Figure 6.9

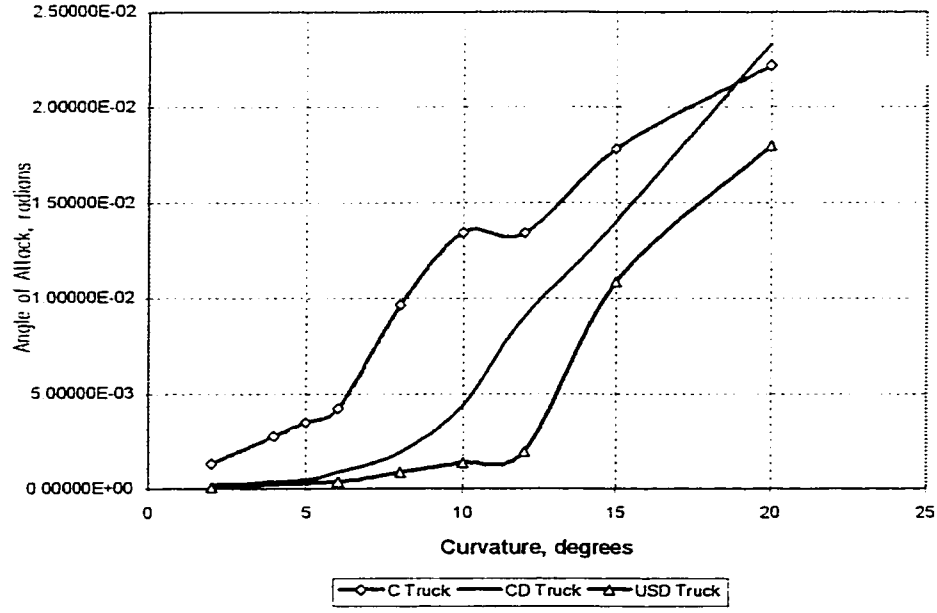

Angle of Attack from NUCARS, Critical Speed = 60 m/s

(K_b values correspond to full creep)

Figure 6.10

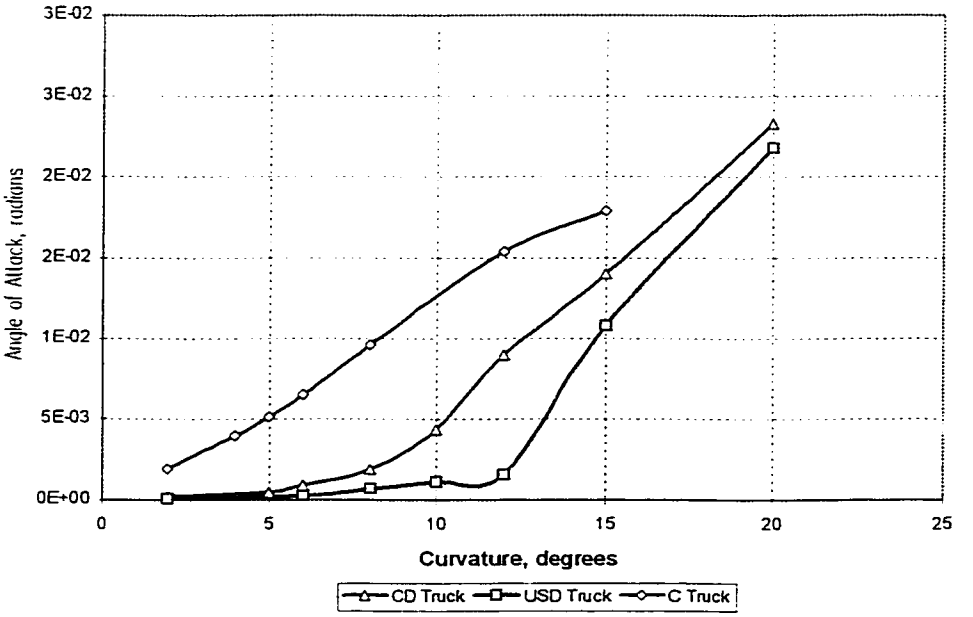

Angle of Attack predicted by NUCARS, Critical Speed = 80 m/s

(K_b values correspond to half creep)

Figure 6.11

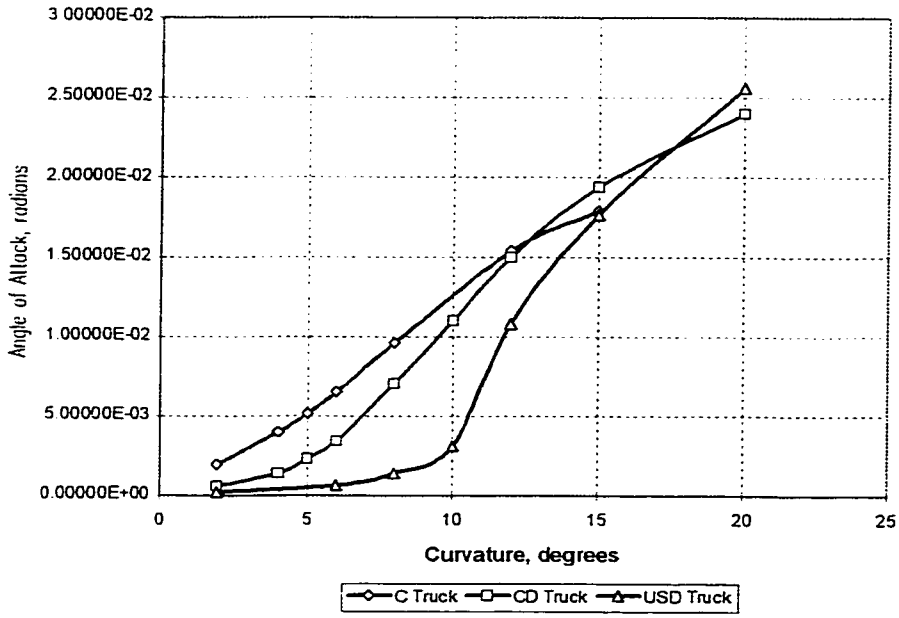

Angle of Attack predicted by NUCARS, Critical Speed = 80 m/s

(K_b values correspond to full creep)

Figure 6.12

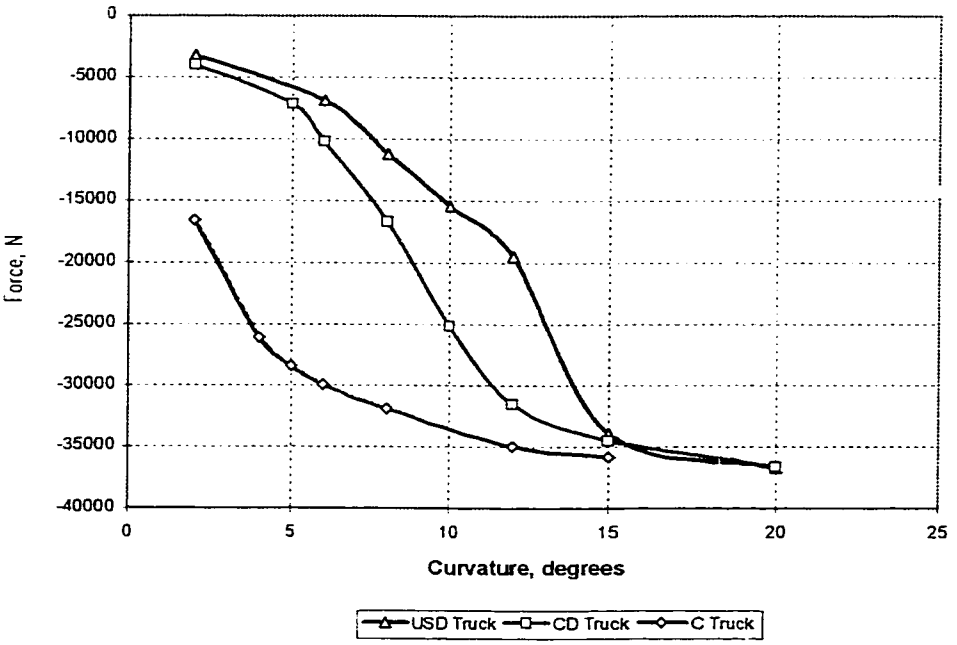

Lateral force on the high rail wheel, critical speed 80 m/s

(K_b values correspond to half creep)

Figure 6.13

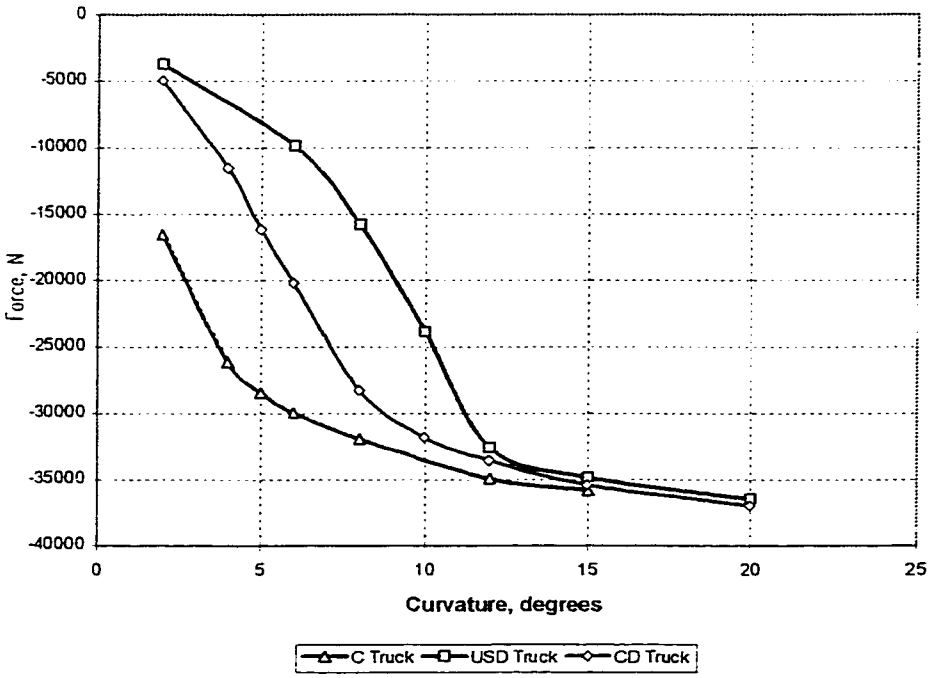

Lateral force on the high rail wheel, critical speed 80 m/s

(K_b values correspond to full creep)

Figure 6.14

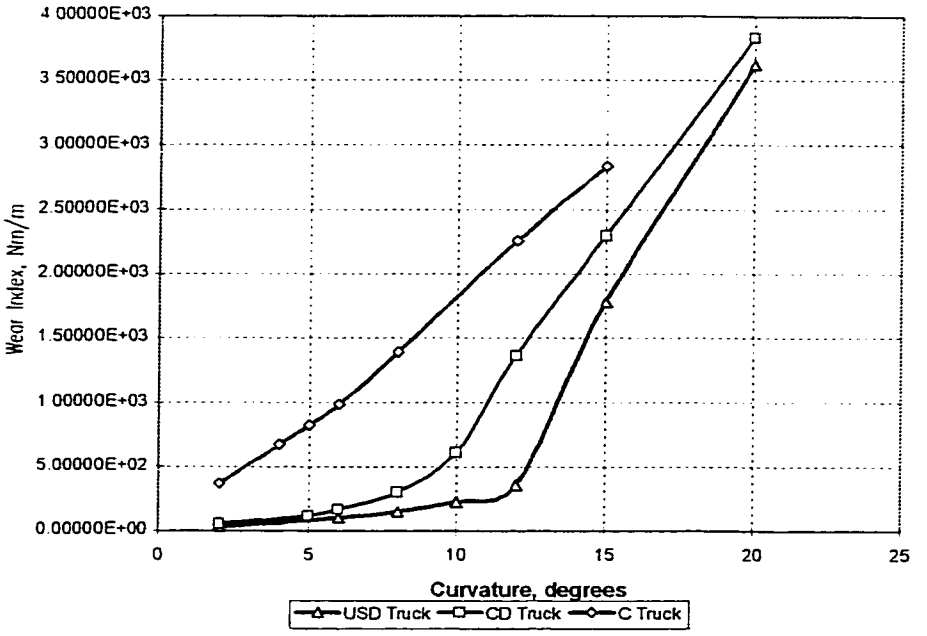

Total Wheel/Rail Resistance predicted by NUCARS

(K_b values correspond to half creep)

Figure 6.15

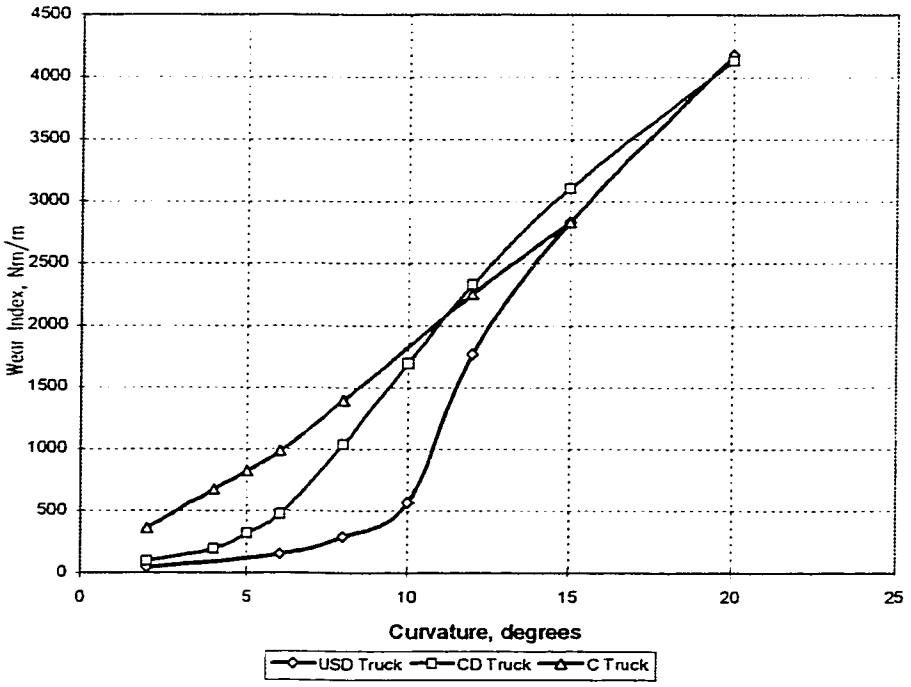

Total Wheel/Rail Resistance predicted by NUCARS

(K_b values correspond to full creep)

Figure 6.16

6.3.4 Comparison of NUCARS simulations with the SS curving model

Tables 6.4, 6.5 and 6.6 compare the values of angle of attack, wheel lateral force and the wear index per truck obtained from NUCARS with that obtained from the steady state curving model on a 12 degree curve for the critical speed 80 m/s. The predicted AOA by the steady state curving program is 15.6 mrad and 1.67 mrad for the front and rear wheelsets. The corresponding values predicted by NUCARS is 15.4 mrad and 0.7 mrad for the front and rear wheelsets respectively. The lateral forces for the high rail wheel are 33483 N and 34936 N for the steady state curving program and NUCARS respectively. Results of CD truck simulations using NUCARS also match reasonably with results of steady state curving simulations. The performance of CD truck is much superior to the C truck as predicted by NUCARS for the truck with stiffness parameters designed for half creep. For CD truck, designed for the critical speed of 80 m/s for full creep coefficients, a lateral force of 33,581 N is predicted by NUCARS. This is in comparison to the value of 33,203 N predicted by the SS curving model. The values of AOA of the lead wheelset predicted by NUCARS for an USD truck on a 12 degree curve is 10.8 mrad and the lateral force is approximately 32,595 N. The corresponding values for the USD truck from the steady state curving model are 7.63 mrad and 30,877 N. Thus the USD truck achieves the best curving performance compared to other truck designs for curvatures up to 15 degrees. This is attributable to the better steering capabilities of the truck with usymmetric suspension and lower bending stiffness for the truck with the yaw dampers.

Truck type	AOA, mrad (NUCARS)		AOA, mrad (SS Curving)	
	Front	Rear	Front	Rear
C Truck	15.4	0.7	15.6	1.7
CD Truck, $K_b = 1.5x10^6$	9	1.6	3.7	1.0
CD Truck, $K_b = 3.5x10^6$	15	1.7	14.3	1.54
USD Truck, $K_b = 7.42x10^5$	1.57	1.58	1.85	0.95
USD Truck, $K_b = 1.485x10^6$	10.8	1.43	7.63	1.1

Comparison of Angle of Attack on a 12 degree curve

Critical Speed = 80 m/s

Table 6.4

Truck type	Lateral Force, N (NUCARS)		Lateral Force, N (SS Curving)	
	Front	Rear	Front	Rear
C Truck	-34936	22231	-33483	22566
CD Truck, $K_b = 1.5x10^6$	-31503	21724	-21343	15783
CD Truck, $K_b = 3.5x10^6$	-33581	21974	-33203	22486
USD Truck, $K_b = 7.42x10^5$	-19495	12503	-18302	10297
USD Truck, $K_b = 1.485x10^6$	-32595	21831	-30877	21770

Comparison of lateral force on a 12 degree curve

Critical Speed = 80 m/s

Table 6.5

Truck type	**Wear index/truck, Nm/m (NUCARS)**	**Wear index/truck, Nm/m (SS Curving)**
C Truck	1129	1079
CD Truck, $K_b = 1.5x10^6$	683	322
CD Truck, $K_b = 3.5x10^6$	1166	996
USD Truck, $K_b = 7.42x10^5$	177.5	257
USD Truck, $K_b = 1.485x10^6$	884	624

Comparison of wear index on a 12 degree curve

Critical Speed = 80 m/s

Table 6.6

The steady state curving attitude of the USD truck on a 10 degree curve is shown in the figure 6.17. The forces and moments shown in the figure are values predicted by NUCARS. This figure can be compared to the results of the steady state curving analysis shown in figure 6.2. For the *C truck*, comparison of results from NUCARS in terms of the angle of attack and lateral force with that of the steady state curving model are given in Figures 6.18 and 6.19 respectively. The corresponding plots for the *USD truck* are given in Figures 6.20 and 6.21.

One of the main differences between the two programs is the computation of wheel/rail interaction forces. In NUCARS, forces are computed using Kalker's non-linear creep theory. The non-linear creep force results for a wide variety of creepage, contact geometry and normal force conditions generated on the basis of Kalker's non-linear theory is stored in a table. This tabular data includes the effect of spin and is referred in the computations. The steady state curving model computes the wheel/rail forces using Kalker's linear theory, and then limits these forces when necessary by an approximate method based on Johnson's non-linear theory. This method ignores the effect of spin creep, which become dominant as the truck negotiates sharp curvatures. This may possibly explain the slight differences in values obtained from the two programs.

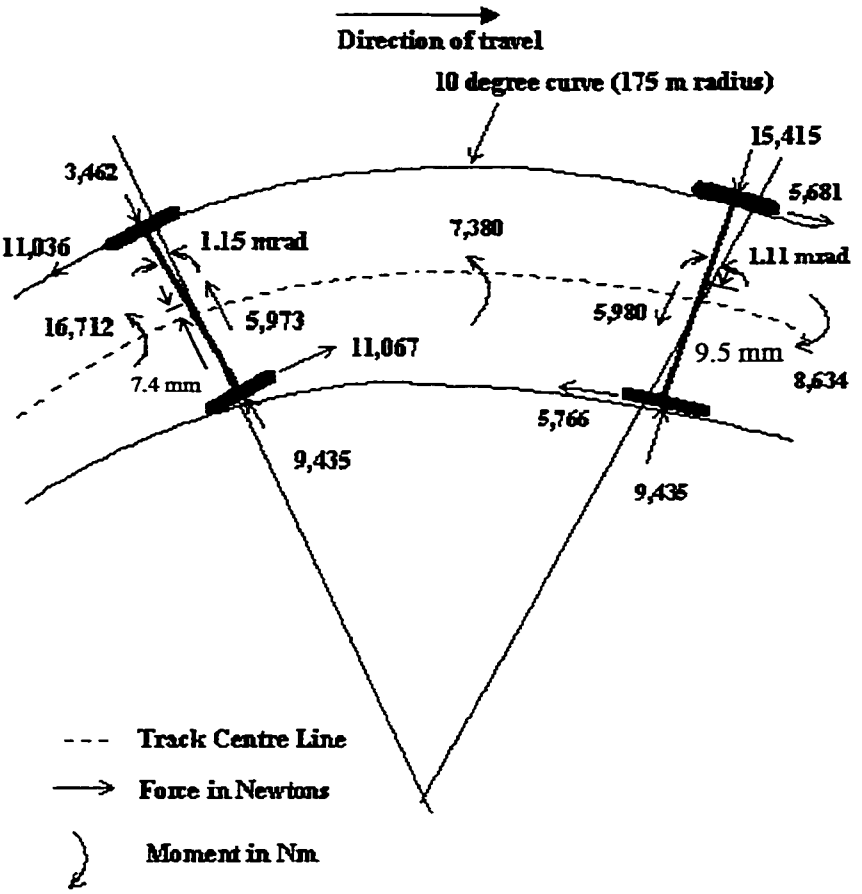

Steady State Curving Attitude of USD Truck predicted by NUCARS

Figure 6.17

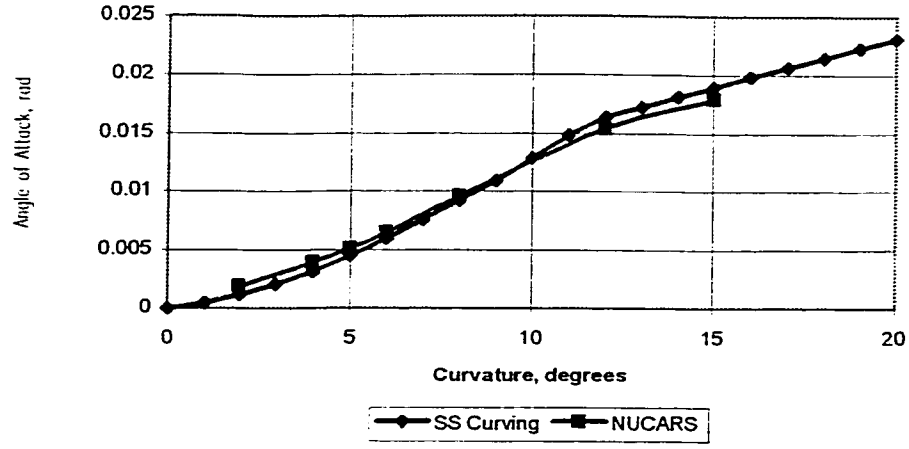

Comparison of AOA from NUCARS with Steady State Curving for C Truck

Figure 6.18

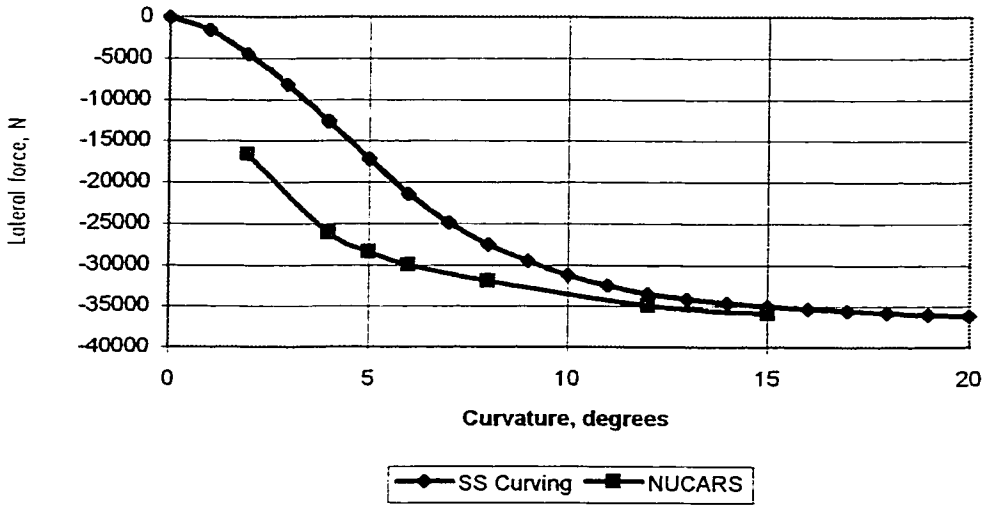

Comparison of Lateral Force from NUCARS with Steady State Curving for C Truck

Figure 6.19

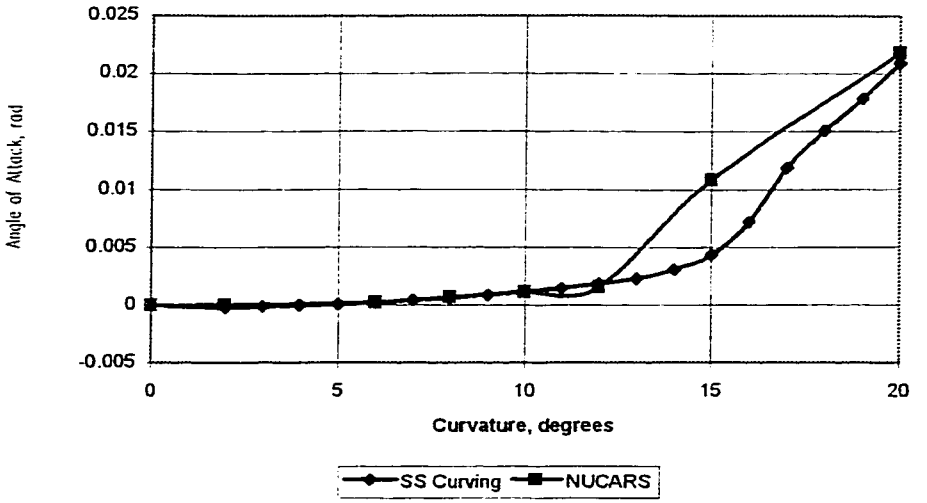

Comparison of AOA from NUCARS with Steady State Curving for USD Truck

Figure 6.20

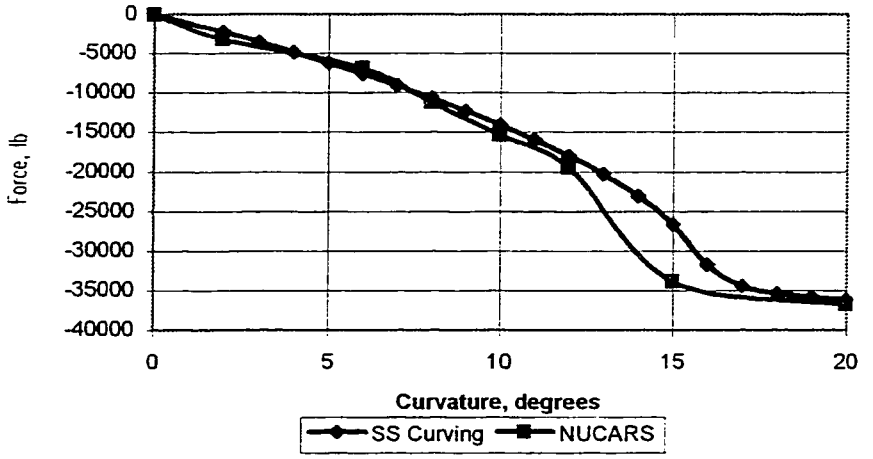

Comparison of Lateral Force from NUCARS with Steady State Curving for USD Truck

Figure 6.21

6.4 Summary

In this chapter, steady state curving behaviour of modified truck designs were studied using a non-linear, steady state curving program. The non-linearities included in the models were wheel/rail geometry, wheel/rail contact forces and the secondary yaw stiffness. The trucks considered for evaluation were the Conventional Truck (*C Truck*), Radial Truck *(R Truck)*, Conventional Truck provided with Yaw Damper (*CD Truck*), and Unsymmetric Suspension Truck with Yaw Damper (*USD truck*). The suspension parameters, bending stiffness and shear stiffness, are chosen for two critical speeds, 80 m/s and 60 m/s from the results presented in Chapter 5.

The results were presented in terms of the angle of attack of the leading wheelset, lateral force on the leading, high rail wheel and wear index. The analysis showed that USD truck could be designed to achieve better over all performance on main line operations where curvatures vary between 1 to 12 degrees. The results of steady state curving program were validated using the commercial software package NUCARS. The comparison of results obtained from NUCARS analysis shows good agreement with the SS curving model. The comparison of steady state curving behaviour of different truck designs using NUCARS also showed that USD truck has the potential to achieve superior performance compared to the other truck designs. For the USD truck to be bi-directional, switched dampers as discussed in Section 3.6 in Chapter 3 have to be provided.

Chapter 7

SUMMARY, CONCLUSIONS AND RECOMMENDATIONS FOR FUTURE RESEARCH

7.1 Summary

In this thesis, modified passenger railway vehicle truck designs have been investigated with an objective to improve the compatibility between the dynamic stability and curving ability. A trade-off analysis of lateral stability on tangent track and curving for conventional truck (*C truck*), radial truck (*R truck*), unsymmetric suspension truck (*US truck*) and unsymmetric wheelset truck (*UW truck*) has been carried out. Based on these off-flange and on-flange trade-off analysis, *C truck* and *US truck* are modified for improved stability performance by providing yaw dampers in the primary suspension. These truck designs are: (a) a conventional truck with the damper referred to as *CD truck* (b) a *US truck* with the damper known as *USD truck*. Suitable design parameters for the yaw damper are selected through the analysis. Suspension design guidelines are developed for the modified truck designs.

A non-linear, steady state curving model has been developed. The curving performance of *C truck, R truck, CD truck* and *USD truck* are evaluated using a non-linear steady state curving model. The creep force saturation and wheel/rail geometry are the non-linear effects considered in the model. Secondary yaw stiffness is the only

suspension non-linearity considered. The curving performance indices used in the steady state curving program are angle of attack, wheel lateral force and truck wear index.

New and Untried Car Analytic Regime Simulation (NUCARS) , a multi-body dynamic program used in the simulation of railway vehicles, has been used to validate the results of the steady state curving program. NUCARS has been developed by the Association of American Railroads (AAR) and has undergone extensive validation since its development. The comparison of results obtained from NUCARS analysis shows good agreement with the steady state curving model.

The technology that would hasten the deployment of a high-speed rail passenger service is that which can improve the safety, reliability, cost-effectiveness and revenue generating potential of such a service. It is shown that the unsymmetric suspension truck with primary yaw damper achieves better compatibility between the dynamic stability and curving behaviour than existing truck designs. Such a railway vehicle with the unsymmetric suspension trucks and primary yaw dampers can potentially be operated on existing rights-of-way without the need for massive investments for new track infrastructure.

7.2 Conclusions

1. It is possible to design a *US truck* to achieve perfect steering on curves. The introduction of asymmetry in the *US truck* improves its curving performance in

comparison to the *C truck*. However, introduction of asymmetry in the US truck deteriorates its lateral stability and lowers the critical speed. An off-flange curving and stability trade-off has been carried out by optimizing suspension parameters for the different truck designs. The analysis shows that the performance of the *US truck* is better than the *C truck*. An optimized *UW truck* has the potential to achieve the best off-flange curving/stability trade-off in comparison to the other truck configurations.

2. The analysis of on-flange curving behaviour revealed that the performance of the *UW truck* deteriorates on curvature greater than 7 degrees in comparison to the *R truck*. This is because the independently rotating wheels in the rear axle of the UW truck do not contribute to proper steering of the truck through sharp trucks. Curvatures in the range of 8 degrees to 12 degrees are common on most main line tracks in North America. Over this range of curvatures, the *UW trucks* show increased angle of attack and flange wear, and hence potentially increased track maintenance and wheel and rail replacement costs in comparison to the *R truck*. From the results of on-flange curving analysis, it appears there will be little benefit in equipping the railway vehicles with independently rotating wheelsets.

3. By choosing suitable values of primary yaw dampers, it is possible for *CD truck* and *USD truck* to achieve higher critical speed in comparison to *C truck* and *US truck* for a given bending stiffness. The non-linear curving analysis has shown that *USD truck* achieves better curving performance in comparison to other truck designs on curvatures up to 12 degrees. On most main line tracks in the North American Railways, the

curvatures are in the range of 1 to 12 degrees. The curving performance of the *USD truck* would be superior to the other truck configurations for main line operations. Thus it is possible for a properly designed *USD truck* to achieve near perfect steering *as well as* good maintain dynamic stability.

4. The analysis of performance using NUCARS also shows that USD truck has better curving behaviour compared to other truck designs for curvatures up to 12 degrees. The trend in performance predicted by NUCARS for the different truck designs is the same as obtained from the steady state curving model.

7.3 Recommendations for future research

1. Tangent track analysis has been carried out in this thesis using linear wheel/rail profile geometry and linear suspension characteristics. A non-linear analysis of the rail vehicle for the stability and forced lateral response will be useful in a quantitative evaluation of the modified truck designs. Such an analysis should include wheel/rail profile, creep force and suspension nonlinearities.

2. The research reported in this thesis has dealt with steady state curving behaviour. To look into the safety implications of the new designs, transient behaviour in curves must be studied. The response of the railway cars in entry and exit spirals should be evaluated. The effects of track irregularities on the response of cars with these modified truck designs need to be analyzed. Any further model refinement should also consider rail flexibility.

3. Experimental investigation of the stability behaviour of the CD truck and USD truck would be useful to study the ability of the dampers to provide increased restraint to achieve desired critical speeds. Of particular importance will be the development of a switched damper for easy bi-directional operation of the railway car.

References

1. Wickens, A.H., "General Aspects of the Lateral Dynamics of Railway Vehicles," *Journal of Engineering for Industry*, Trans. ASME, Series B, Vol. 91, Nov. 3, Aug. 1969, pp.869-878.

2. Newland, D.E., "Steering Characteristics of Bogies," *The Railway Gazette*, Oct. 4 1968, pp. 745-750.

3. Boocock, D., "Steady State Motion of Railway Vehicles on Curved Tracks," *Journal of Mechanical Engineering Science*, Vol. 11, No. 6, 1969, pp. 556-566.

4. Garg, V.K., and Dukkipati, R.V., *Dynamics of Railway Vehicle Systems*, Academic Press, Toronto, 1984.

5. Law, E.H. and Cooperrider, N.K., "A Survey of Railway Vehicle Dynamics Research," *ASME Transactions*, Vol. 98, Series G, No. 2, June 1974, pp. 132-146.

6. Wickens, A.H., " Steering and Dynamic Stability of Railway Vehicles, " *Vehicle System Dynamics*, Vol. 5, 1975/1976, pp. 15-46.

7. Wormley, D., Hedrick, K., Horak, D., Bell, C., "Rail Passenger Vehicle Truck Design Methodology," *FRA Report No. FRA/ORD-81/11*, January, 1981.

8. Gasch, R. et al, "Stability and Forced Vibrations of a 4-Axled Railway Vehicle with Elastic Car Body," *Proceedings of 5th VSD - 2nd IUTAM Symposium, Vienna, September*, 1977, pp. 464-480.

9. Hedrick, J.K. and Arslan, A.V., "Nonlinear Analysis of Rail Vehicle Forced Lateral Response and Stability," Transactions of the ASME, *Journal of Dynamic Systems, Measurement & Control*, Vol. 101, September 1979, pp. 230-237.

10. Elkins, J.A. and Gostling, R.J., "A general quasi-static curving theory for railway vehicles," *Proceedings of 5th VSD - 2nd IUTAM Symposium*, Vienna, September, 1977, pp. 388-406.

11. Elkins, J.A., and Eickhoff, B.M., "Advances in Nonlinear Wheel/Rail Force Prediction Methods and Their Validation," *Journal of Dynamic Systems, Measurement and Control*, Transactions of the ASME, Vol. 104, June 1982, pp. 133-142.

12. Elkins, J.A. and Allen, R.A., "Verification of a Transit Vehicle's Curving Behaviour and Projected Wheel/Rail Wear Performance," *Journal of Dynamic Systems, Measurement and Control*, Transactions of the ASME, Vol. 104, September 1982, pp. 247-255.

13. Hannebrink, D.N., Lee, H.S.H., Weinstock, H. and Hedrick, J.K., "Influence of Axle Load, Track Gauge, and Wheel Profile on Rail-Vehicle Hunting," Transactions of the ASME, *Journal of Engineering for Industry*, Feb. 1977, pp. 186-195.

14. Hull, R., and Cooperider, N.K., "Influence of Non-Linear Wheel/Rail Contact Geometry on Stability of Rail Vehicles," Transactions of the ASME, *Journal of Engineering for Industry*, Feb. 1977, pp. 172-185.

15. Horak, D. and Wormley, D.N., "Nonlinear Stability and Tracking of Rail Passenger Trucks," Transactions of the ASME, Journal of Dynamic Systems, Measurement and Control, Vol. 104, Sept. 1982, pp. 256-263.

16. Scheffel, H., "The Hunting Stability and Curving Ability of Railway Vehicles," *Rail International*, No. 2, Feb. 1974, pp. 154-177.

17. Scheffel, H., "The influence of the suspension on the hunting stability of railway vehicles," *Rail International*, August 1979, pp. 662-696.

18. Scheffel, H., "Unconventional Bogie Designs - Their Practical Basis and Historical Background," *Vehicle System Dynamics*, Vol. 24, 1995, pp. 497-524.

19. Pollard, M.G., "Studies of the dynamics of vehicles with cross-braced bogies," *Proceedings of 5th VSD - 2nd IUTAM Symposium*, Vienna, September, 1977, pp. 518-526.

20. Pollard, M.G., "The development of cross-braced freight bogies," *Rail International*, September 1979, pp. 736-750.

21. List, H.A., and Bailey, E.C., "Development of a retrofit steering assembly for standard freight car trucks," *Proc. of the Economics and Performance of Freight Car Trucks Conference*, Montreal, Canada, 1983, pp. 109-116.

22. Horak, D., Bell, C.E., and Hedrick, J.K., "A Comparison of the Stability and Curving Performance of Radial and Conventional Rail Vehicle Trucks," *Journal of Dynamic Systems, Measurement and Control*, Transactions of the ASME, Vol. 103, September 1981, pp. 191-200.

23. Smith, R.E. and Anderson, R.J., "Characteristics of Guided-Steering Railway Trucks," *Vehicle System Dynamics*, Vol. 17,, 1988, pp. 1-36.

24. Bell, C.E. and Hedrick, J.K., "Forced Steering of Rail Vehicles: Stability and Curving Mechanics," *Vehicle System Dynamics*, Vol. 10, 1981, pp. 357-386.

25. Goodall, R.M. and Kortum, W., "Active controls in ground transportation - a review of the state-of-the-art and future potential," *Vehicle System Dynamics*, Vol. 12, 1983, pp. 225-257.

26. Celniker, G.M. and Hedrick, J.K., "Rail vehicle active suspensions for lateral ride and stability improvement," Transactions of the ASME, *Journal of Dynamic Systems, Measurement & Control*, Vol. 104, 1982, pp. 100-106.

27. Wickens, "Dynamics of Actively Guided Vehicles," *Vehicle System dynamics*, Vol. 20, 1991, pp.219-242.

28. Narayanaswamy, S., Osman, M.O.M. and Dukkipati, R.V., "Performance of a rail car system equipped with Independently Rotating Wheelset having yaw control," ASME Winter Annual Meeting, Transportation Systems - 1992, DSC - Vol. 44, pp. 75-88.

29. Dukkipati, R.V., Narayanaswamy, S. and Osman, M.O.M., "Independently Rotating Wheel Systems for Railway Vehicles - A State of the Art Review," *Vehicle Systems Dynamics*, Vol. 21, 1992, pp. 297-330.

30. Kaplan, A. and Short, S.A., "Dynamics of Independently Rotating Wheel Systems, *TRW Systems Group Report 06818-6045-R0-00*, 1970.

31. Eickhoff, B.M., and Harvey, R.F., "Theoretical and experimental evaluation of Independently Rotating Wheels for Railway Vehicles," *Proceedings of the 11th IAVSD Symposium*, 1989, pp. 190-202.

32. Eickhoff, B.M., "The application of independently rotating wheels to railway vehicles," *Proceedings of Institution of Mechanical Engineers*, Vol. 205, 1991, pp. 43-54.

33. Elkins, J.A., "The performance of three-piece trucks equipped with independently rotating wheelsets," *Proceedings of 11th IAVSD Symposium*, Kingston, Canada, 1989, pp. 203-216.

34. Benington, C.K. and Greenhorn, J.W.R., "A proposal for improving the performance of two-axle rail-guided vehicle," *Journal of Mechanical Engineering Sciences*, Vol. 13, No. 3, 1971, pp. 157-167.

35. Ahmed, A.K.W., "Lateral Stability and Steady State Curving Behaviour of Railway Freight Car System with Elasto-Damper Coupled Wheelset," *Ph.D. Thesis*, Concordia University, Montreal, Canada, 1986.

36. Geuenich, W., Gunther C.H. and Leo, R., "The Dynamics of Fibre Composite Bogies with Creep Controlled Wheelsets," *Vehicle System Dynamics*, Vol. 12, 1983, pp. 134-140.

37. Frederich, F., "Possibilities as yet unknown or unused regarding the wheel/rail tracking mechanism - Development of modern rolling stock running gear," *Rail International*, 1985, pp. 33-41.

38. Lombardi, E.J., "Amtrak's High-Speed Trainset Program," *Proceedings of the 1995 IEEE/ASME Joint Railroad Conference*, Baltimore, Maryland, April 4-6, 1995, ASME RTD-Vol. 9, pp. 1-7.

39. McCowan, R. and Tsai, T., "The Next Generation High-Speed Rail Technology Program at FRA," *Proceedings of the 1995 IEEE/ASME Joint Railroad Conference*, Baltimore, Maryland, April 4-6, 1995, ASME RTD-Vol. 9, pp. 9-14.

40. Tsai, T. and Jamieson, D., "Testing of Rail Vehicles for Higher Speeds on Existing Lines," *Proceedings of the 1995 IEEE/ASME Joint Railroad Conference*, Baltimore, Maryland, April 4-6, 1995, ASME RTD-Vol. 9, pp. 15-18.

41. Kolig, H. and Hesser, R.K., "Tilt System for Amtrak High Speed Trainsets," *Proceedings of the 1997 IEE/ASME Joint Railroad Conference*, Boston, Massachusetts, March 1997, IEEE Catalog Number 97CH36047, pp.59-64.

42. Federal Railroad Administration, "Ground Transportation for America," *U.S. Department of Transportation Report*, August 1996.

43. J.G. Bell and R.J. Annechini, "Program Update - Amtrak's High Speed Train Set Program," *Proceedings of the 1997 IEEE/ASME Joint Railroad Conference*, IEEE Catalog Number 97CH36047, March 1997, pp. 109-113.

44. Wickens, A.H., "The dynamics of railway vehicles on straight track: fundamental considerations of lateral stability," *Proceedings of Institution of Mechanical Engineers*, Vol. 180, 1965-66, pp. 29-44.

45. Wickens, A.H., "The dynamic stability of a simplified four-wheeled railway vehicle having profiled wheels," *International Journal of Solids Structures*, Vol. 1, 1965, pp. 385-406.

46. Cooperrider, N.K. and Heller, R., "User's Manual for asymmetric wheel-rail contact characterization program," Report No. FRA/ORD-78/05, 1977.

47. Kalker, J.J., "Survey of Wheel-Rail Contact Theory," *Vehicle Systems Dynamics*, Vol. 5, 1979, pp. 317-358.

48. Wickens, A.H. "Stability Criteria for Articulated Railway Vehicles Possessing Perfect Steering," *Vehicle System Dynamics*, Vol. 7, 1978, pp. 165-182.

49. Wickens, A.H., "Steering and Stability of Unsymmetric Articulated Railway Vehicles," *Journal of Dynamic Systems, Measurement and Control*, Transactions of ASME, Vol. 101, September 1979, pp.256-262.

50. Suda, Yoshihiro, "Improvement of High Speed Stability and Curving Performance by Parameter Control of Trucks for Rail Vehicles Considering Independently Rotating Wheelsets and Unsymmetric Structure," *JSME International Journal*, Series III, Vol. 33, No. 2, 1990, pp. 176-182.

51. Fujioka, T., Suda, Y. and Iguchi, M., "Representation of Primary Suspensions of Rail Vehicles and Performance of Radial Trucks," Bulletin of JSME, Vol. 27, No.232, October 1984.

52. Pennington, K.W., Harwood, N.A. and Peat, D.M. , "A steering bogie for the British Rail Class 37 locomotive," *Proceedings of Institution of Mechanical Engineers*, Vol. 200, No. D3, 1986, pp. 211-218.

53. Suda, Y., "High Speed Stability and Curving Performance of Longitudinally Unsymmetric Trucks with Semi-active Control," Vehicle System Dynamics, Vol. 23, 1994, pp.29-52.

54. Narayanaswamy, S., Dukkipati, R.V. and Osman, M.O.M., "A comparative study on lateral stability and steady state curving behaviour of unconventional rail truck models," *Proceedings of Institution of Mechanical Engineers*, Vol. 208, 1994, pp. 1-13.

55. Wickens, A.H., "Steering and stability of the bogie: vehicle dynamics and suspension design," *Proceedings of Institution of Mechanical Engineers*, Vol. 205, 1991, pp.109-122.

56. Shen, Z.Y., Hedrick, J.K. and Elkins, J.A., "A comparison of alternative creep force models for rail vehicle dynamic analysis," *Proceedings of the 8th International Conference on Vehicle System Dynamics*, Swets and Zeitlinger, Amsterdam, 1981, p.591.

57. Narayanaswamy, S., Dukkipati, R.V. and Osman, M.O.M., "Analysis of modified railway passenger truck designs to improve lateral stability/curving behaviour compatibility," *Proceedings of Institution of Mechanical Engineers*, Vol. 209, 1995, pp. 49-59.

58. Shaopu Yang and Mehdi Ahmadian, "The Hopf Bifurcation in a Rail Wheelset with Nonlinear Damping,", ASME - Rail Transportation 1996, RTD-Vol.12, pp. 113-120.

59. Association of American Railroads, "User's Manual for NUCARS Version 2.1," Report No. SD-043, September 1995.

60. Eickhoff, B.M., Evans, J.R. and Minnis, A.J., "A Review of Modelling Methods for Railway Vehicle Suspension Components," Vehicle System Dynamics, Vol. 24, 1995, pp. 469-496.

Appendix A

Wheelset Coordinate System

The coordinate system, i_e, j_e, k_e shown in Figure A-1 has its origin at the track center line and moves at a constant forward velocity V with respect to a fixed inertial frame. The axes system i_i, j_i, k_i is an intermediate frame that is rotated through an angle ψ about the k_e axis. The axes system i_b, j_b, k_b form the wheel-axle set body coordinate system and has its origin at the center of mass. Two more contact axes i_l, j_l, k_l and i_r, j_r, k_r are used that are attached to the left-rail and right-rail instantaneous points respectively. These are defined in Fig. A2 and are used to calculate wheel-rail contact forces.

The transformation equations between the wheelset body axis and intermediate frame are written as [4]

$$\begin{bmatrix} i_b \\ j_b \\ k_b \end{bmatrix} = \begin{bmatrix} 1 & 0 & 0 \\ 0 & \cos\phi & \sin\phi \\ 0 & -\sin\phi & \cos\phi \end{bmatrix} \begin{bmatrix} i_i \\ j_i \\ k_i \end{bmatrix} \tag{A-1}$$

and between the intermediate frame and the equilibrium axis is

$$\begin{bmatrix} i_i \\ j_i \\ k_i \end{bmatrix} = \begin{bmatrix} \cos\psi & \sin\psi & 0 \\ -\sin\psi & \cos\psi & 0 \\ 0 & 0 & 1 \end{bmatrix} \begin{bmatrix} i_e \\ j_e \\ k_e \end{bmatrix} \tag{A-2}$$

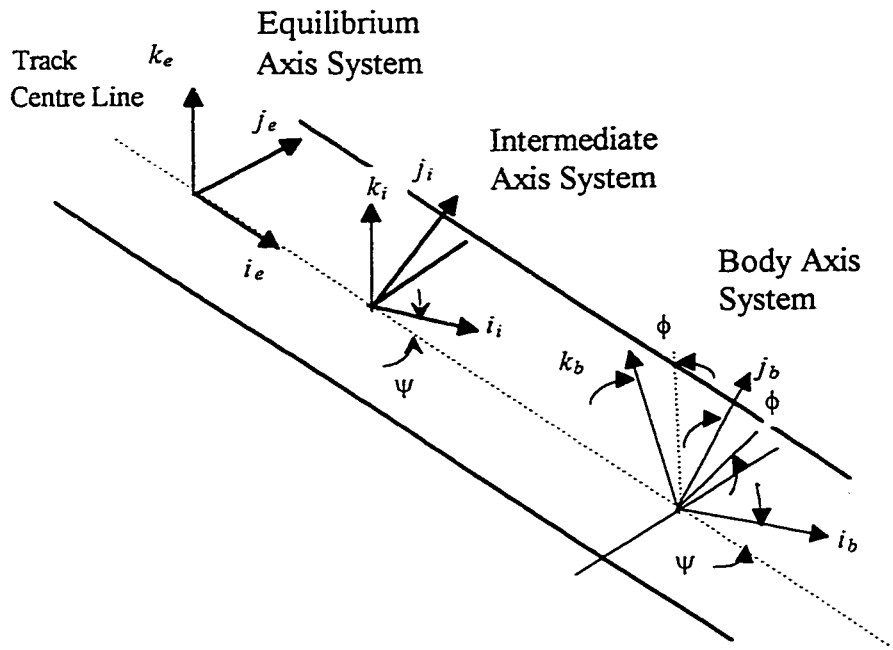

Axis System for Wheelset Model

Figure A-1

The transformation between the wheelset body axis and equilibrium axis is then written as

$$\begin{bmatrix} i_b \\ j_b \\ k_b \end{bmatrix} = \begin{bmatrix} \cos\psi & \sin\psi & 0 \\ -\cos\phi\sin\psi & \cos\phi\cos\psi & \sin\phi \\ \sin\phi\sin\psi & -\sin\phi\cos\psi & \cos\phi \end{bmatrix} \begin{bmatrix} i_e \\ j_e \\ k_e \end{bmatrix} \tag{A-3}$$

For small ϕ and ψ equation (A-3) becomes

$$\begin{bmatrix} i_b \\ j_b \\ k_b \end{bmatrix} = \begin{bmatrix} 1 & \psi & 0 \\ -\psi & 1 & \phi \\ 0 & -\phi & 1 \end{bmatrix} \begin{bmatrix} i_e \\ j_e \\ k_e \end{bmatrix} \tag{A-4}$$

In Figure A-2, δ_l and δ_r refer to the left and right contact angles, r_l and r_r are the left and right contact rolling radii. The transformation from the contact-point axes and the wheelset body axes are given by

$$\begin{bmatrix} i_l \\ j_l \\ k_l \end{bmatrix} = \begin{bmatrix} 1 & 0 & 0 \\ 0 & \cos\delta_l & \sin\delta_l \\ 0 & -\sin\delta_l & \cos\delta_l \end{bmatrix} \begin{bmatrix} i_b \\ j_b \\ k_b \end{bmatrix} \tag{A-5}$$

$$\begin{bmatrix} i_r \\ j_r \\ k_r \end{bmatrix} = \begin{bmatrix} 1 & 0 & 0 \\ 0 & \cos\delta_r & -\sin\delta_r \\ 0 & \sin\delta_r & \cos\delta_r \end{bmatrix} \begin{bmatrix} i_b \\ j_b \\ k_b \end{bmatrix} \tag{A-6}$$

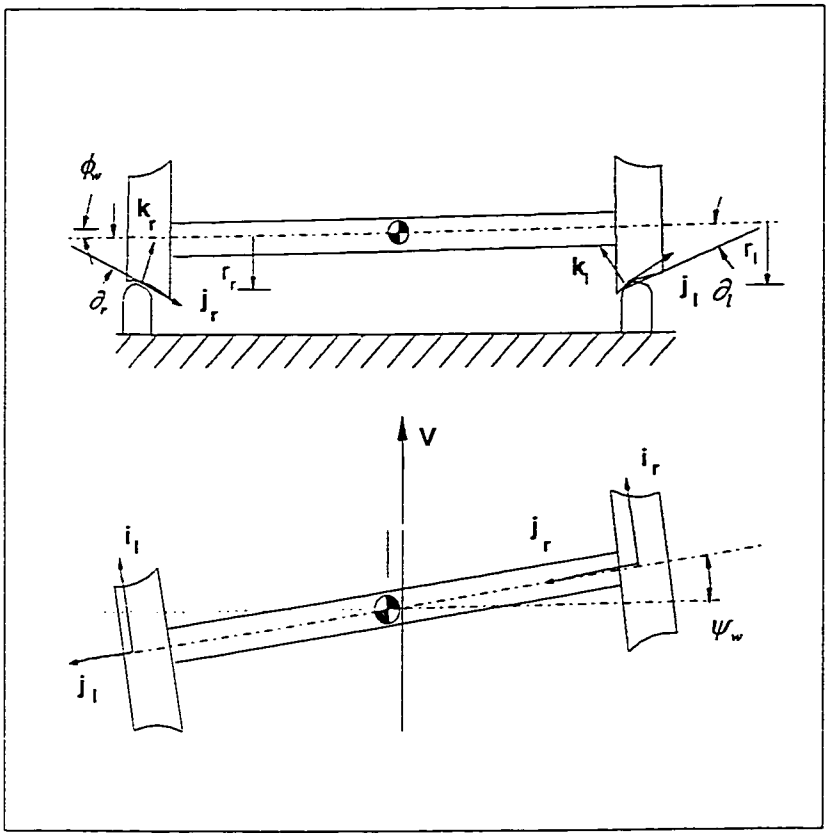

Axis Systems at Wheel/Rail Contact Points

Figure A-2

For small angles using equations (A-4) in (A-5), the expression for transformation from left wheel contact plane axes to wheelset equilibrium axes is given by:

$$\begin{bmatrix} i_l \\ j_l \\ k_l \end{bmatrix} = \begin{bmatrix} 1 & \psi & 0 \\ -\psi & 1 & \delta_l + \phi \\ 0 & -(\delta_l + \phi) & 1 \end{bmatrix} \begin{bmatrix} i_e \\ j_e \\ k_e \end{bmatrix} \tag{A-7}$$

Similarly for the right wheel contact plane:

$$\begin{bmatrix} i_r \\ j_r \\ k_r \end{bmatrix} = \begin{bmatrix} 1 & \psi & 0 \\ -\psi & 1 & -(\delta_r - \phi) \\ 0 & (\delta_r - \phi) & 1 \end{bmatrix} \begin{bmatrix} i_e \\ j_e \\ k_e \end{bmatrix} \tag{A-8}$$

For the curved track, equations (A-7) and (A-8) should be modified to include an extra term b^* in the equation. In the curved track coordinate system, the wheelset is radially aligned with the track when $(\psi + \frac{b^*}{R})$ is zero. The term $\frac{b^*}{R}$ will then equal to $+\frac{b}{R}$ for the leading wheelset and $-\frac{b}{R}$ for the trailing wheelset.

The transformation between contact axes and equilibrium axis is given by

$$\begin{bmatrix} i_l \\ j_l \\ k_l \end{bmatrix} = \begin{bmatrix} 1 & (\psi + \frac{b^*}{R}) & 0 \\ -(\psi + \frac{b^*}{R}) & 1 & \delta_l + \phi \\ 0 & -(\delta_l + \phi) & 1 \end{bmatrix} \begin{bmatrix} i_e \\ j_e \\ k_e \end{bmatrix} \tag{A-9}$$

$$\begin{bmatrix} i_r \\ j_r \\ k_r \end{bmatrix} = \begin{bmatrix} 1 & (\psi + \frac{b^*}{R}) & 0 \\ -(\psi + \frac{b^*}{R}) & 1 & -(\delta_r - \phi) \\ 0 & (\delta_r - \phi) & 1 \end{bmatrix} \begin{bmatrix} i_e \\ j_e \\ k_e \end{bmatrix} \qquad \text{(A-10)}$$

Appendix B

Creepage Derivation

Each wheel experiences relative linear and angular motions between the wheel and rail which are called lateral, longitudinal and spin creepages.

Longitudinal and lateral creepages are defined as

$$\xi_x = \frac{\text{Longitudinal component of } \mathbf{V}_c}{\text{nominal forward velocity}} \tag{B-1}$$

$$\xi_y = \frac{\text{Lateral component of } \mathbf{V}_c}{\text{nominal forward velocity}} \tag{B-2}$$

where $\mathbf{V}_c$ is the absolute velocity of the wheel at the contact point.

Spin creepage is defined as

$$\xi_{sp} = \frac{\text{Angular velocity component } \Omega_z}{\text{nominal forward velocity}} \tag{B-3}$$

where Ω_z is the component of the absolute angular velocity Ω perpendicular to the contact plane.

Figure B-1 shows the wheelset body axes from which we can write the velocity at the contact point $\mathbf{V}_c$ as

$$\mathbf{V}_c = \mathbf{V}_b + \Omega \times \mathbf{R}_c + \mathbf{V}_r \tag{B-4}$$

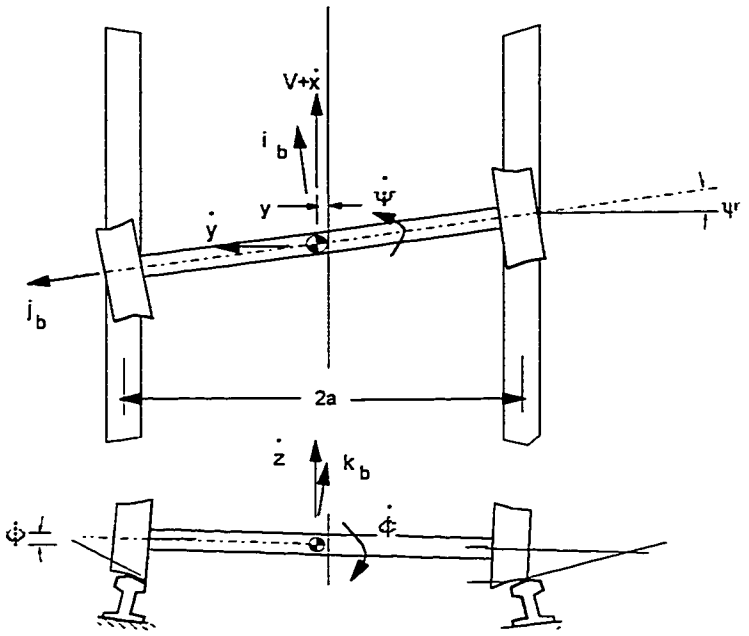

Wheelset axes and velocity of centre of mass

Figure B-1

in which V_b is the angular velocity of wheelset axes, Ω is the angular velocity of the wheelset axes excluding the wheelset rolling velocity and R_c is the position vector of the contact point in the wheelset body axes and $\mathbf{V}_r$ is the velocity of point of contact measured with respect to the wheelset body axes.

From figure B-1, the velocity $\mathbf{V}_b$ can be written as

$$\mathbf{V}_b = (V + \dot{x} - \dot{y}\psi)\mathbf{i}_b + (\dot{y} - V\psi)\mathbf{j}_b + \dot{z}\mathbf{k}_b \tag{B-5}$$

In the model, we assume the vehicle is travelling at constant velocity and hence $\dot{x} = 0$. Neglecting the term $\dot{y}\psi$ because it is small, we get,

$$\mathbf{V}_b = V\mathbf{i}_b + (\dot{y} - V\psi)\mathbf{j}_b + \dot{z}\mathbf{k}_b \tag{B-6}$$

The angular velocity Ω is given in wheelset axes as

$$\Omega = \dot{\phi}\mathbf{i}_b + (\tfrac{V}{R} + \dot{\psi})\mathbf{k}_b \tag{B-7}$$

The position vector for the left and right wheel contact points are

$$\mathbf{R}_{cl} = a\mathbf{j}_b - r_l\mathbf{k}_b \tag{B-8}$$

$$\mathbf{R}_{cr} = -a\mathbf{j}_b - r_r\mathbf{k}_b \tag{B-9}$$

From equations (B-7) and (B-8), we can write,

$$\Omega \times \mathbf{R}_{cl} = -a(\tfrac{V}{R} + \dot{\psi})\mathbf{i}_b + r_l\dot{\phi}\mathbf{j}_b + a\dot{\phi}\mathbf{k}_b \qquad \text{(B-10)}$$

The relative velocity $\mathbf{V}_r$ in equation (B-4) is written as

$$\mathbf{V}_r = -(\omega + \dot{\beta})r_l\mathbf{i}_b \qquad \text{(B-11)}$$

where ω is the nominal rolling velocity of the wheelset and $\dot{\beta}$ is the perturbation in the wheel spin.

The absolute velocity of the contact point $\mathbf{V}_{cl}$ can be written from equations (B-4), (B-6), (B-10) and (B-11) as

$$\mathbf{V}_{cl} = (V - a(\tfrac{V}{R} + \dot{\psi}) - (\omega + \dot{\beta})r_l)\mathbf{i}_b + (\dot{y} - V\psi + r_l\dot{\phi})\mathbf{j}_b + (\dot{z} + a\dot{\phi})\mathbf{k}_b \qquad \text{(B-12)}$$

Similarly, the expression for the absolute velocity of contact point at the right wheel is given by

$$\mathbf{V}_{cr} = (V + a(\tfrac{V}{R} + \dot{\psi}) - (\omega + \dot{\beta})r_r)\mathbf{i}_b + (\dot{y} - V\psi + r_r\dot{\phi})\mathbf{j}_b + (\dot{z} - a\dot{\phi})\mathbf{k}_b \qquad \text{(B-13)}$$

The absolute angular velocity at a contact point Ω_c is written from equation (B-7) after adding the wheelset rolling velocity as

$$\Omega_c = \dot{\phi}\mathbf{i}_b + (\omega + \dot{\beta})\mathbf{j}_b + (\tfrac{V}{R} + \dot{\psi})\mathbf{k}_b \qquad \text{(B-14)}$$

Creepages in general are expressed in contact axes. By using the

transformation matrices in equations (A-5) and (A-6), equations (B-12), (B-13) and (B-14) are written in contact axes coordinates as

$$V_{cl} = (V - a(\frac{V}{R} + \dot{\psi}) - (\omega + \dot{\beta})r_l)\mathbf{i}_l + ((\dot{y} - V\psi + r_l\dot{\phi})\cos\delta_l + (\dot{z} + a\dot{\phi})\sin\delta_l)\mathbf{j}_l + (-(\dot{y} - V\psi + r_l\dot{\phi})\sin\delta_l + (\dot{z} + a\dot{\phi})\cos\delta_l)\mathbf{k}_l \quad \text{(B-15)}$$

$$V_{cr} = (V + a(\frac{V}{R} + \dot{\psi}) - (\omega + \dot{\beta})r_r)\mathbf{i}_r + ((\dot{y} - V\psi + r_r\dot{\phi})\cos\delta_r + (\dot{z} - a\dot{\phi})\sin\delta_r)\mathbf{j}_r + (-(\dot{y} - V\psi + r_r\dot{\phi})\sin\delta_r + (\dot{z} + a\dot{\phi})\cos\delta_r)\mathbf{k}_r \quad \text{(B-16)}$$

$$\omega_{cl} = \dot{\phi}\mathbf{i}_l + ((\omega + \dot{\beta})\cos\delta_l + (\frac{V}{R} + \dot{\psi})\sin\delta_l)\mathbf{j}_l + ((\frac{V}{R} + \dot{\psi})\cos\delta_l - (\omega + \dot{\beta})\sin\delta_l)\mathbf{k}_l \quad \text{(B-17)}$$

$$\omega_{cr} = \dot{\phi}\mathbf{i}_r + ((\omega + \dot{\beta})\cos\delta_r - (\frac{V}{R} + \dot{\psi})\sin\delta_r)\mathbf{j}_r + ((\frac{V}{R} + \dot{\psi})\cos\delta_r + (\omega + \dot{\beta})\sin\delta_r)\mathbf{k}_r \quad \text{(B-18)}$$

From the longitudinal component of equation (B-15), the longitudinal creepage for the left wheel can be written as

$$\xi_{xl} = \frac{V - a(\frac{V}{R} + \dot{\psi}) - (\omega + \dot{\beta})r_l}{V} \quad \text{(B-19)}$$

and the lateral creepage,

$$\xi_{yl} = \frac{(\dot{y} - V\psi + r_l\dot{\phi})\cos\delta_l + (\dot{z} + a\dot{\phi})\sin\delta_l}{V} \quad \text{(B-20)}$$

The spin equation can be obtained from equation (B-17) as

$$\xi_{sl} = \frac{(\frac{V}{R}+\dot{\psi})\cos\delta_l - (\omega+\dot{\beta})\sin\delta_l}{V} \tag{B-21}$$

The creepage terms for the right wheel can similarly be written as

$$\xi_{xr} = \frac{V+a(\frac{V}{R}+\dot{\psi})-(\omega+\dot{\beta})r_r}{V} \tag{B-22}$$

$$\xi_{yr} = \frac{(\dot{y}-V\psi+r_r\dot{\phi})\cos\delta_r - (\dot{z}-a\dot{\phi})\sin\delta_r}{V} \tag{B-23}$$

$$\xi_{sr} = \frac{(\frac{V}{R}+\dot{\psi})\cos\delta_r + (\omega+\dot{\beta})\sin\delta_r}{V} \tag{B-24}$$

The $\mathbf{k}_l$ component of equation (B-15) is zero since it is assumed that wheel lift is not possible. Therefore, we get,

$$\dot{z} + a\dot{\phi} = (\dot{y} - V\psi + r_l\dot{\phi})\tan\delta_l \tag{B-25}$$

which is used in equation (B-20) to get

$$\xi_{yl} = \frac{(\dot{y}-V\psi+r_l\dot{\phi})}{V\cos\delta_l} \tag{B-26}$$

The right wheel lateral creepage can similarly be simplified as

$$\xi_{yr} = \frac{(\dot{y}-V\psi+r_r\dot{\phi})}{V\cos\delta_r} \tag{B-27}$$

B.1 Linearized creepage expressions for tangent track

For the tangent track hunting model, the creepage terms derived above are linearized by making use of equations (2.1), (2.2) and (2.3). The simplified creepage expressions are

$$\xi_{xl} = -(\frac{\lambda}{r_o}y + \frac{a\dot{\psi}}{V}) \tag{B-28}$$

$$\xi_{yl} = \frac{\dot{y}}{V} - \psi + \frac{\Gamma r_o \dot{y}}{Va} \tag{B-29}$$

$$\xi_{sl} = \frac{\dot{\psi}}{V} - \frac{\delta_l}{r_o} \tag{B-30}$$

$$\xi_{xr} = (\frac{\lambda}{r_o}y + \frac{a\dot{\psi}}{V}) \tag{B-31}$$

$$\xi_{yr} = \frac{\dot{y}}{V} - \psi + \frac{\Gamma r_o \dot{y}}{Va} \tag{B-32}$$

$$\xi_{sr} = \frac{\dot{\psi}}{V} + \frac{\delta_r}{r_o} \tag{B-33}$$

Expressions for longitudinal, lateral and spin creep forces can be derived by making use of the above terms in equation (2.4).

B.2 Linearized creepage expressions for curved track

B.2.1 Wheel load shift

In curving wheel loads redistribute under the influence of cant deficiency. The wheel load $N_l(2a) - \frac{M_{cg}}{4}(a) = \frac{M_{cg}}{4}\phi_d h_{cg}$ shift can be approximated by summing moment about right wheel contact point (refer figure B-2),

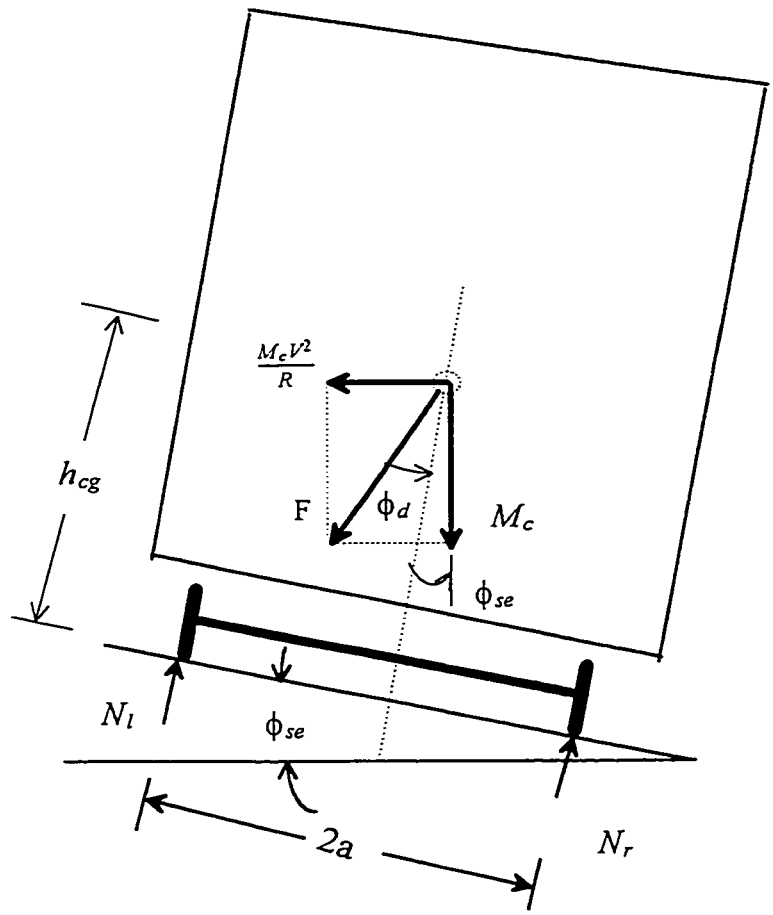

Load distribution during curving

Figure B-2

where a is the half track gauge, h_{cg} is the height of C.G. of the car from the top of rail and ϕ_d is the cant deficiency. This is simplified as

$$\frac{N_l - N_w}{N_w} = \frac{h_{cg}}{a}\phi_d \tag{B-34}$$

where $N_w = \frac{M_{cg}}{8}$, the nominal wheel load per wheel. The expression for the normal wheel load on the left wheel is

$$N_l = N_w(1 + \frac{h_{cg}}{a}\phi_d) \tag{B-35}$$

Similarly, normal wheel load on the right wheel is

$$N_r = N_w(1 - \frac{h_{cg}}{a}\phi_d) \tag{B-36}$$

B.2.2 Creepages

Longitudinal creepage

The expressions for curved track longitudinal creepage given in equations (B-19) and (B-22) are simplified by ignoring the $\dot{\psi}$ term for the steady state curving analysis considered here. The expressions are rewritten by using the linearizing approximations for r_l and r_r in terms of y_w as

$$\xi_{xl} = \frac{a}{R} - \frac{\lambda y}{r_o} - \frac{\dot{\beta} r_o}{V} \tag{B-37}$$

$$\xi_{xr} = -\frac{a}{R} + \frac{\lambda y}{r_o} - \frac{\dot{\beta} r_o}{V} \tag{B-38}$$

The longitudinal creep forces are

$$F_{xl} = -f_{11l}\xi_{xl} \tag{B-39}$$

$$F_{xr} = -f_{11r}\xi_{xr} \tag{B-40}$$

$$f_{11l}f_{11r} = f_{11}(1 \pm \tfrac{2h\phi_d}{3}) \tag{B-41}$$

The wheelset is assumed to be rolling with constant rotational velocity and the net couple about the wheelset rolling axis provided by the longitudinal creep forces must be zero (assuming no driving or braking torque). This gives the following expressions for the torque balance about the wheelset axis:

$$F_{xl}r_l + F_{xr}r_r = 0 \tag{B-42}$$

Substituting expressions derived before in the above equation yields the following:

$$\dot{\beta} = -\tfrac{2Vh\phi_d\lambda}{3r_o^2}(y - \tfrac{r_o a}{\lambda R}) \tag{B-43}$$

Equations (B-37) and (B-38) can now be written as follows:

$$\xi_{xl} = -\tfrac{\lambda}{r_o}(y - \tfrac{r_o a}{\lambda R})(1 - \tfrac{2h\phi_d}{3}) \tag{B-44}$$

$$\xi_{xr} = \tfrac{\lambda}{r_o}(y - \tfrac{r_o a}{\lambda R})(1 + \tfrac{2h\phi_d}{3}) \tag{B-45}$$

Lateral creepage

Lateral creepage for the steady state curving analysis can be obtained from (B-26) and (B-27) by neglecting the velocity terms

$$\xi_{yl},\xi_{yr} = -(\psi + \frac{b^*}{R}) \tag{B-46}$$

where b^* is $+b$ for the leading wheelset in a truck and $-b$ is for the trailing wheelset in a truck.

Spin creepage

$$\xi_{sl} = \frac{-(\frac{V}{R} + \frac{V}{r_o}\delta_l)}{V} \tag{B-47}$$

$$\xi_{sr} = \frac{-(\frac{V}{R} - \frac{V}{r_o}\delta_r)}{V} \tag{B-48}$$

Appendix C

Derivation of Equations of Motion

C.1 Wheel-axle set force balance

The angular velocity ω of the wheel-axle set is given as

$$\omega = \dot{\phi}\mathbf{i}_i + (\Omega + \dot{\beta})\mathbf{j}_b + \dot{\psi}\mathbf{k}_i \tag{C.1}$$

Transforming the above equation into body axes system,

$$\omega = \dot{\phi}\mathbf{i}_b + (\Omega + \dot{\beta} + \dot{\psi}\sin\phi)\mathbf{j}_b + \dot{\psi}\cos\phi\mathbf{k}_b \tag{C.2}$$

$$= \omega_x\mathbf{i}_b + \omega_y\mathbf{j}_b + \omega_z\mathbf{k}_b \tag{C.3}$$

The angular momentum of the wheel-axle set in the body coordinate system is

$$\mathbf{H} = I_{wx}\omega_x\mathbf{i}_b + I_{wy}\omega_y\mathbf{j}_b + I_{wz}\omega_z\mathbf{k}_b \tag{C.4}$$

where I_{wx}, I_{wy} and I_{wz} are the principal mass moment of inertia of the wheelset.

The angular velocity of the body coordinate axes is written as

$$\omega_{axis} = \dot{\phi}\mathbf{i}_b + \dot{\psi}\mathbf{k}_i$$

$$= \dot{\phi}\mathbf{i}_b + \dot{\psi}\sin\phi\mathbf{j}_b + \dot{\psi}\cos\phi\mathbf{k}_b \tag{C.5}$$

The rate of change of momentum is obtained as

$$\frac{d\mathbf{H}}{dt} = I_{wx}\dot{\omega}_x\mathbf{i}_b + I_{wy}\dot{\omega}_y\mathbf{j}_b + I_{wz}\dot{\omega}_z\mathbf{k}_b + \omega \times \mathbf{H} \tag{C.6}$$

The rate of change of momentum is obtained as

$$\frac{d\mathbf{H}}{dt} = (I_{wx}\ddot{\phi} - I_{wy}\Omega\dot{\psi})\mathbf{i}_e + I_{wy}\ddot{\beta}\mathbf{j}_e + (I_{wy}\Omega\dot{\phi} + I_{wx}\ddot{\psi})\mathbf{k}_e \tag{C.7}$$

The equations of motion are written in the equilibrium axes, from Newton's law, as

$$m_w\ddot{r} = \Sigma\mathbf{F} \tag{C.8}$$

$$\frac{d\mathbf{H}}{dt} = \Sigma\mathbf{M} \tag{C.9}$$

where m_w is the mass of the wheel-axle set.

Neglecting the lateral displacements of the contact points from the equilibrium position, the position vectors for the left and right contact points in terms of the body coordinate system are (refer figure B-1)

$$\mathbf{R}_r = -a\mathbf{j}_b - r_r\mathbf{k}_b \tag{C-10}$$

$$\mathbf{R}_l = a\mathbf{j}_b - r_l\mathbf{k}_b \tag{C-11}$$

In terms of the equilibrium coordiantes, components of these position vectors are

$$R_{xr} = a\cos\phi\sin\psi - r_r\sin\phi\sin\psi \tag{C-12}$$
$$R_{yr} = -a\cos\phi\cos\psi + r_r\sin\phi\cos\psi \tag{C-13}$$
$$R_{zr} = -a\sin\phi - r_r\cos\phi \tag{C-14}$$

and

$$R_{xl} = -a\cos\phi\sin\psi - r_l\sin\phi\sin\psi \tag{C-15}$$
$$R_{yl} = a\cos\phi\cos\psi + r_l\sin\phi\cos\psi \tag{C-16}$$
$$R_{zl} = a\sin\phi - r_l\cos\phi \tag{C-17}$$

The equilibrium equations for the wheel-axle set can be written from the force-moment system shown in figure C-1. From the free-body diagram of a wheelset the summation of forces and moments are given by

$$\Sigma\mathbf{F} = \mathbf{F}_l + \mathbf{F}_r + \mathbf{N}_l + \mathbf{N}_r + \mathbf{F}_s + W_A\mathbf{k}_z \tag{C-18}$$

$$\Sigma\mathbf{M} = \mathbf{R}_{xr}(\mathbf{F}_r + \mathbf{N}_r) + \mathbf{R}_{xl}(\mathbf{F}_l + \mathbf{N}_l) + \mathbf{M}_l + \mathbf{M}_r + \mathbf{M}_s \tag{C-19}$$

By expressing the components of the above mentioned forces and position vectors in the equilibrium coordinate system, and making use of equations (C.8) and (C.9), the following six equations for the wheelset can be written:

Longitudinal equation

$$m_w\ddot{x}_w = F_{xl} + F_{xr} + N_{xl} + N_{xr} + F_{xs} \tag{C-20}$$

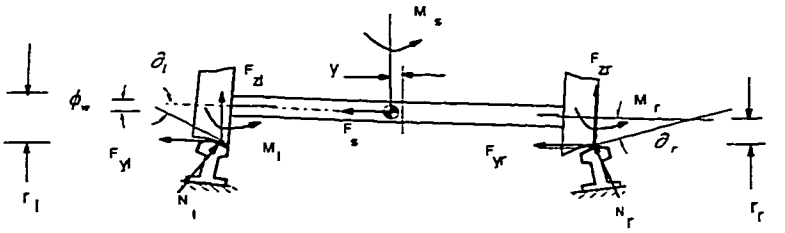

Free body diagram of a wheelset

Figure C-1

Lateral equation

$$m_w \ddot{y}_w = F_{yl} + F_{yr} + N_{yl} + N_{yr} + F_{ys} \tag{C-21}$$

Vertical Equation

$$m_w \ddot{z}_w = F_{zl} + F_{zr} + N_{zl} + N_{zr} + F_{zs} - W_A \tag{C-22}$$

Roll Equation

$$I_{wx}\ddot{\phi}_w - I_{wy}(V/r_o)\dot{\psi}_w = R_{yr}(F_{zr} + N_{zr}) - R_{zr}(F_{yr} + N_{yr}) + R_{yl}(F_{zl} + N_{zl}) - R_{zl}(F_{yl} + N_{yl}) + M_{xl} + M_{xr} + M_{xs} \tag{C-23}$$

Spin Equation

$$I_{wy}\ddot{\beta}_w = R_{zr}F_{xr} - R_{xr}(F_{zr} + N_{zr}) + R_{zl}F_{xl} - R_{xl}(F_{zl} + N_{zl}) + M_{yl} + M_{yr} + M_{ys} \tag{C-24}$$

Yaw Equation

$$I_{wx}\ddot{\psi}_w + I_{wy}(\tfrac{V}{r_o})\dot{\phi}_w = R_{xr}(F_{yr} + N_{yr}) + R_{xl}(F_{yl} + N_{yl}) - R_{yl}F_{xl} - R_{yr}F_{xr} + M_{zl} + M_{zr} + M_{zs} \tag{C-25}$$

By using the values of linearized creep force terms derived in Appendix B and making use of equations (C-13),(C-14), C(1-16) and (C-17), equation (C-23) can be simplified as [4]

$$I_{wx}\ddot{\phi} - I_{wy}\tfrac{V}{r_o}\dot{\psi} + \tfrac{2f_{11}}{V}((1 + \tfrac{r_o\Gamma}{a})\dot{y} - V\psi) + f_{12}(\tfrac{2r_o}{V}\dot{\psi} + (\delta_l - \delta_r)) - a(N_l - N_r) - M_{xs} = 0 \tag{C-26}$$

Multiplying equation (C-22) by a and adding it to equation (C-26), we get,

$$N_l = \frac{1}{2a}((m\ddot{z} + W_A - F_{zl} - F_{zr})a + (I_{wx}\ddot{\phi} - I_{wy}\frac{V}{r_o}\dot{\psi} + \frac{2f_{11}}{V}(\dot{y} + \frac{r_o\Gamma}{a}\dot{y} - V\psi) + f_{12}(\frac{2r_o}{V}\dot{\psi} + (\delta_l - \delta_r)) - M_{xs})$$

(C-27)

$$N_r = \frac{1}{2a}((m\ddot{z} + W_A - F_{zl} - F_{zr})a - (I_{wx}\ddot{\phi} - I_{wy}\frac{V}{r_o}\dot{\psi} + \frac{2f_{11}}{V}(\dot{y} + \frac{r_o\Gamma}{a}\dot{y} - V\psi) + f_{12}(\frac{2r_o}{V}\dot{\psi} + (\delta_l - \delta_r)) - M_{xs})$$

(C-28)

From equations (C-27) and (C-28), we get,

$$(N_l\delta_l - N_r\delta_r) = \frac{(\delta_l - \delta_r)}{2}W_A - I_{wy}\frac{V}{r_o}\dot{\psi}(\frac{\delta_l + \delta_r}{2}) = W_A(\frac{\Delta}{a})y - I_{wy}(\frac{V}{r_o})\dot{\psi}\delta_o$$

(C-29)

C.2 Truck force balance

Figure C-2 shows the free body diagram for the front truck forces.

Front truck lateral

$$m_t\ddot{y}_t^f = F_{yt}^f - \sum_{i=1}^{2} F_{yli} - \sum_{i=1}^{2} F_{yri} - F_{yl}^f - F_{yr}^f \qquad \text{(C-30)}$$

Front truck yaw

$$I_{\psi t}\ddot{\psi}_t^f = -(F_{yl1} + F_{yr1})b + (F_{yl2} + F_{yr2})b - \sum_{i=1}^{2}(F_{xri} - F_{xli})d_p - M_{\psi t}^f \qquad \text{(C-31)}$$

Front truck roll

$$I_{\phi t}\ddot{\phi}_t^f = (F_{zr1} - F_{zl1})d_p + (F_{zr2} - F_{zl2})d_p + (F_{zr}^f - F_{zl}^f)d_s \qquad \text{(C-32)}$$

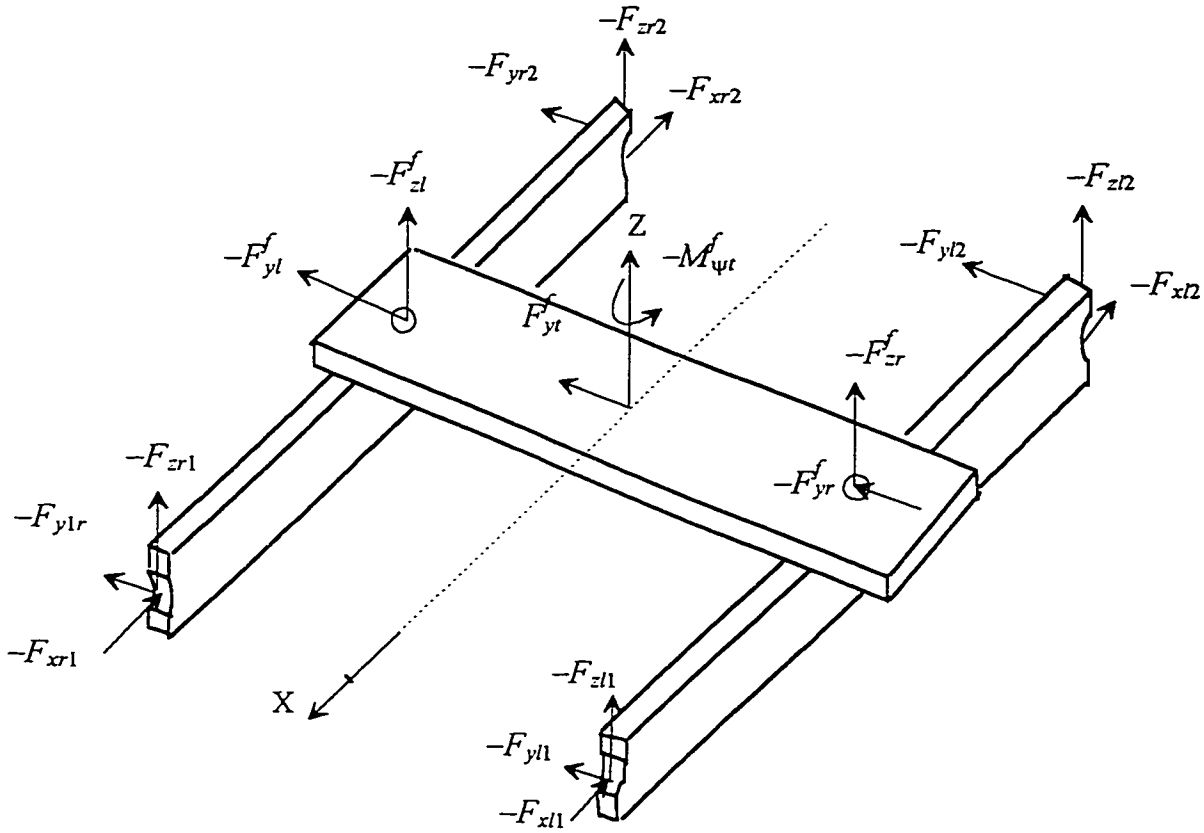

Free body diagram of front truck

Figure C-2

Similarly, equations for the rear truck can be derived as follows.

Rear truck lateral

$$m_t \ddot{y}_t^r = F_{yt}^r - \sum_{i=3}^{4} F_{yli} - \sum_{i=3}^{4} F_{yri} - F_{yl}^r - F_{yr}^r \tag{C-33}$$

Rear truck yaw

$$I_{\psi t} \ddot{\psi}_t^r = -(F_{yl3} + F_{yr3})b + (F_{yl4} + F_{yr4})b - \sum_{i=3}^{4} (F_{xri} - F_{xli})d_p - M_{\psi t}^r \tag{C-34}$$

Rear truck roll

$$I_{\phi t} \ddot{\phi}_t^r = (F_{zr3} - F_{zl3})d_p + (F_{zr4} - F_{zl4})d_p + (F_{zr}^r - F_{zl}^r)d_s \tag{C-35}$$

C.3 Carbody force balance

Figure C-3 shows the carbody force balance.

Lateral

$$M_c \ddot{y}_c = F_{yl}^f + F_{yr}^f + F_{yl}^r + F_{yr}^r + F_{cy} \tag{C-36}$$

Yaw

$$I_c \ddot{\psi}_c = (F_{yl}^f + F_{yr}^f)l_s - (F_{yl}^r + F_{yr}^r)l_s + M_{\psi t}^f + M_{\psi t}^r + M_{\psi c} \tag{C-37}$$

Roll

$$I_c \ddot{\phi}_c = (F_{yl}^f + F_{yr}^f)h_{cs} + (F_{yl}^r + F_{yr}^r)h_{cs} + (F_{zl}^f - F_{zr}^f)d_s + (F_{zl}^r - F_{zr}^r) + M_{c\phi} \tag{C-38}$$

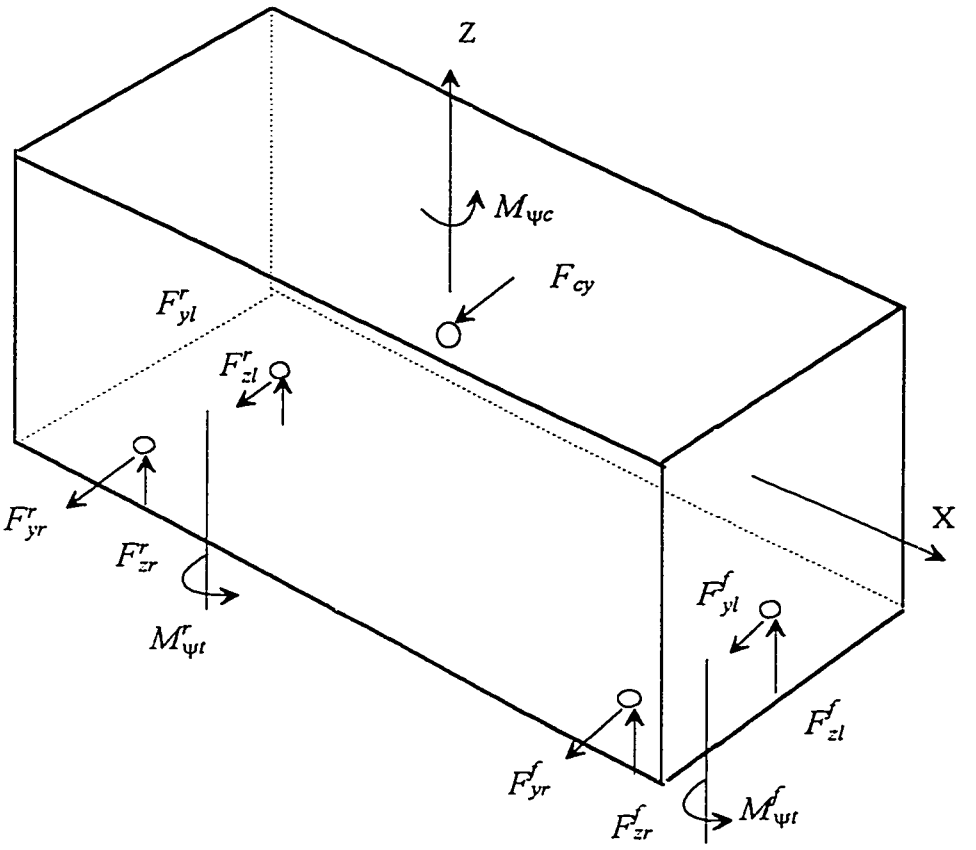

Free body diagram of car

Figure C-3

C.4 Suspension forces

The suspension forces acting on the wheelset are:

$$F_{yl1} = -k_{py}(y_{w1} - y_{t1} - b\psi_{t1} - h_{tp}\phi_{t1})$$

Expressing truck roll in terms of wheelset roll angle and making use of equation (2.3), we have,

$$F^k_{yl1} = -k_{py}(y_{w1} - y_{t1} - b\psi_{t1} - h_{tp}\frac{\Gamma}{2a}(y_{w1} + y_{w2})) \quad \text{(C-39)}$$

$$F^k_{yr1} = F^k_{yl1} \quad \text{(C-40)}$$

$$F^k_{xr1} = -k_{px}d_p(\psi_{w1} - \psi_{t1}) \quad \text{(C-41)}$$

$$F^k_{xl1} = k_{px}d_p(\psi_{w1} - \psi_{t1}) \quad \text{(C-42)}$$

$$F^k_{yl2} = -k_{py}(y_{w2} - y_{t1} - b\psi_{t1} - h_{tp}\frac{\Gamma}{2a}(y_{w1} + y_{w2})) \quad \text{(C-43)}$$

$$F^k_{yr2} = F^k_{yl2} \quad \text{(C-44)}$$

$$F^k_{xl2} = k_{px}d_p(\psi_{w2} - \psi_{t1}) \quad \text{(C-45)}$$

$$F^k_{xr2} = -k_{px}d_p(\psi_{w2} - \psi_{t1}) \quad \text{(C-46)}$$

The suspension forces acting on the car body are (Figure C.3):

$$F^{fk}_{yl} = k_{sy}(y_{t1} - y_c - (l_s - l_e)\psi_c - h_{cs}\phi_c - h_{ts}\frac{\Gamma}{2a}(y_{w1} + y_{w2})) \quad \text{(C-47)}$$

$$F^{fk}_{yr} = F^{fk}_{yl} \quad \text{(C-48)}$$

$$F^{fk}_{zl} = k_{sz}d_s(\phi_c - \frac{\Gamma}{2a}(y_{w1} + y_{w2})) - \frac{M_{cg}}{4} \quad \text{(C-49)}$$

$$F^{fk}_{zr} = k_{sz}d_s(\frac{\Gamma}{2a}(y_{w1} + y_{w2}) - \phi_c) - \frac{M_{cg}}{4} \quad \text{(C-50)}$$

$$F^{rk}_{yl} = k_{sy}(y_{t2} - y_c + (l_s - l_e)\psi_c - h_{cs}\phi_c - h_{ts}\frac{\Gamma}{2a}(y_{w3} + y_{w4})) \quad \text{(C-51)}$$

$$F^{rk}_{yr} = F^{rk}_{yl} \quad \text{(C-52)}$$

$$F^{rk}_{zl} = k_{sz}d_s(\phi_c - \frac{\Gamma}{2a}(y_{w3} + y_{w4})) - \frac{M_{cg}}{4} \quad \text{(C-53)}$$

$$F^{rk}_{zr} = k_{sz}d_s(\frac{\Gamma}{2a}(y_{w3} + y_{w4}) - \phi_c) - \frac{M_{cg}}{4} \quad \text{(C-54)}$$

$$M^{fk}_{\psi} = k_{s\psi}(\psi_{t1} - \frac{l_s}{R} - \psi_c)$$
$$= -T_{s\psi} \quad \text{with yaw break away} \quad \text{(C-55)}$$

$$M^{rk}_{\psi} = k_{s\psi}(\psi_{t2} - \frac{l_s}{R} - \psi_c)$$
$$= T_{s\psi} \quad \text{with yaw break away} \quad \text{(C-56)}$$

Suspension forces acting on the truck are negative of the values given above.

In the above equations, force terms relating to stiffness parameters F^k are given. The terms for suspension forces relating to dampers F^c can be obtained by using velocity terms instead of displacements and by using damping coefficients instead of stiffness constants.

C.5 Gravitational Stiffness Force and Moment:

Refering to Figure 2.1, Section 2.1.2, the equation of lateral gravitational stiffness force as given in equation (2-23) can be simplified by using equation (C-29) and linearizing:

$$N_y = \frac{I_{wy} V \delta_o}{a r_o} \dot{\psi}_w - \frac{W_A(\Gamma+\Delta)}{a} y_w \qquad \text{(C-57)}$$

Multiplying (C-27) by δ_l and (C-28) by δ_r and adding, we get an expression for the yaw gravitational stiffness given in the equation (2-24). The following simplified expression is obtained after neglecting the higher order terms.

$$N_\psi = W_A a \delta_o \psi_w \qquad \text{(C-58)}$$

On curved track, the effect of wheel load shift is taken into account. Equation (2-23) after linearization is

$$N_y = -(N_l - N_r)\delta_o - (N_l + N_r)\frac{(\Delta+\Gamma)}{a} y_w \qquad \text{(C-59)}$$

Using equations (B-35)and (B-36), the above equation can be rewritten as

$$N_y = -W_A \frac{h_{cg}}{a}\phi_d\delta_o - \frac{W_A(\Gamma+\Delta)y_w}{a} \qquad \text{(C-60)}$$

The yaw gravitational moment for the curved track is

$$\begin{aligned} N_\psi &= a(-N_{yl}+N_{yr})(\psi_w + \tfrac{b^*}{R}) \\ &= W_A a\delta_o(\psi_w + \tfrac{b^*}{R}) \end{aligned} \qquad \text{(C-61)}$$

C.6 Equations of Motion - Tangent Track Hunting Model

The equations of motion for the linear hunting model can be written by inputting terms derived for creep forces, gravitational force and moment, and suspension forces into the set of force balance equations obtained for the case of each rigid body, i.e. wheelsets, trucks and carbody (equations C-21, C-25, C-30 to C-38). The model has 17 degrees of freedom: lateral and yaw for 4 wheelsets, lateral, yaw and roll for 2 trucks and lateral, yaw and roll for 1 carbody.

Wheelset lateral (for $i = 1,2, j = 1$; for $i = 3,4, j = 2$)

$$\begin{aligned} &m_w\ddot{y}_{wi} + (2c_{py} + \tfrac{2f_{22}}{V} + \tfrac{2f_{22}r_o\Gamma}{Va})\dot{y}_{wi} + (\tfrac{2f_{23}}{V} - \tfrac{I_{wy}V\delta_o}{ar_o})\dot{\psi}_{wi} - 2c_{py}\dot{y}_{tj} \mp 2c_{py}b\dot{\psi}_{tj} - 2c_{py}h_{tp}\dot{\phi}_{tj} + \\ &+(2k_{py} + \tfrac{W(\Gamma+\Delta)}{a} - \tfrac{2f_{23}\Delta}{r_o a})y_{wi} - 2f_{22}\psi_{wi} - 2k_{py}y_{tj} - 2k_{py}b\psi_{tj} - 2k_{py}h_{tp}\phi_{tj} = 0 \end{aligned} \qquad \text{(C-62)}$$

Wheelset yaw (for $i = 1,2, j = 1$; for $i = 3,4, j = 2$)

$$I_{wz}\ddot{\psi}_{wi} + (\tfrac{I_{wy}V\Gamma}{ar_o} - \tfrac{2f_{23}}{V} - \tfrac{2f_{23}r_o\Gamma}{aV})\dot{y}_{wi} + (2c_{px}d_p^2 + \tfrac{2f_{11}a^2}{V} + \tfrac{2f_{33}}{V})\dot{\psi}_{wi} - 2c_{px}d_p^2\dot{\psi}_{tj} +$$

$$(\frac{2f_{11}a\lambda}{r_o} - \frac{2f_{33}\Delta}{ar_o})y_{wi} + (2k_{px}d_p^2 + 2f_{23} - W_A a\delta_o)\psi_{wi} - 2k_{px}d_p^2\psi_{tj} = 0 \qquad \text{(C-63)}$$

Truck lateral (for $j = 1, i = 1$; for $j = 2, i = 3$)

$$m_{tj}\ddot{y}_{tj} - 2c_{sy}\dot{y}_c - 2c_{sy}h_{cs}\dot{\phi}_c + (2c_{sy} + 4c_{py})\dot{y}_{tj} - 2c_{py}(\dot{y}_{wi} + \dot{y}_{w(i+1)}) + (4c_{py}h_{tp} - 2c_{sy}h_{ts})\dot{\phi}_{tj} \mp 2c_{sy}(l_s - l_e)\dot{\psi}_c - 2k_{sy}y_c - 2k_{sy}h_{cs}\phi_c + (2k_{sy} + 4k_{py})y_{tj} - 2k_{py}(y_{wi} + y_{w(i+1)}) + (4k_{py}h_{tp} - 2k_{sy}h_{ts})\phi_{tj} \mp 2k_{sy}(l_s - l_e)\psi_c = 0 \qquad \text{(C-64)}$$

Truck yaw (for $j = 1, i = 1$; for $j = 2, i = 3$)

$$I_{tz}\ddot{\psi}_{tj} - c_{s\psi}\dot{\psi}_c + (c_{s\psi} + 4c_{px}d_p^2 + 4c_{py}b^2)\dot{\psi}_{tj} - 2c_{py}b(\dot{y}_{wi} - \dot{y}_{w(i+1)}) - 2c_{px}d_p^2 (\dot{\psi}_{wi} + \dot{\psi}_{w(i+1)}) - k_{s\psi}\psi_c + (k_{s\psi} + 4k_{px}d_p^2 + 4k_{py}b^2)\psi_{tj} - 2k_{py}b(y_{wi} - y_{w(i+1)}) - 2k_{px}d_p^2 (\psi_{wi} + \psi_{w(i+1)}) = 0 \qquad \text{(C-65)}$$

Truck roll (for $j = 1, i = 1$; for $j = 2, i = 3$)

$$I_{tx}\ddot{\phi}_{tj} + 2h_{ts}c_{sy}\dot{y}_c \pm 2h_{ts}c_{sy}(l_s \mp l_e)\dot{\psi}_c + (2h_{ts}h_{cs}c_{sy} - 2c_{sz}d_s^2)\dot{\phi}_c + (2d_s^2c_{sz} + 2h_{ts}^2c_{sy} + 4c_{py}h_{tp}^2 + 4d_p^2c_{pz})\dot{\phi}_{tj} + (4c_{py}h_{tp} - 2c_{sy}h_{ts})\dot{y}_{tj} - 2c_{py}h_{tp}(\dot{y}_{wi} + \dot{y}_{w(i+1)}) + 2h_{ts}k_{sy}y_c + 2h_{ts}k_{sy}(l_s - l_e)\psi_c + (2h_{ts}h_{cs}k_{sy} - 2k_{sz}d_s^2)\phi_c + (2d_s^2k_{sz} + 2h_{ts}^2k_{sy} + 4k_{py}h_{tp}^2 + 4d_p^2k_{pz})\phi_{tj} (4k_{py}h_{tp} - 2k_{sy}h_{ts})y_{tj} - 2k_{py}h_{tp}(y_{wi} + y_{w(i+1)}) = 0 \qquad \text{(C-66)}$$

Carbody lateral

$$m_c\ddot{y}_c + 4c_{sy}\dot{y}_c - 4c_{sy}l_e\dot{\psi}_c + 4c_{sy}h_{cs}\dot{\phi}_c + 2c_{sy}h_{ts}(\dot{\phi}_{t1} + \dot{\phi}_{t2}) - 2c_{sy}(\dot{y}_{t1} + \dot{y}_{t2}) + 2k_{sy}y_c - 4k_{sy}y_c - 4k_{sy}l_e\psi_c + 4k_{sy}h_{cs}\phi_c + 2k_{sy}h_{ts}(\phi_{t1} + \phi_{t2}) - 2k_{sy}y_{t1} - 2k_{sy}y_2 = 0 \qquad \text{(C-67)}$$

Carbody yaw

$$I_{zc}\ddot{\psi}_c + (2c_{s\psi} + 4c_{sy}l_s^2)\dot{\psi}_c - 2c_{sy}l_s(\dot{y}_{t1} - \dot{y}_{t2}) + 2c_{sy}l_sh_{ts}(\dot{\phi}_{t1} - \dot{\phi}_{t2}) - c_{s\psi}(\dot{\psi}_{t1} + \dot{\psi}_{t2}) + (2k_{s\psi} + 4k_{sy}l_s^2)\psi_c - 2k_{sy}l_s(y_{t1} - y_{t2}) + 2k_{sy}l_sh_{ts}(\phi_{t1} - \phi_{t2}) - k_{s\psi}(\psi_{t1} + \psi_{t2}) = 0 \qquad \text{(C-68)}$$

Carbody roll

$$I_{xc}\ddot{\phi}_c + 4c_{sy}h_{cs}\ddot{y}_c + 4(c_{sz}d_s^2 + c_{sy}h_{cs}^2)\dot{\phi}_c - 4c_{sy}h_{cs}l_e\dot{\psi}_c - 2c_{sy}h_{cs}(\dot{y}_{t1} + \dot{y}_{t2}) + 2(h_{cs}h_{ts}c_s - d_s^2c_{sz})(\dot{\phi}_{t1} + \dot{\phi}_{t2}) + 4k_{sy}h_{cs}y_c + 4(k_{sz}d_s^2 + k_{sy}h_{cs}^2)\phi_c - 4k_{sy}h_{cs}l_e\psi_c - 2k_{sy}h_{cs}(y_{t1} + y_{t2}) + 2(h_{cs}h_{ts}k_{sy} - d_s^2k_{sz})(\phi_{t1} + \phi_{t2}) = 0$$

(C-69)

C.7 Equations of Motion - Steady State Curving Model

The equations for the linear curving model are obtained by including terms due to curvature and cant deficiency as derived in Appendix B.2. For the steay state curving model, velocity and acceleration terms are omitted from the force balance equations given in Sections C.1 to C.3 above. The model has 8 degrees of freedom: lateral and yaw of two wheelsets, lateral and yaw of a truck and lateral and roll of car body.

Leading Wheelset lateral

$$2f_{22}\psi_{w1} + (\frac{2f_{23}\Delta}{ar_o} - \frac{W_A(\Gamma+\Delta)}{a} - 2k_{py} + k_{py}h_{tp}\frac{\Gamma}{a})y_{w1} + k_{py}h_{tp}\frac{\Gamma}{a}y_{w2} + 2k_{py}y_{t1} + 2k_{py}b\psi_{t1} = -2f_{22}\frac{b}{R} - \frac{2f_{23}}{R} - \frac{2f_{23}h_{cf}\phi_d\delta_o}{ar_o} - m_wg\phi_d + W_A\frac{h_{cg}}{a}\phi_d\delta_o$$

(C-70)

Wheelset yaw

$$\left[-2af_{11}\left(1 - \frac{4h_{cg}^2\phi_d^2}{9a^2}\right)\frac{\lambda}{r_o} + \frac{2f_{33}\Delta}{ar_o}\right]y_{w1} + \left(aW_A\delta_o - 2f_{23} - 2d_p^2k_{px}\right)\psi_{w1} + 2d_p^2k_{px}\psi_t = -\left(1 - \frac{4h_{cg}^2\phi_d^2}{9a^2}\right)\frac{2f_{11}a^2}{R} - \frac{2f_{33}}{R} - \frac{8f_{33}h_{cg}\phi_d\delta_o}{3ar_o} + \frac{2f_{23}b}{R} - \frac{Wa\delta_o b}{R}$$

(C-71)

Trailing Wheelset Lateral

$$2f_{22}\psi_{w2}+(\tfrac{2f_{23}\Delta}{ar_o}-\tfrac{W_A(\Gamma+\Delta)}{a}-2k_{py}+k_{py}h_{tp}\tfrac{\Gamma}{a})y_{w2}+k_{py}h_{tp}\tfrac{\Gamma}{a}y_{w2}+2k_{py}y_{t1}-$$
$$2k_{py}b\psi_{t1}=2f_{22}\tfrac{b}{R}-\tfrac{2f_{23}}{R}-\tfrac{2f_{23}h_{cs}\phi_d\delta_o}{ar_o}-m_wg\phi_d+W_A\tfrac{h_{cg}}{a}\phi_d\delta_o$$

(C-72)

Trailing Wheelset Yaw

$$\left[-2af_{11}\left(1-\tfrac{4h_{cg}^2\phi_d^2}{9a^2}\right)\tfrac{\lambda}{r_o}+\tfrac{2f_{33}\Delta}{ar_o}\right]y_{w2}+\left(aW_A\delta_o-2f_{23}-2d_p^2k_{px}\right)\psi_{w2}+2d_p^2k_{px}\psi_t$$
$$=-\left(1-\tfrac{4h_{cg}^2\phi_d^2}{9a^2}\right)\tfrac{2f_{11}a^2}{R}-\tfrac{2f_{33}}{R}-\tfrac{8f_{33}h_{cg}\phi_d\delta_o}{3ar_o}+\tfrac{2f_{23}b}{R}+\tfrac{W_Aa\delta_ob}{R}$$

(C-73)

Truck Lateral

$$(2k_{py}-2k_{py}h_{tp}\tfrac{\Gamma}{a}+k_{sy}h_{ts}\tfrac{\Gamma}{a})(y_{w1}+y_{w2})-(4k_{py}+2k_{sy})y_t+2k_{sy}y_c+2k_{sy}(l_s+l_e)\psi_c$$
$$+2k_{sy}h_{cs}\phi_c=-m_tg\phi_d$$

(C-74)

Truck yaw

$$2bk_{py}(y_{w1}-y_{w2})+2d_p^2k_{px}(\psi_{w1}+\psi_{w2})-(4d_p^2k_{px}+4b^2k_{py}+k_{s\psi})\psi_t+k_{s\psi}\psi_c=-k_{s\psi}\tfrac{l_s}{R}$$

(C-75)

Carbody Lateral

$$-k_{sy}h_{ts}\tfrac{\Gamma}{a}(y_{w1}+y_{w2})+2k_{sy}y_t-2k_{sy}y_c+2k_{sy}l_e\psi_c-2k_{sy}h_{cs}\phi_c=-m_cg\phi_d$$

(C-76)

Carbody Roll

$$(k_{sz}d_s^2-k_{sy}h_{cs}h_{ts})\tfrac{\Gamma}{a}(y_{w1}+y_{w2})+2k_{sy}h_{cs}y_t-2k_{sy}h_{cs}y_c+2k_{sy}l_eh_{cs}\psi_c-2k_{sy}h_{cs}^2\phi_c$$
$$-2k_{sz}d_s^2\phi_c=0$$

(C-77)

APPENDIX - D

Cubic Saturation Model

The non-linear effect of contact forces is to be taken into account in a curving model. The cubic saturation model developed by Vermuelen and Johnson has been used to account for the saturation of creep forces imposed by the coefficient of friction. In this process, the linear longitudinal and lateral creep forces are first calculated using the following equations:

$$F_{xlin} = f_{11}\xi_x \tag{D-1}$$

$$F_{ylin} = f_{22}\xi_y + f_{23}\xi_s \tag{D-2}$$

The total creep force is then caculated and non-dimensionalized.

$$F' = \frac{\sqrt{F_{xlin}^2 + F_{ylin}^2}}{\mu N} \tag{D-3}$$

A saturation variable α is now calculated based on the following cubic law,

$$\alpha = \frac{1}{F'}\left(F' - \frac{F'^2}{3} + \frac{F'^3}{27}\right) \qquad \text{for} \qquad F' \le 3 \tag{D-4}$$

$$\alpha = \frac{1}{F'} \qquad \text{for} \qquad F' > 3 \tag{D-5}$$

The linear forces are then multiplied by the saturation variable α to obtain the non-linear creep force relationships,

$$F_x = \alpha F_{xlin} \tag{D-6}$$

$$F_y = \alpha F_{ylin} \tag{D-7}$$

Appendix E

Summary of Vehicle Parameters

Parameter	Dimension
Half of wheelset contact distance, a	0.7163 m
Half of wheelbase, b	1.295 m
Half of primary spring lateral spacing, d_p	0.5852 m
Half of secondary spring lateral spacing, d_s	1.143 m
Height of carbody c.g. to secondary lateral springs, h_{cs}	0.896 m
Height of truck c.g. to secondary lateral springs, h_{ts}	0.512 m
Height of truck c.g. above axle centre, h_{tp}	0.1067 m
Half of truck centre spacing, l_s	9.068 m
Carbody mass, M_c	41,738 kg
Truck frame mass, M_t	3649 kg
Wheelset mass, M_w	1751 kg
Roll moment of inertia of carbody, I_{cx}	103,500 kg-m^2
Pitch moment of inertia of carbody, I_{cy}	2.391×10^6 kg-m^2
Yaw moment of inertia of carbody, I_{cz}	2.391×10^6 kg-m^2
Roll moment of inertia of truck frame, I_{tx}	2790 kg-m^2
Pitch moment of inertia of truck frame, I_{ty}	588 kg-m^2
Yaw moment of inertia of truck frame, I_{tz}	3371 kg-m^2

Parameter	Dimension
Roll moment of inertia of wheelset, I_{wx}	761 kg-m^2
Pitch moment of inertia of wheelset, I_{wy}	152 kg-m^2
Yaw moment of inertia of wheelset, I_{wz}	761 kg-m^2
Centred wheel rolling radius, r_o	0.4572 m
Centred contact angle, δ_o	0.06775 rad
Wheelset roll coefficient, Γ_o	0.06775
Contact angle difference coefficient, Δ	10.35
Creep Coefficients (50% of Kalker values)	
Longitudinal creep coefficient, f_{11}	6.1×10^6 N
Lateral creep coefficient, f_{22}	5.27×10^6 N
Spin creep coefficient, f_{33}	121.9 N-m^2